

UCSF

UC San Francisco Electronic Theses and Dissertations

Title

Engineering Cellular Therapeutics

Permalink

<https://escholarship.org/uc/item/8059s8rs>

Author

Park, Jason Sun-Hyung

Publication Date

2013

Supplemental Material

<https://escholarship.org/uc/item/8059s8rs#supplemental>

Peer reviewed|Thesis/dissertation

Engineering Cellular Therapeutics

by

Jason Sun-Hyung Park

DISSERTATION

Submitted in partial satisfaction of the requirements for the degree of

DOCTOR OF PHILOSOPHY

in

Bioengineering

in the

GRADUATE DIVISION

of the

UNIVERSITY OF CALIFORNIA, SAN FRANCISCO

AND

UNIVERSITY OF CALIFORNIA, BERKELEY

Copyright 2013

by

Jason Sun-Hyung Park

Acknowledgments

My graduate education at UCSF has been an amazing time of growth and learning. I could not possibly have asked for a better environment in which to develop as a scientist and enjoy learning the discipline and craft of scientific research. I have many people to thank:

My advisor Wendell Lim – for his mentorship and for teaching me how to do great science; for showing me the importance of maintaining creativity and an agile mind in addition to rigor in one’s work; for his excitement and fearlessness in pursuing new ideas; for his tireless work on behalf of the lab; for always demanding the best from me and for putting faith in me; for building the Lim Lab and bringing together all of the amazing people who make the lab the special place that it is.

My co-advisor Bruce Conklin – for teaching me how to propose, pursue, and present science with clarity; for his advice and guidance over the years; for his love of scientific research and passion for world-changing ideas; for showing me how to be a great scientific collaborator; for supporting me in my aspirations as a future physician-scientist.

My thesis committee members Art Weiss and Zena Werb – for their kindness and caring about a young physician-scientist in training; for showing such generosity with their time, knowledge, and advice; for their active leadership in the MSTP especially in my early years at UCSF when Art was Director; for asking incisive questions; for being my advocates.

My MSTP advisors Christoph Schreiner and Tejal Desai – for helping me find my footing as I entered the Ph.D. program, and for their advice throughout grad school. And Tejal, for giving me a fantastic experience with my first lab rotation all those years ago and for serving as my qualifying exam committee chair.

James Onuffer, associate director of the Cell Propulsion Lab – for his mentorship and willingness to share from his immense research experience and knowledge base; for countless conversations about my research (and about non-scientific topics); for playing a critical role in the build-up of the translational work that defines the CPL Pathway to Medicine lab today.

My labmate Benjamin Rhau, with whom I guided many iGEM students, survived two lab moves, set up an entirely empty new lab space from scratch (spending countless thousands in the process), and ventured into the world of preclinical mouse models of disease – for his careful and rigorous approach to science; for teaching me the ins and outs of the notoriously finicky HL-60 cell line; for all of our discussions about science; for being a great person to work with; for always-ready recommendations on places to eat and to drink coffee.

My labmate / rotation advisor Aynur Tasdemir a.k.a. “Big Bird” – for welcoming me into the lab with open arms; for her passion for life; for her diligent teaching; for making my rotation and first year in the lab an enjoyable experience.

My labmates Ping “Andy” Wei and Wilson Wong – for countless interesting discussions; for our work together on the work presented in Chapter 4 of this dissertation and published in Nature; for teaching me how they do (and enjoy) science; for being great colleagues.

My labmates Krista McNally and Silinda Neou – for all of our work together; for helping me be clear in my thinking; for their patience; for doing what it takes to keep the lab and its equipment running; for making life in the lab enjoyable; for saving me sandwiches when I was late to Lim Lab birthday lunches.

My labmates Chia Wu and Kole Roybal – for all of our scientific discussions and work together in the lab; for being great colleagues; for thoughtful feedback and for helping me think critically about my research.

My labmates Faith Kreitzer, Alice Sheehan, Po-Lin So, Miller Huang, Matt Spindler, Nate Huebsch, Kenta Nakamura, and others in the Conklin Lab – for our work together in stem cell differentiation and motility; for sharing with me your knowledge and insights and for being great colleagues.

My labmate Jared Toettcher – for our exploratory work into the guidance of neurite outgrowth and axon guidance together; for sharing his infectious joy for doing scientific research on a daily basis.

Edwin Rodriguez, my MSTP classmate – for always being generous and helpful in technical and scientific brainstorming; for our conversations on the future of medicine; for help with cell sorting on so many occasions; for being a great person to bounce ideas off of to get thoughtful insights and questions; for making me a more creative scientist.

My iGEM and summer students of past years: Carmen Zhou, Jackie Tam, Eric Wong, Ryan Liang, Ethan Chan, and many others – for being engaged and energetic learners; for their contributions to our lab's research; for teaching me how to mentor; for making research a great deal of fun.

Orion Weiner and my colleagues in the Weiner Lab including Arthur Millius, Andrew Houk, and Sheel Dandekar, all of whom I leaned on heavily for advice especially during my early days in the lab studying chemotaxis in HL-60 neutrophils.

Zev Gartner and my colleagues in the Gartner Lab, especially Nicholas Selden – for providing an open environment and fun place to talk about science and big ideas for

synthetic chemistry in biology; for being fantastic collaborators on a project exploring the use of cells as cargo-delivery vehicles; for being enjoyable people to work with.

Karl Saldanha from the Majumdar Lab – for teaching me about Nuclear Magnetic Resonance and for his generosity with his time in our work together on using cells as delivery vehicles for diagnostic payloads for magnetic resonance imaging; for being such a positive presence and great person to work with.

For Byron Hann, Donghui Wang, Don Hom, and Paul Phojanakong of the UCSF Preclinical Therapeutics Core – for being a wonderful resource and for our years of work and discussions together.

Jana Toutolmin and Catherine Norton in the UCSF MSTP Office – for solving every problem big and small.

Art Weiss, Kevin Shannon, and Mark Anderson: past and current directors of the UCSF MSTP – for their guidance, support, and tireless work on behalf of all of the trainees in the program.

All of my other colleagues at the Lim and Conklin Labs, too many to name – for teaching me so many things; for sharing your love of science; for making the labs two of the most fun, interesting, and intellectually stimulating places I have ever had the fortune of working.

My parents Chan and Mitzie and my brother Ryan – for always encouraging me in good times and bad; for always being supportive about my work and aspirations; for

giving me perspective in life; for their love and guidance not just over the last five years, but over the past twenty nine.

My wife Christine – for always standing by my side with endless patience and tireless encouragement; for her unwavering support of me in all of my hopes and dreams.

Chapter 2 contains material that will soon be submitted for publication with contributions from several authors:

Jason S. Park, Benjamin Rhau, Aynur Tasdemir, Krista A. McNally, Carmen Zhou, Orion D. Weiner, Bruce R. Conklin, James J. Onuffer, Wendell A. Lim. Engineering synthetic control over mammalian cell migration to an orthogonal bio-inert small molecule. *In preparation*.

Chapter 4 is based on a manuscript previously published in *Nature* with contributions from several authors:

Ping Wei, Wilson W. Wong, Jason S. Park, Ethan E. Corcoran, Sergio G. Peisajovich, James J. Onuffer, Arthur Weiss, and Wendell A. Lim. Bacterial virulence proteins as tools to rewire kinase pathways in yeast and immune cells. *Nature*, 488(7411), 384-388 (2012).

My contributions to this work included the conception and design of experiments, methods development, experimental planning, lab work, and data analysis for aspects of the project involving primary human T cells (particularly Figure 4 and related supplementary figures and text).

Engineering Cellular Therapeutics

Jason Park

Abstract

Living cells act as smart and powerful therapeutic agents within the body. With their ability to sense multiple environmental signals, integrate a wide array of information to make critical decisions, and execute complex tasks, cells exert disease-fighting effects in the body with a precision and sophistication that far exceeds that of the small molecule and protein-based therapeutics that currently dominate modern medicine. The remarkable disease-fighting capabilities of cells can be harnessed for therapeutic use, and cellular therapies are currently being explored for the treatment of conditions ranging from cancer and autoimmunity to spinal cord injury and neurodegenerative disorders.

Most cell therapy strategies today rely on the endogenous abilities of cells, but there is great untapped potential in using genetic engineering to tune, optimize, and direct their capabilities. A recent example is the use of genetic modification by researchers in adoptive T cell cancer immunotherapy to generate tumor-targeted T cells with highly potent anti-tumor and proliferative activity to effectively treat chemotherapy-resistant cancer patients.

We present several new tools for enhancing the therapeutic capabilities of engineered cells through genetic engineering. First, we describe a synthetic biology approach to orthogonal control over cell migration. Migration is a core capability of many cell types in the body that truly sets cells apart from small molecules and biologics.

Specifically, we demonstrate the use of an engineered G protein-coupled receptor to direct the homing and migration of a variety of cell types toward an orthogonal small molecule drug source both *in vitro* and in a mouse. We also describe ongoing work using the engineered cell migration tool described above to enhance the infiltration of tumors by anti-tumor T cells.

Next, we discuss a project exploring the usage of two bacterial pathogen proteins, OspF from *Shigella*, and YopH from *Yersinia Pestis*, as reagents to precisely modulate MAPK signaling in yeast and in human T cells. Tools like these hold potential for use in the precise regulation of cellular signaling in therapeutic cells.

Finally, I conclude this dissertation with closing remarks on some of the challenges and opportunities ahead for this exciting field of scientific research.

Table of Contents

Copyright.....	ii
Acknowledgments	iii
Abstract.....	viii
Table of Contents	x
List of Tables.....	xii
List of Figures.....	xiii
Chapter 1. The Use of Engineered Cells as Therapeutic Agents	1
Cells as Therapeutic Agents	1
Enhancing cellular therapeutics through genetic engineering.....	2
A synthetic biology “toolkit” for engineering therapeutic cells.....	4
Overview of chapters two through four.....	6
References	8
Chapter 2. Engineering synthetic control over mammalian cell migration to an orthogonal bio-inert small molecule	12
Introduction	12
References	14
Manuscript: Engineering synthetic control over mammalian cell migration to an orthogonal bio-inert small molecule.....	15
Figures.....	42
Chapter 3. Use of an orthogonal cell migration tool to enhance the infiltration of tumors by adoptively transferred anti-tumor T cells	50

Introduction	50
T cell-based immunotherapy for cancer	50
Overcoming suboptimal infiltration of tumors by anti-tumor T cells	51
Results	54
Anti-CD19 CAR-expressing T cells respond to CD19-expressing target tumor cells <i>in vitro</i>	54
Establishment of a CD19+ Daudi subcutaneous tumor model to test CAR T cell efficacy	56
Anti-CD19 CAR T cells efficiently expand <i>in vivo</i> and treat subcutaneous Daudi xenograft tumors	57
Use of an orthogonal cell migration tool augments the homing of CAR T cells to Daudi tumors	58
Discussion	59
Figures	63
References	70
Chapter 4. Building a “pause” safety switch for safer T cell therapeutics	74
Introduction	74
Manuscript: Bacterial Virulence Proteins as Tools to Rewire Kinase Pathways in Yeast and Immune Cells	76
Figures	106
Supplementary Information	110
Chapter 5. Concluding Remarks	138

List of Tables

Chapter 3

Supplementary Table 1 – Plasmids used in yeast experiments	124
Supplementary Table 2 - Yeast strains used in this study	124
Supplementary Table 3 – Expression vectors used in the study with Jurkat T cell	125
Supplementary Table 4 – Gateway donor vector used to generate the expression vector	126
Supplementary Table 5 – Gateway destination vector used to generate the expression Vector	126
Supplementary Table 6 – Other vectors used to generate the expression vector	126
Supplementary Table 7 – Plasmids used in the transfection	127
Supplementary Table 8 – Plasmids used in the human primary CD4+ T cell experiments	128

List of Figures

Figure 2.1 – Expression of engineered Gai-coupled GPCRs is sufficient to induce cytoskeletal changes and direct the chemotaxis of neutrophils up a gradient of a bio-inert small molecule drug CNO	42
Figure 2.2 – Microscopic analysis and quantitation of neutrophil cell migration in response to a gradient of CNO	43
Figure 2.3 – The engineered chemotaxis receptor Di is “portable” to a range of cell types and is sufficient to mediate both chemotaxis and transendothelial migration	44
Figure 2.4 – Intravenously administered primary T lymphocytes expressing Di specifically localize to a subcutaneously implanted depot of CNO slow-release biodegradable microspheres	45
Supp. Figure 2.1 – CNO induces adhesion / spreading in engineered Gai-coupled GPCR-expressing HL-60 neutrophils, as determined using a real-time impedance-based assay	46
Supp. Figure 2.2 – Integrity of tight endothelial cell monolayers grown on porous inserts is demonstrated by blockage of FITC-dextran diffusion in a permeability assay	48
Supp. Figure 2.3 – Fabricated PLGA microspheres show typical morphology and size distribution suitable for subcutaneous injection	49
Figure 3.1 – Anti-CD19 chimeric antigen receptor design	64
Figure 3.2 – Anti-CD19 CAR-transduced primary T cells express CAR on cell surface	65

Figure 3.3 – Anti-CD19 CAR T cells are functional against a CD19-expressing tumor cell line <i>in vitro</i>	66
Figure 3.4 – rLuc/Daudi tumor cell lines grow robustly as subcutaneous tumors in immunodeficient NSG mice	67
Figure 3.5 – Anti-CD19 CAR-transduced primary T cells expand in rLuc/Daudi tumor-bearing NSG mice and reduce the size of subcutaneous tumors	68
Figure 3.6 – Anti-CD19 CAR- and Di receptor-transduced primary T cells preferentially localize to rLuc/Daudi tumors (right flank) injected with CNO microspheres relative to tumors in the contralateral flank (left) injected with control microspheres	69
Figure 4.1 – Bacterial effector OspF can block selective MAP kinase pathways in yeast	106
Figure 4.2 – Tuning frequency dependent response of yeast osmolarity pathway using synthetic OspF feedback loop	107
Figure 4.3 – OspF can be used to precisely control T cell activation amplitude and duration in Jurkat T cells	108
Figure 4.4 – OspF can be used as a synthetic pause switch to control human primary CD4+ T cell activation	109
Supplementary Figure 4.1 – Pathogen effectors can be harnessed to inhibit specific MAPKs through scaffold protein recruitment with leucine zippers in yeast	129

Supplementary Figure 4.2 – Simulation indicates that synthetic negative feedback loops can alter the frequency dependent activation of the HOG MAPK pathway	130
Supplementary Figure 4.3 – Single cell assaying with microfluidic device	131
Supplementary Figure 4.4 – OspF mediated feedback renders the cell less responsive to a second step of osmostress stimulation	132
Supplementary Figure 4.5 - Other TCR responses - ERK activation and CD69 expression - were also inhibited by YopH and OspF when cells are induced with an anti-TCR antibody (C305), while overexpression of mammalian SHP-1 phosphatase does not inhibit T cell response	133
Supplementary Figure 4.6 – Specific OspF mutant can be used to derive negative regulator that is specific for pERK vs pp38 MAPK inhibition in Jurkat T cells	134
Supplementary Figure 4.7 – Mechanism of amplitude limiter circuit: Introduction of OspF negative feedback loop causes transient Erk activation (instead of sustained), leading to lower steady pathway output amplitude	135
Supplementary Figure 4.8 – Synthetic pause switch: Transient inhibition of TCR activation with a pulse induction of bacterial effectors	136
Supplementary Figure 4.9 – OspF was engineered into a synthetic pause switch to control the activation of primary human T cells	137

Chapter 1. The Use of Engineered Cells as Therapeutic Agents

Cells as Therapeutic Agents

Living cells act as smart and powerful therapeutic agents within the body. With their ability to sense multiple environmental signals, integrate a wide array of information to make critical decisions, and execute complex tasks, cells exert disease-fighting effects in the body with a precision and sophistication that far exceeds that of the small molecule and protein-based therapeutics that currently dominate modern medicine.

Take for instance the human immune system. Natural Killer cells sense virally infected or malignant cells and deliver powerful cytotoxic payloads directly to their targets. Macrophages and dendritic cells of the innate immune system engulf and destroy pathogens, and recruit lymphocytes of the adaptive immune system for further help and to initiate the development of long-lasting immune memory against these foreign invaders to safeguard against future attacks.

There are countless other mechanisms built into the body's cells and organ systems to keep it in homeostasis and ward off disease. Pancreatic islet cells sense glucose concentrations and secrete hormones such as glucagon and insulin to precisely regulate glucose metabolism. The kidney regulates electrolyte, pH, and blood pressure through hormone secretion and by actively balancing the reabsorption and excretion of salts, bicarbonate ions, and waste. The liver is home to cells that serve the body as factory, warehouse, and detoxification center – it is a site for carbohydrate, protein, and lipid metabolism, production of coagulation factors and various hormones, the breakdown of toxic substance, and the storage of glycogen and vitamins. Stem and progenitor cells

throughout the body provide a constant stream of new cells to replenish old and damaged cells and tissues in reparative and regenerative processes.

The remarkable disease-fighting and regenerative capabilities of cells can also be harnessed for modern-day medicine. In fact, cells have been used as therapeutic agents at least since James Blundell's first successful human-to-human blood transfusion in 1818 as a last-resort treatment for blood loss in obstetrical procedures (1–3). Since then, the direct uses for cells and tissues in medicine have expanded from simple blood product derivatives (30 million transfusions per year in the U.S. in 2006 per the American Red Cross) to include organ transplants (28,358 in the U.S. in 2007 per the National Organ Procurement and Transplantation Network), *in vitro* fertilization (47,849 live births in 2011 per CDC report), immune cell therapy, and hematopoietic stem cell transplants (50,417 worldwide in 2006 per the Worldwide Network for Blood and Marrow Transplantation). There is also currently great enthusiasm for stem cell-based therapies for conditions ranging from heart disease and spinal cord injury to blindness and autoimmune diabetes. Many of these potential treatments are still in the research phase with a steadily increasing number reaching human clinical trials.

Enhancing Cellular Therapeutics Through Genetic Engineering

Cellular therapeutics in use today rely mostly on the endogenous capabilities of cells, in some cases with the help of proteins or small molecules in *ex vivo* culture to stimulate proliferation or effect some other useful phenotype. However, there is great untapped potential in modifying therapeutic cells using genetic engineering tools to tune, optimize, and direct their therapeutic capabilities.

For example, genetic engineering has already had a huge impact on adoptive T cell immunotherapy for cancer, a field that has become a leader in the cell therapy arena. T

cell-based immunotherapies have shown impressive efficacy in recent clinical trials for cancer types ranging from metastatic melanoma to lymphomas and leukemias, even in heavily pre-treated and chemotherapy-resistant patients (4).

The general strategy for T cell immunotherapy is as follows: T cells are collected and isolated from patient peripheral blood. To endow them with the ability to recognize and respond to cancer antigens by proliferating, secreting pro-inflammatory cytokines, and killing target cells, the cells are genetically modified to express recombinant T cell receptor (TCR) chains cloned from tumor antigen-reactive T cells or chimeric antigen receptors (CARs), which are protein fusions of tumor antigen-specific single-chain antibody fragments (scFv) and intracellular signaling domains of key components of immune cell activation signaling cascades (5–11). Additional background is available in the introduction section of Chapter 3 of this dissertation.

Recently, investigators accomplished an important feat in CAR engineering to overcome a major impediment to success in cell therapy. After years of study in mouse models and human clinical trials, it had become well-known that poor *in vivo* persistence and expansion of infused cells was a limiting factor in therapeutic efficacy (11–13). Based on prior work showing that the costimulatory signaling from the 4-1BB (CD137) receptor is critical for the expansion and memory phenotype of CD8+ cytotoxic lymphocytes – which are responsible for much of the direct cell-killing effect in anti-tumor T cell therapy – researchers demonstrated that the inclusion of the costimulatory signaling domain from 4-1BB (CD137) in the design of a CAR targeting CD19+ malignancies was sufficient to significantly increase the anti-tumor activity, memory phenotype, and *in vivo* persistence of transferred T cells in cell-based assays, in mouse tumor models, and in patients (14–19). In three chemotherapy-resistant chronic lymphocytic leukemia patients treated in a pilot clinical trial, two out of three patients had

complete responses and one had a partial response. Each infused T cell and its progeny eliminated more than 1000 leukemia cells on average, proliferated robustly, and persisted for greater than 6 months in the blood and bone marrow (18).

Genetic modification has also been used to engineer safety controls into cellular therapeutics. One of the simplest possible controls is a “kill switch” that can be activated with a drug or other signal to eliminate modified cells in case of adverse events. For example, expression of the herpes simplex-thymidine kinase gene in engineered cells has been shown to be sufficient for their depletion upon administration of the antiviral drug ganciclovir (20–22). However, this early approach was slow (days for cell killing to take place), precluded the future use of an important class of antiviral prodrugs, and suffered from concerns about immunogenicity from the use of virus-derived protein (23). A newer tool that overcame these obstacles is known as iCasp9 and is composed of a modified human caspase 9 fused to a human FK506 binding protein(24–26). The presence of a bio-inert small molecule drug AP1903 causes dimerization of the iCasp9 construct, rapidly inducing apoptosis of modified cells.

A synthetic biology “toolkit” for engineering therapeutic cells

Could we develop systematic ways of using genetic engineering techniques to further precisely control cellular therapeutics, thereby unlocking their full potential? For cell therapies to be a viable and effective treatment for a broad range of disease indications in the future, a long-term goal for the field must be to learn how to predictably and reproducibly design cellular therapeutic agents that are safe and effective (27). Such a feat will likely involve intensive interdisciplinary work including the building and refinement of models to understand “cellular control theory”, extensive experimental work to test the effects of systematic cellular modifications in meaningful biological

assays and disease models, and continued advancements in core enabling technologies including genome editing, gene synthesis, and genetic modification.

Synthetic biology is an emerging scientific discipline that is poised to make a significant impact in this effort. Practitioners in the field seek to build, characterize, and utilize biological “parts” and “devices” for useful purposes. Key principles in synthetic biology include the importance of standardization in the design and characterization of DNA “parts” and the use of the concept of abstraction to manage the complexity of biological systems and allow for better predictive modeling and understanding of systems (28).

The synthetic biology community has been building, characterizing, and using a variety of DNA parts to build basic biological circuits and systems. Some of the interesting types of parts that have been made include gene expression controllers that respond to exogenous and endogenous signals, orthogonal tools for control over receptor or intracellular signaling (e.g. with small molecule drugs or light), and sophisticated cellular signal processing systems including switches, oscillators, logic gates, feedback loops, engineered scaffold proteins, and transistors (29–35) (36, 37) (38–41) (30, 42–45). Much of this work has been done in bacteria and yeast though an increasing amount of work in recent years has been conducted in mammalian cells.

Significant work remains to build on current tools and techniques in synthetic biology and use them in a focused manner that is guided by our understanding of cell and disease biology to predictably engineer effective therapeutic cells. One clear area in which progress is needed is in the building of robust therapeutic cell “control modules” to control key cellular behaviors. Among other things, these modules could include circuits to sense and target disease, control cell proliferation and death, direct cell migration,

tune cellular signaling, program cellular communication, produce secreted therapeutic molecules, and direct cell fate (27).

This dissertation covers some of my contributions to our laboratory's work over the past five years in building, testing, and characterizing new parts for the therapeutic cellular engineering toolkit.

Overview of Chapters Two through Four

Chapter 2 describes a synthetic biology approach to orthogonal control over cell migration, a capability of many cell types in the body that is not only critical for their natural function but also one that can truly sets cells apart from small molecules and biologics when they are used as therapeutic agents. Specifically, we demonstrate the use of an engineered G protein-coupled receptor called a Receptor Activated Solely by a Synthetic Ligand (RASSL) to direct the homing and migration of a variety of cell types toward an orthogonal small molecule drug source both *in vitro* and in a mouse. This work is in the process of being submitted for peer review and publication.

Chapter 3 describes our ongoing work on enhancing the infiltration of tumors by anti-tumor T cells through the use of the engineered cell migration tool detailed in Chapter 2. We express in human T cells the engineered RASSL receptor Di and an anti-tumor chimeric antigen receptor, and demonstrate in a mouse subcutaneous tumor model that these engineered therapeutic cells show greater localization to tumors injected with a slow-release source of the small molecule drug for the Di receptor than to tumors injected with a vehicle control. Work for this project is ongoing in the lab at the time of writing of this dissertation

Chapter 4 is comprised of research performed in the lab with co-authors including co-lead authors Ping Wei and Wilson Wong. This work explored the usage of two

bacterial pathogen proteins, OspF from *Shigella*, and YopH from *Yersinia Pestis*, as reagents to precisely modulate MAPK signaling, both in yeast and in human T cells. In the latter cell type, we demonstrated the ability to modulate T cell activation. Constitutive expression of the effectors blocked activation, introducing them in a synthetic negative feedback loop limited the amplitude of activation, and inducible expression transiently paused activation. This work was published in *Nature* in 2012.

Finally, I conclude this dissertation with a summary of the work described and closing remarks on some of the challenges and opportunities ahead for this exciting field of scientific research.

References

1. J. Blundell, Experiments on the transfusion of blood by the syringe, *Medico-chirurgical transactions* **9**, 56 (1818).
2. J. Blundell, Successful case of transfusion, *Lancet* **1**, 431–432 (1829).
3. J. Blundell, Observations on Transfusion of Blood. With a Description of His Gravitator, *Lancet* **2**, 321–324 (1828).
4. S. A. Rosenberg, Raising the bar: the curative potential of human cancer immunotherapy., *Science translational medicine* **4**, 127ps8 (2012).
5. T. M. Clay *et al.*, Efficient Transfer of a Tumor Antigen-Reactive TCR to Human Peripheral Blood Lymphocytes Confers Anti-Tumor Reactivity, *J. Immunol.* **163**, 507–513 (1999).
6. Z. Eshhar, T. Waks, G. Gross, D. G. Schindler, Specific activation and targeting of cytotoxic lymphocytes through chimeric single chains consisting of antibody-binding domains and the gamma or zeta subunits of the immunoglobulin and T-cell receptors., *Proceedings of the National Academy of Sciences of the United States of America* **90**, 720–4 (1993).
7. B. Irving, A. Weiss, The cytoplasmic domain of the T cell receptor chain is sufficient to couple to receptor-associated signal transduction pathways, *Cell* **64**, 891–901 (1991).
8. C. J. Turtle, M. Hudecek, M. C. Jensen, S. R. Riddell, Engineered T cells for anti-cancer therapy., *Current opinion in immunology* **24**, 633–9 (2012).
9. K. J. Curran, H. J. Pegram, R. J. Brentjens, Chimeric antigen receptors for T cell immunotherapy: current understanding and future direction, *The Journal of Gene Medicine* (2012) (available at <http://onlinelibrary.wiley.com/doi/10.1002/jgm.2604/abstract>).
10. M. Kalos, Muscle CARs and TcRs: turbo-charged technologies for the (T cell) masses., *Cancer immunology, immunotherapy: CII* , 127–135 (2011).
11. T. S. Park, S. a Rosenberg, R. a Morgan, Treating cancer with genetically engineered T cells., *Trends in biotechnology* **29**, 550–557 (2011).
12. M. Sadelain, R. Brentjens, I. Rivière, The promise and potential pitfalls of chimeric antigen receptors., *Current opinion in immunology* **21**, 215–23 (2009).
13. B. Jena, G. Dotti, L. J. N. Cooper, Redirecting T-cell specificity by introducing a tumor-specific chimeric antigen receptor., *Blood* **116**, 1035–44 (2010).

14. H. Zhang *et al.*, 4-1BB is superior to CD28 costimulation for generating CD8+ cytotoxic lymphocytes for adoptive immunotherapy., *Journal of immunology (Baltimore, Md. : 1950)* **179**, 4910–8 (2007).
15. M. C. Milone *et al.*, Chimeric receptors containing CD137 signal transduction domains mediate enhanced survival of T cells and increased antileukemic efficacy in vivo., *Molecular therapy : the journal of the American Society of Gene Therapy* **17**, 1453–64 (2009).
16. D. L. Porter, M. Kalos, Z. Zheng, B. Levine, C. June, Chimeric Antigen Receptor Therapy for B-cell Malignancies., *Journal of Cancer* **2**, 331–2 (2011).
17. D. L. Porter, B. L. Levine, M. Kalos, A. Bagg, C. H. June, Chimeric antigen receptor-modified T cells in chronic lymphoid leukemia., *The New England journal of medicine* **365**, 725–33 (2011).
18. M. Kalos *et al.*, T Cells with Chimeric Antigen Receptors Have Potent Antitumor Effects and Can Establish Memory in Patients with Advanced Leukemia, *Science Translational Medicine* **3**, 95ra73–95ra73 (2011).
19. C. Carpenito *et al.*, Control of large, established tumor xenografts with genetically retargeted human T cells containing CD28 and CD137 domains., *Proceedings of the National Academy of Sciences of the United States of America* **106**, 3360–5 (2009).
20. P. Tiberghien *et al.*, Administration of herpes simplex-thymidine kinase-expressing donor T cells with a T-cell-depleted allogeneic marrow graft., *Blood* **97**, 63–72 (2001).
21. P. Tiberghien *et al.*, Ganciclovir treatment of herpes simplex thymidine kinase-transduced primary T lymphocytes: an approach for specific in vivo donor T-cell depletion after bone marrow transplantation?, *Blood* **84**, 1333–41 (1994).
22. F. Ciceri *et al.*, Infusion of suicide-gene-engineered donor lymphocytes after family haploidentical haemopoietic stem-cell transplantation for leukaemia (the TK007 trial): a non-randomised phase I-II study., *The lancet oncology* **10**, 489–500 (2009).
23. S. R. Riddell *et al.*, T-cell mediated rejection of gene-modified HIV-specific cytotoxic T lymphocytes in HIV-infected patients., *Nature medicine* **2**, 216–23 (1996).
24. C. Quintarelli *et al.*, Co-expression of cytokine and suicide genes to enhance the activity and safety of tumor-specific cytotoxic T lymphocytes., *Blood* **110**, 2793–802 (2007).
25. A. Di Stasi *et al.*, Inducible apoptosis as a safety switch for adoptive cell therapy., *The New England journal of medicine* **365**, 1673–83 (2011).
26. K. C. Straathof *et al.*, An inducible caspase 9 safety switch for T-cell therapy., *Blood* **105**, 4247–54 (2005).

27. M. A. Fischbach, J. A. Bluestone, W. A. Lim, Cell-based therapeutics: the next pillar of medicine., *Science translational medicine* **5**, 179ps7 (2013).
28. D. Endy, Foundations for engineering biology., *Nature* **438**, 449–53 (2005).
29. D. Auel, M. Fussenegger, Mammalian synthetic biology--from tools to therapies., *BioEssays : news and reviews in molecular, cellular and developmental biology* **32**, 332–45 (2010).
30. A. S. Khalil, J. J. Collins, Synthetic biology: applications come of age., *Nature reviews. Genetics* **11**, 367–79 (2010).
31. H. Ye, M. Daoud-El Baba, R.-W. Peng, M. Fussenegger, A synthetic optogenetic transcription device enhances blood-glucose homeostasis in mice., *Science (New York, N.Y.)* **332**, 1565–8 (2011).
32. J. Mulhbach, P. St-Pierre, D. a Lafontaine, Therapeutic applications of ribozymes and riboswitches., *Current opinion in pharmacology* **10**, 551–6 (2010).
33. S. J. Culler, K. G. Hoff, C. D. Smolke, Reprogramming cellular behavior with RNA controllers responsive to endogenous proteins., *Science (New York, N.Y.)* **330**, 1251–5 (2010).
34. C. Kemmer *et al.*, Self-sufficient control of urate homeostasis in mice by a synthetic circuit., *Nature biotechnology* **28**, 355–60 (2010).
35. M. Gitzinger, C. Kemmer, M. D. El-Baba, W. Weber, M. Fussenegger, Controlling transgene expression in subcutaneous implants using a skin lotion containing the apple metabolite phloretin., *Proceedings of the National Academy of Sciences of the United States of America* **106**, 10638–43 (2009).
36. B. R. Conklin *et al.*, Engineering GPCR signaling pathways with RASSLs, *Nature methods* **5**, 673–678 (2008).
37. B. N. Armbruster, X. Li, M. H. Pausch, S. Herlitze, B. L. Roth, Evolving the lock to fit the key to create a family of G protein-coupled receptors potently activated by an inert ligand., *Proceedings of the National Academy of Sciences of the United States of America* **104**, 5163–5168 (2007).
38. R. D. Airan, K. R. Thompson, L. E. Fenno, H. Bernstein, K. Deisseroth, Temporally precise in vivo control of intracellular signalling., *Nature* **458**, 1025–9 (2009).
39. A. Levskaya, O. D. Weiner, W. a Lim, C. a Voigt, Spatiotemporal control of cell signalling using a light-switchable protein interaction., *Nature* **461**, 997–1001 (2009).
40. J. E. Toettcher, C. A. Voigt, O. D. Weiner, W. A. Lim, The promise of optogenetics in cell biology: interrogating molecular circuits in space and time, *nature methods* **8**, 35–38 (2010).

41. J. E. Toettcher, D. Gong, W. a Lim, O. D. Weiner, Light-based feedback for controlling intracellular signaling dynamics, *Nature Methods* **8** (2011), doi:10.1038/nmeth.1700.
42. D. Greber, M. Fussenegger, Mammalian synthetic biology: engineering of sophisticated gene networks., *Journal of biotechnology* **130**, 329–45 (2007).
43. W. A. Lim, Designing customized cell signalling circuits, *Nature Reviews Molecular Cell Biology* **11**, 393–403 (2010).
44. M. C. Good, J. G. Zalatan, W. A. Lim, Scaffold proteins: hubs for controlling the flow of cellular information., *Science (New York, N.Y.)* **332**, 680–6 (2011).
45. J. Bonnet, P. Yin, M. E. Ortiz, P. Subsoontorn, D. Endy, Amplifying genetic logic gates., *Science (New York, N.Y.)* **340**, 599–603 (2013).

Chapter 2. Engineering synthetic control over mammalian cell migration to an orthogonal bio-inert small molecule

Introduction

The remarkable capability of many cell types to efficiently home and migrate to specific sites in the body is critical to their roles in developmental and normal homeostatic processes. This targeted chemotactic action is also one of the potential key advantages that cells have over traditional therapeutics such as small molecules and biologics, which diffuse widely and often have broad side effect profiles.

The ability of cells to migrate has not been effectively harnessed by most cell therapies being tested today. Most current cell therapy trials rely only on the native homing abilities of the particular cell types being used for sufficient migration to sites of disease. For example, neural stem cells and mesenchymal stem cells have been shown to naturally home to certain types of tumors and sites of inflammation in a manner that is largely dependent on cytokines being produced at these target sites (1–3). Work has also been done to specifically redirect the homing of anti-tumor T cells by forcing “matched” expression of chemotactic chemokine receptors in the T cells that correspond to chemokines produced by particular tumor model cell lines.

However, from a foundational tool engineering standpoint, it would be beneficial to have a strategy to direct cells to novel and arbitrary user-specified sites independent from natural homing signals. In this chapter, we explore a simple synthetic biology approach for controlling mammalian cellular migration toward a bio-inert small molecule drug, both *in vitro* and *in vivo*, via expression of orthogonal engineered G-protein

coupled receptors known as Receptors Activated Solely by a Synthetic Ligand (RASSLs, a.k.a. Designer Receptors Exclusively Activated by a Designer Drug - DREADDs). The receptors are activated only by a small drug molecule that does not bind to native receptors. Conversely these receptors are not activated by natural ligands.

We are able to show that:

- The expression of particular G α i-coupled RASSLs is sufficient to cause HL-60 neutrophil cells to efficiently chemotax towards the target drug, clozapine-N-oxide (CNO).
- This orthogonal receptor is “portable” to a range of interesting cell types used in cell therapy (neutrophils, T cells, keratinocytes, endothelial cells) – expression of the receptor is sufficient to direct chemotaxis to CNO of each of these cell types.
- Neutrophils and T cells expressing this orthogonal receptor will migrate through an endothelial monolayer in response to a gradient of CNO *in vitro*, suggesting that they can overcome the challenge of extravasation to exit the vasculature and enter target tissues.
- In a proof of principle *in vivo* study, T cells expressing the orthogonal receptor were shown to localize specifically to a subcutaneously implanted depot of CNO-emitting microspheres after being injected intravenously.

Overall, we establish a new strategy for retargeting the localization of engineered therapeutic cells, and suggest that the development of more orthogonal receptors of this type could be a great boon to the development of next generation cell-based therapeutics.

This work is currently being prepared as a manuscript for submission for publication.

References

1. J. M. Karp, G. S. Leng Teo, Mesenchymal stem cell homing: the devil is in the details., *Cell stem cell* **4**, 206–16 (2009).
2. J. Imitola *et al.*, Directed migration of neural stem cells to sites of CNS injury by the stromal cell-derived factor 1alpha/CXC chemokine receptor 4 pathway., *Proceedings of the National Academy of Sciences of the United States of America* **101**, 18117–22 (2004).
3. M. R. Reagan, D. L. Kaplan, Concise review: Mesenchymal stem cell tumor-homing: detection methods in disease model systems., *Stem cells (Dayton, Ohio)* **29**, 920–7 (2011).

Engineering synthetic control over mammalian cell migration to an orthogonal bio-inert small molecule

Jason S. Park^{1,2,3}, Benjamin Rhau^{1,2}, Aynur Tasdemir^{1,2}, Krista McNally^{1,2},
Carmen Zhou^{1,2}, Orion D. Weiner^{2,4}, Bruce R. Conklin^{1,2,3,4,5}, James Onuffer^{1,2},
Wendell A. Lim^{1,2,6‡}

¹Department of Cellular & Molecular Pharmacology, University of California San Francisco, San Francisco, CA 94158

²The Cell Propulsion Lab, an NIH Nanomedicine Development Center

³Gladstone Institute of Cardiovascular Disease, University of California, San Francisco San Francisco, CA 94158, USA

⁴Cardiovascular Research Institute and Department of Biochemistry, University of California San Francisco, San Francisco, CA 94143, USA

⁵Department of Medicine, University of California San Francisco

⁶Howard Hughes Medical Institute

‡To whom correspondence should be addressed: lim@cmp.ucsf.edu

Cells are increasingly being explored as therapeutic agents for a growing array of diseases¹⁻¹⁰. A significant potential advantage of cells over traditional therapeutics such as small molecules and biologics lies in their ability to specifically and actively migrate to target sites, thereby concentrating their activities to maximize efficacy while limiting off-target effects elsewhere in the body. However, in many settings, suboptimal cell homing remains a significant impediment to effective treatment¹¹⁻¹⁹. Here we describe a simple but powerful approach: genetic modification of cells with an engineered G-protein coupled receptor such that their migration is controlled by a bioinert drug-like small molecule, clozapine-N-oxide (CNO)²⁰. The engineered receptor and small molecule ligand form an orthogonal pair - the receptor does not respond to native ligands, and the inert drug does not bind to native cells²⁰⁻²². CNO responsive migration can be engineered into a variety of cell types currently being used in cellular therapy, including neutrophils, T lymphocytes, keratinocytes, and endothelial cells. The engineered cells migrate up a gradient of the drug CNO, and transmigrate through endothelial monolayers. For one clinically useful cell type - T lymphocytes - we show that the modified cells can specifically migrate *in vivo* to CNO-releasing beads implanted in a live mouse. This work represents a step forward in the development of generalizable genetic tools for user-defined orthogonal control over cell migration in future therapeutic applications.

(229 words)

In order to be effective in treating disease, cellular therapeutics must efficiently and specifically home to the desired site of action in significant numbers. Cells that are

currently used in clinical trials, including immune cells and stem cells, largely rely on the natural "tropism" of particular cell types for certain tissues (e.g. hematopoietic stem cell homing to the bone marrow niche²³) or for disease-associated signals (e.g. mesenchymal and neural stem cell homing to inflammation^{16-18,24} or monocytes into tumors^{25,26}). The ability to redirect the migration of therapeutic cells to any user-specified location in the body would be a powerful enabling technology for future applications, but there are currently few easily generalizable strategies to accomplish this goal. We conceived of an approach to direct cellular homing to small molecules by expressing, in motile cells, engineered G-protein coupled receptors (GPCRs) called Receptors Activated Solely by a Synthetic Ligand (RASSLs)^{20,27}.

RASSLs are engineered to be unresponsive to endogenous ligands but can be activated by pharmacologically inert orthogonal small molecules (**Fig. 1A**). Versions of these receptors exist for the three major GPCR signaling pathways (Gas-, Gai-, and Gαq-coupled receptors) and the design of a new arrestin-biased variant has recently been reported^{27,28}. Because GPCRs control many important physiological functions including cell migration, we hypothesized that by expressing these engineered receptors in motile cells we could develop a general strategy for establishing user control over cell homing (**Fig. 1B**). Here we use a family of second generation RASSLs known as Designer Receptors Exclusively Activated by a Designer Drug (DREADDs) that are only activated by the small molecule clozapine-N-oxide (CNO), an inert metabolite of the FDA approved anti-psychotic drug clozapine²⁰. CNO is highly bioavailable in rodents and humans, lacks affinity for any known receptors, channels, and transporters, and does not cause any appreciable physiological effects when systemically administered in normal mice²⁰⁻²².

To rapidly test if this family of engineered orthogonal receptors could be used to control cell morphology and motility, we first transiently expressed several variants of these receptors (Dq, Di3, and Di) along with green fluorescent protein (GFP) in HL-60 neutrophils. Transfection efficiencies were routinely 40-45% as measured by co-electroporation with GFP and determination of % GFP-positive cells via flow cytometry (data not shown). We tested these engineered cells in a high-throughput impedance-based adhesion / spreading assay in which cells are plated on a fibronectin-coated electrode array and exposed to putative chemoattractants (**Fig. 1C**). Cells that morphologically respond to the chemoattractant adhere tightly to the surface and spread out, and this cytoskeletal change is measured as an increase in electrical impedance in real-time. We found that cells expressing the Gai-coupled receptors Di3 and Di responded to the drug CNO whereas cells expressing the Gaq-coupled receptor Dq did not. This result was consistent with the known fact that many natural Gai-coupled receptors are associated with chemotaxis²⁹. None of the cells responded to vehicle treatment, and all of the cells responded to the positive control chemoattractant formyl-Met-Leu-Phe (fMLP), which strongly attracts neutrophils (**Fig. 1C and Supplementary Fig. 1**).

We tested whether HL-60 neutrophils expressing the same three engineered receptors would migrate directionally through a porous membrane in response to a gradient of the drug CNO in a Boyden chamber transwell migration assay (**Fig. 1D**). The number of migrating cells was quantitated by flow cytometry using a fluorescent bead counting standard. Consistent with the results of the cell-spreading assay, cells expressing the Gai-coupled receptors Di3 and Di migrated in response to a gradient of CNO whereas cells expressing the Gaq-coupled receptor Dq did not. All of the cells also

migrated in response to a gradient of the positive control chemoattractant, formyl-Met-Leu-Phe (fMLP) (**Fig. 1D**).

Next we used a micropipet migration assay with time-lapse microscopy to visualize the dynamic process of migration. This assay allows for visualization of individual cell behavior and provides: 1) a very steep concentration gradient and 2) the ability to rapidly move the source of the gradient (**Fig. 2A**). Transiently transfected HL-60 neutrophils expressing Di and GFP (as a co-electroporation control) migrated robustly and directionally to the micropipet point-source of CNO, whereas cells transfected with an irrelevant plasmid control exhibited random migration (**Fig 2A and Supplementary Videos 1A and 1B**). Further, cells migrating to CNO were able to re-orient to a changing gradient of the drug as can be appreciated when the micropipet is moved in **Supplementary Videos 1B**.

To facilitate further quantitation of migration metrics of engineered HL-60 neutrophil chemotaxis *in vitro*, we used a microfluidic gradient generator developed and optimized in collaboration with CellASIC Corp. We generated HL-60 cell lines stably expressing the Di receptor with a YFP fluorescent protein fusion in order to improve homogeneity of receptor expression in the cell pool. Cells loaded into the device were allowed to adhere to the fibronectin-coated glass surface, and unbound cells were washed away as can be seen at the beginning of **Supplementary Video 2**. A diffusive CNO gradient was applied (visualized by a fluorescent red tracer dye), and cells were tracked by time lapse microscopy. Image analysis was performed, and cell tracks were generated with initial cell positions plotted at the origin (**Fig. 2B**). Di receptor-expressing cells migrated directionally in response to the CNO gradient as compared to vehicle control, as determined by comparing the track velocity, displacement rate, and directionality metrics between the two treatment conditions (**Fig. 2B**).

Having established that the Di receptor is a potent mediator of CNO-chemotaxis in HL-60 neutrophils, we asked whether this engineered chemotaxis receptor is "portable" to other cell types. We therefore generated a lentiviral vector to efficiently express an mCherry fluorescent protein-tagged Di receptor construct in a variety of cell types. Stable Di receptor-expressing cell lines were then established from HL-60 cells, primary human T lymphocytes, primary neonatal human epidermal keratinocytes, and primary human umbilical vein endothelial cells (HUVECs) (**Fig. 3A**). We tested each of these cell types in Boyden chamber transwell migration assays. In each case, Di receptor-expressing cells migrated toward a gradient of CNO. Control cells not expressing the Di receptor did not migrate to CNO (**Fig. 3B**).

Cellular migration in the body is complicated by mammalian anatomy. Most cellular therapies are delivered intravenously such that therapeutic cells must exit blood vessels through the process of diapedesis, or transendothelial migration, in order to reach their target tissues (**Fig. 3C**). Therefore in our next experiment, we tested whether motile cells expressing the Di receptor could migrate through an endothelial monolayer *in vitro* in response to a gradient of CNO. We grew a tight monolayer of HUVECs on a fibronectin-coated porous transwell membrane for four days. Monolayer integrity was assessed by an observed increase in transendothelial electrical resistance from a baseline of $< 7 \Omega$ to $> 60 \Omega$ and barrier function in a FITC-dextran permeability assay (**Supplemental Fig. 2**). We then proceeded with a transwell migration assay using HL-60 neutrophils and primary human T lymphocytes as the motile cell types. Both engineered HL-60 neutrophils and primary human T lymphocytes exhibited a directed transendothelial migration response to CNO as well as to a positive control chemoattractant (fMLP for HL-60 neutrophils and SDF-1a for T lymphocytes) (**Fig. 3D**).

Finally, we tested whether our approach of redirecting cellular homing using a small molecule drug could be feasible for use *in vivo*. Adoptive transfer of T lymphocytes is commonly used in human clinical trials and in preclinical models. Thus, we tested whether the homing of engineered T lymphocytes could be redirected to the orthogonal CNO signal in a mouse. Mouse T lymphocytes were retrovirally transduced with a bicistronic construct encoding both an mCherry-tagged Di receptor and an enhanced firefly luciferase to allow tracking of modified cells³⁰. Biodegradable CNO-loaded poly-lactide-co-glycolide (PLGA) microspheres were formulated using standard techniques to generate a slow-release source of CNO in the body (**Supplementary Fig. 3**). The encapsulated drug concentration was determined to be 4.1 ug/mg (encapsulation efficiency of 19.6%). Vehicle control microspheres were generated in parallel by omission of CNO in the protocol. CNO-loaded and vehicle control microspheres were injected subcutaneously (suspension in PBS) into opposing flanks of albino B6 mice. Di receptor- and luciferase-transduced T lymphocytes were injected intravenously via lateral tail vein.

In this experiment, we observed that the Di receptor-expressing T lymphocytes preferentially localized to sites of injection of CNO-loaded beads versus vehicle control beads injected on the contralateral flanks (**Fig. 4A**). This preferential localization was also observed in mice where the injected flanks were switched (CNO-left and vehicle-right versus CNO-right and vehicle-left flank) (data points combined and analyzed together in **Fig. 4B**). The luminescence of the T cells localized at each site was quantitated at six hours, four days, and seven days after T cell injection (**Fig. 4B and Fig. 4C**).

The approach we describe for engineering synthetic control over cell migration is both complementary to and conceptually distinct from past strategies reported in the

literature for directing migration. Some interesting previously described approaches include chemical or enzymatic modification of the cell surface with specific adhesion molecules^{31,32}, materials engineering of artificial scaffolds and tunable matrices to direct cell adhesion and migration³³, expression or direct injection of natural homing ligands such as chemokines into sites where increased cell migration is desired^{34,35}, and the expression in therapeutic cells of natural receptors such as chemokine receptors whose ligands are upregulated in inflammation or cancer^{11-13,36}. Challenges faced by approaches that use naturally existing homing receptors or ligands to direct cell migration include the observations that many ligands are present in multiple locations throughout the body, the expression of these ligands may vary in time throughout the natural course of disease or in response to therapy, many ligands (such as chemokines) interact with multiple receptors and vice versa, and native receptors for natural ligands can sometimes be found not only on therapeutic cell types but also on cell types that are detrimental for therapy^{19,34,37-41}. Another intriguing strategy is the use of optogenetics for controlling cell motility (such as through photoactivated control of Rac)⁴²⁻⁴⁴. Tools for guiding cellular migration with light are invaluable in basic research and may have potential for use in future clinical applications, but the requirement for consistent *in vivo* delivery of light remains an obstacle for broader use in therapeutic contexts. Thus the use of an orthogonal receptor-drug pair provides many potential benefits for the strategy demonstrated in this work. The drug has a low toxicity profile, which decreases concerns of side effects in therapeutic settings. The homing receptor for the drug is expressed uniquely on the cell type of one's choosing (and not on native cells). The user can better control when, where, and how much drug is present at a given site, and the drug cannot naturally be produced at off-target sites. Cellular homing can be directed not only to sites of disease where there are known chemotactic ligands or migration signals, but to any site where a drug can be delivered.

While we have presented a proof-of-principle demonstration that mammalian cell migration and homing can be directed *in vitro* and *in vivo* using an orthogonal small molecule / receptor pair, further work remains to optimize this technology. For example, the small molecule drug could be modified through synthetic chemistry to optimize its properties as a gradient-generating homing molecule. Alternative delivery formulations of the drug (such as smart liposomes with antibody-based targeting and triggered release characteristics⁴⁵) could be used for delivery to sites of disease in a targeted manner. In the longer term, it may be possible to develop genetically encodable orthogonal receptor/ligand pairs to allow for biological expression of the homing signal by cells. Protein engineering of the receptor could also be used to develop variants with altered drug affinity, recycling properties, or signaling capabilities.

A paradigm of orthogonal, synthetic control over cell migration could be generally useful in therapeutic applications. By allowing physicians to better direct powerful cellular therapeutic activities such as cell killing, repair / regeneration, sensing disease^{46,47}, and delivering therapeutic molecules⁴⁸⁻⁵¹, we envision that this technology could broaden the range of uses for cells in medicine.

Current word count excluding intro paragraph, online methods, etc: 1994 words (2000 limit)

Full Methods and any associated references are available in the online version of the paper at www.nature.com/nature.

Works cited

1. Tang, Q., Bluestone, J. A. & Kang, S.-M. CD4(+)Foxp3(+) regulatory T cell therapy in transplantation. *Journal of molecular cell biology* **4**, 11–21 (2012).
2. Burrell, B. E., Nakayama, Y., Xu, J., Brinkman, C. C. & Bromberg, J. S. Regulatory T cell induction, migration, and function in transplantation. *Journal of immunology (Baltimore, Md. : 1950)* **189**, 4705–11 (2012).
3. Restifo, N. P., Dudley, M. E. & Rosenberg, S. A. Adoptive immunotherapy for cancer: harnessing the T cell response. *Nature reviews. Immunology* **12**, 269–81 (2012).
4. Riddell, S. R. *et al.* Restoration of viral immunity in immunodeficient humans by the adoptive transfer of T cell clones. *Science (New York, N.Y.)* **257**, 238–41 (1992).
5. Heslop, H. E. *et al.* Long-term restoration of immunity against Epstein–Barr virus infection by adoptive transfer of gene–modified virus–specific T lymphocytes. *Nature Medicine* **2**, 551–555 (1996).
6. Kavanagh, D. P. J. & Kalia, N. Hematopoietic stem cell homing to injured tissues. *Stem cell reviews* **7**, 672–82 (2011).
7. Branski, L. K., Gauglitz, G. G., Herndon, D. N. & Jeschke, M. G. A review of gene and stem cell therapy in cutaneous wound healing. *Burns : journal of the International Society for Burn Injuries* **35**, 171–80 (2009).
8. Lu, P. *et al.* Long-distance growth and connectivity of neural stem cells after severe spinal cord injury. *Cell* **150**, 1264–73 (2012).
9. Bliss, T., Guzman, R., Daadi, M. & Steinberg, G. K. Cell transplantation therapy for stroke. *Stroke; a journal of cerebral circulation* **38**, 817–26 (2007).
10. Chang, Y.-C., Shyu, W.-C., Lin, S.-Z. & Li, H. Regenerative therapy for stroke. *Cell transplantation* **16**, 171 (2007).
11. Craddock, J. A. *et al.* Enhanced tumor trafficking of GD2 chimeric antigen receptor T cells by expression of the chemokine receptor CCR2b. *Journal of immunotherapy (Hagerstown, Md. : 1997)* **33**, 780–8 (2010).
12. Di Stasi, A. *et al.* T lymphocytes coexpressing CCR4 and a chimeric antigen receptor targeting CD30 have improved homing and antitumor activity in a Hodgkin tumor model. *Blood* **113**, 6392–402 (2009).
13. Moon, E. K. *et al.* Expression of a functional CCR2 receptor enhances tumor localization and tumor eradication by retargeted human T cells expressing a mesothelin-specific chimeric antibody receptor. *Clinical cancer research : an*

official journal of the American Association for Cancer Research **17**, 4719–30 (2011).

14. Pockaj, B. A. *et al.* Localization of ¹¹¹indium-labeled tumor infiltrating lymphocytes to tumor in patients receiving adoptive immunotherapy. Augmentation with cyclophosphamide and correlation with response. *Cancer* **73**, 1731–7 (1994).
15. Fisher, B. *et al.* Tumor localization of adoptively transferred indium-111 labeled tumor infiltrating lymphocytes in patients with metastatic melanoma. *Journal of clinical oncology : official journal of the American Society of Clinical Oncology* **7**, 250–61 (1989).
16. Karp, J. M. & Leng Teo, G. S. Mesenchymal stem cell homing: the devil is in the details. *Cell stem cell* **4**, 206–16 (2009).
17. Ankrum, J. & Karp, J. M. Mesenchymal stem cell therapy: Two steps forward, one step back. *Trends in molecular medicine* **16**, 203–9 (2010).
18. Wagner, J., Kean, T., Young, R., Dennis, J. E. & Caplan, A. I. Optimizing mesenchymal stem cell-based therapeutics. *Current opinion in biotechnology* **20**, 531–6 (2009).
19. Penn, M. S. *et al.* An Open Label Dose Escalation Study to Evaluate the Safety of Administration of Non-Viral SDF-1 Plasmid to Treat Symptomatic Ischemic Heart Failure. *Circulation research* **112**, 816–825 (2013).
20. Armbruster, B. N., Li, X., Pausch, M. H., Herlitz, S. & Roth, B. L. Evolving the lock to fit the key to create a family of G protein-coupled receptors potently activated by an inert ligand. *Proceedings of the National Academy of Sciences of the United States of America* **104**, 5163–8 (2007).
21. Bender, D., Holschbach, M. & Stöcklin, G. Synthesis of n.c.a. carbon-11 labelled clozapine and its major metabolite clozapine-N-oxide and comparison of their biodistribution in mice. *Nuclear Medicine and Biology* **21**, 921–925 (1994).
22. Ray, R. S. *et al.* Impaired respiratory and body temperature control upon acute serotonergic neuron inhibition. *Science (New York, N.Y.)* **333**, 637–42 (2011).
23. Peled, A. Dependence of Human Stem Cell Engraftment and Repopulation of NOD/SCID Mice on CXCR4. *Science* **283**, 845–848 (1999).
24. Imitola, J. *et al.* Directed migration of neural stem cells to sites of CNS injury by the stromal cell-derived factor 1 α /CXC chemokine receptor 4 pathway. *Proceedings of the National Academy of Sciences of the United States of America* **101**, 18117–22 (2004).

25. De Palma, M., Murdoch, C., Venneri, M. A., Naldini, L. & Lewis, C. E. Tie2-expressing monocytes: regulation of tumor angiogenesis and therapeutic implications. *Trends in immunology* **28**, 519–24 (2007).
26. Lewis, C. E. & Pollard, J. W. Distinct role of macrophages in different tumor microenvironments. *Cancer research* **66**, 605–12 (2006).
27. Conklin, B. R. *et al.* Engineering GPCR signaling pathways with RASSLs. *Nature methods* **5**, 673–678 (2008).
28. Nakajima, K. & Wess, J. Design and functional characterization of a novel, arrestin-biased designer G protein-coupled receptor. *Molecular pharmacology* **82**, 575–82 (2012).
29. Neptune, E. R. Receptors induce chemotaxis by releasing the beta gamma subunit of Gi, not by activating Gq or Gs. *Proceedings of the National Academy of Sciences* **94**, 14489–14494 (1997).
30. Rabinovich, B. A. *et al.* Visualizing fewer than 10 mouse T cells with an enhanced firefly luciferase in immunocompetent mouse models of cancer. *Proceedings of the National Academy of Sciences of the United States of America* **105**, 14342–6 (2008).
31. Sarkar, D. *et al.* Engineered cell homing. *Blood* **118**, e184–91 (2011).
32. Sackstein, R. *et al.* Ex vivo glycan engineering of CD44 programs human multipotent mesenchymal stromal cell trafficking to bone. *Nature Medicine* **14**, 181 (2008).
33. Lutolf, M. P. & Hubbell, J. A. Synthetic biomaterials as instructive extracellular microenvironments for morphogenesis in tissue engineering. *Nature biotechnology* **23**, 47–55 (2005).
34. Homey, B., Müller, A. & Zlotnik, A. Chemokines: agents for the immunotherapy of cancer? *Nature reviews. Immunology* **2**, 175–84 (2002).
35. Chada, S., Ramesh, R. & Mhashilkar, A. M. Cytokine- and chemokine-based gene therapy for cancer. *Current opinion in molecular therapeutics* **5**, 463–74 (2003).
36. Kershaw, M. H. *et al.* Redirecting migration of T cells to chemokine secreted from tumors by genetic modification with CXCR2. *Human gene therapy* **13**, 1971–80 (2002).
37. Tan, M. C. B. *et al.* Disruption of CCR5-dependent homing of regulatory T cells inhibits tumor growth in a murine model of pancreatic cancer. *Journal of immunology (Baltimore, Md. : 1950)* **182**, 1746–55 (2009).
38. Abastado, J.-P. The next challenge in cancer immunotherapy: controlling T-cell traffic to the tumor. *Cancer research* **72**, 2159–61 (2012).

39. Hong, M. *et al.* Chemotherapy induces intratumoral expression of chemokines in cutaneous melanoma, favoring T-cell infiltration and tumor control. *Cancer research* **71**, 6997–7009 (2011).
40. Piccio, L. *et al.* Changes in B- and T-lymphocyte and chemokine levels with rituximab treatment in multiple sclerosis. *Archives of neurology* **67**, 707–14 (2010).
41. Torikai, E., Kageyama, Y., Suzuki, M., Ichikawa, T. & Nagano, A. The effect of infliximab on chemokines in patients with rheumatoid arthritis. *Clinical rheumatology* **26**, 1088–93 (2007).
42. Wu, Y. I. *et al.* A genetically encoded photoactivatable Rac controls the motility of living cells. *Nature* **461**, 104–8 (2009).
43. Yoo, S. K. *et al.* Differential regulation of protrusion and polarity by PI3K during neutrophil motility in live zebrafish. *Developmental cell* **18**, 226–36 (2010).
44. Levskaya, A., Weiner, O. D., Lim, W. a & Voigt, C. a Spatiotemporal control of cell signalling using a light-switchable protein interaction. *Nature* **461**, 997–1001 (2009).
45. Allen, T. M. & Cullis, P. R. Liposomal drug delivery systems: From concept to clinical applications. *Advanced drug delivery reviews* **65**, 36–48 (2013).
46. Folcher, M. & Fussenegger, M. Synthetic biology advancing clinical applications. *Current opinion in chemical biology* **16**, 345–54 (2012).
47. Khalil, A. S. & Collins, J. J. Synthetic biology: applications come of age. *Nature reviews. Genetics* **11**, 367–79 (2010).
48. Ruoslahti, E., Bhatia, S. N. & Sailor, M. J. Targeting of drugs and nanoparticles to tumors. *The Journal of cell biology* **188**, 759–68 (2010).
49. Stephan, M. T. & Irvine, D. J. Enhancing Cell therapies from the Outside In: Cell Surface Engineering Using Synthetic Nanomaterials. *Nano today* **6**, 309–325 (2011).
50. Stephan, M. T., Moon, J. J., Um, S. H., Bershteyn, A. & Irvine, D. J. Therapeutic cell engineering with surface-conjugated synthetic nanoparticles. *Nature medicine* **16**, 1035–41 (2010).
51. Yoo, J.-W., Irvine, D. J., Discher, D. E. & Mitragotri, S. Bio-inspired, bioengineered and biomimetic drug delivery carriers. *Nature reviews. Drug discovery* **10**, 521–35 (2011).
52. Peisajovich, S. G., Garbarino, J. E., Wei, P. & Lim, W. A. Rapid diversification of cell signaling phenotypes by modular domain recombination. *Science (New York, N.Y.)* **328**, 368–72 (2010).

53. Millius, A., Dandekar, S. N., Houk, A. R. & Weiner, O. D. Neutrophils establish rapid and robust WAVE complex polarity in an actin-dependent fashion. *Current biology : CB* **19**, 253–9 (2009).
54. Astete, C. E. & Sabliov, C. M. Synthesis and characterization of PLGA nanoparticles. *Journal of biomaterials science. Polymer edition* **17**, 247–89 (2006).

Acknowledgements

We thank the Conklin lab, the Weiner lab, and the Lim lab for helpful discussions and Jason Cyster, Henry Bourne, and Arthur Weiss for critical reading of the manuscript. We acknowledge the UCSF Preclinical Therapeutics Core Facility, especially Byron Hann, Don Hom, Donghui Wang, and Paul Phojanakong for mouse experimental support and helpful discussions. We also acknowledge the 2009 UCSF iGEM team (especially Katja Kolar, Ryan Liang, Cathy Liu, Hansi Liu, Jackie Tam, and Eric Wong) for their work on HL-60 neutrophil chemotaxis experiments and molecular cloning. This work was supported by NIH grant R01 HL60664-07 (to BRC), pilot study funds from the Gladstone Institutes, NIH Nanomedicine Development Center grant PN2EY016546 (The Cell Propulsion Laboratory: Center for Synthetic Signaling and Motility Systems Engineering) (W.A.L.), NIH grant RO1 GM084040 (to ODW), a California Institute for Regenerative Medicine fellowship (Grant Number TG2-01153) (J.S.P.), and the Howard Hughes Medical Institute (W.A.L.).

Author Contributions

B.R., A.T., B.R.C., O.D.W., and W.A.L. initiated the project in HL-60 cells. J.S.P., B.R., J.O., and W.A.L. initiated the project in T lymphocytes. J.S.P., C.Z., K.M., and W.A.L. initiated the project in keratinocytes and endothelial cells. J.S.P., B.R., B.R.C., J.O., and W.A.L. initiated the project in mice. J.S.P. and W.A.L. wrote the manuscript. J.S.P., B.R., A.T., K.M., and C.Z. performed experiments.

Author Information

Reprints and permissions information is available at www.nature.com/reprints. The authors declare no competing financial interests. Readers are welcome to comment on the online version of this article at www.nature.com/nature. Correspondence and requests for materials should be addressed to W.A.L. (lim@cmp.ucsf.edu).

Figure Legends

Figure 1. Engineered Gai-coupled GPCRs Di3 and Di mediate cytoskeletal

changes and chemotaxis of HL-60 neutrophils in response to CNO. a, RASSLs are engineered GPCRs that interact orthogonally with a bio-inert small molecule drug.

Natural ligands do not interact with the engineered receptors, and the bio-inert drug that activates the engineered receptors does not interact with native receptors. **b,** We tested whether certain second generation RASSLs known as DREADDs could mediate cell motility. **c,** Changes in electrical impedance as a result from cell spreading in response

to drug or ligand are detected by an electrode array. Expression of Di3 or Di causes HL-60 neutrophils to respond to CNO. All cells respond to the positive control

chemoattractant fMLP. Mean +/- SEM for n=3 replicates is shown. **d,** Cell migration

through a porous transwell membrane is measured in a Boyden chamber assay. HL-60 neutrophils transiently expressing Di3 or Di migrate in response to a CNO gradient. Cells in all conditions migrated in response to a gradient of fMLP (positive control). Mean +/- SEM for n=3 replicates is shown.

Figure 2. Microscopic analysis of HL-60 neutrophil polarization and cell migration

in response to CNO. a, HL-60 neutrophils co-electroporated with Di and GFP migrate up a steep, micropipet-generated gradient of CNO. Fluorescent dye Alexa 594 tracer is mixed with CNO solution in micropipet to visualize the diffusive gradient. Micropipet gradient source is marked by magenta asterisk. Track start locations are marked by black squares and red triangles mark cell location and direction in each frame. Traces (black and grey) connect track start locations (black squares) and cell location (red triangles). See **Supplementary Videos 1a and 1b** for full videos. **b,** Quantitation of

migration metrics of stably Di-expressing HL-60 neutrophils in a microfluidic chemotaxis assay device. Cells migrate toward the CNO gradient (trajectories plotted with cell start

locations at origin) and show increased track velocity, displacement rate, and directionality as compared to basal motility in the presence of vehicle control. Mean +/- SEM is shown for n=61 cells tracked (**, $p < 0.0001$ by Student's t-test).

See **Supplementary Video 2** for full video.

Figure 3. The engineered chemotaxis receptor Di is "portable" to a range of cell

types. **a**, Gene construct with N-terminal signal sequence followed by mCherry fluorescent protein fused to Di was inserted into a lentiviral plasmid backbone for viral expression in various cell types. **b**, Transwell experiments demonstrate that HL-60 neutrophils, primary human T lymphocytes, primary human epidermal keratinocytes, and primary human umbilical vein endothelial cells expressing Di migrate through a porous membrane in response to a CNO gradient. Mean +/- SEM is shown for three repeats (***, $p < 1e-4$, **, $p = 0.001$, *, $p = 0.02$ by Student's t-test). **c**, Transendothelial migration is a critical step in the overall process of cellular homing that also includes adhesion to endothelium and chemotaxis. **d**, HL-60 neutrophils and primary human T lymphocytes transmigrate through a tight endothelial monolayer grown on a porous fibronectin-coated transwell membrane in response to both a CNO gradient as well as a positive control chemoattractant (fMLP and SDF-1a, respectively). Mean +/- SEM for n=3 (HL-60) or n=4 (T cells) replicates is shown (**, $p < 1e-4$, *, $p = 0.02$ by Student's t-test).

Figure 4. Intravenously administered primary T lymphocytes expressing Di specifically localize to a subcutaneously implanted depot of CNO slow-release biodegradable microspheres.

a, Systemically administered (intravenous) mouse T lymphocytes expressing Di specifically localize to CNO-releasing biodegradable PLGA microspheres implanted subcutaneously in a mouse. T lymphocytes express a bicistronic construct coding for Di and firefly luciferase to enable *in vivo* bioluminescent imaging of modified cells. Location of spleen is denoted by the letter "s". **b**, Quantitative

analysis of bioluminescent imaging. Specific localization of T lymphocytes persists for at least 7 days. Quantitation shown for four and seven days post-injection of T lymphocytes and for two different doses of implanted microspheres (analyzed for statistical significance separately). Microsphere injection doses were 2mg (triangles) and 6mg (squares). Mean shown for n=6 mice for each microsphere dose (dashed line for 2mg dose, solid line for 6mg dose) (*, p=0.013 for Day 4 - 2mg, p=0.022 for Day 4 - 6mg, p=0.017 for Day 7 - 2mg, p<0.001 for Day 7 - 6mg by Student's t-test). **c**, Fold-differences in T lymphocyte luminescent signal in CNO microsphere-injected flanks (black circles) versus vehicle microsphere-injected flanks (grey circles) at six hours, four days, and seven days after T lymphocyte injection. Mean +/- SEM shown for n=6 mice (*, p<0.01 by Student's t-test).

Supplementary Figure 1. CNO induces adhesion / spreading in engineered Gai-coupled GPCR-expressing HL-60 neutrophils, as determined using a real-time impedance-based assay. Changes in electrical impedance as a result from cell spreading in response to drug or ligand are detected real-time by an electrode array. Expression of Di3 or Di causes HL-60 neutrophils to respond to CNO. All cells respond to the positive control chemoattractant fMLP. Mean +/- SEM for n=3 replicates is shown. Peak responses in this figure correspond to the bar graph in Figure 1C.

Supplementary Figure 2. Integrity of tight endothelial cell monolayers grown on porous inserts is demonstrated by blockage of FITC-dextran diffusion in a permeability assay. Human umbilical vein endothelial cells were seeded on fibronectin-coated porous transwell inserts to generate a tight monolayer, and monolayer integrity was assessed in a standard FITC-dextran permeability assay. Fluorescent dye diffusing through the porous inserts with or without endothelial cell monolayers was quantitated at 30 minute timepoints. Mean +/- SEM for n=4 replicates is shown.

Supplementary Figure 3. Fabricated PLGA microspheres show typical morphology and size distribution suitable for subcutaneous injection. Biodegradable PLGA microspheres loaded with CNO were generated using a standard oil-in-water emulsion method and visualized by standard bright field light microscopy.

Supplementary Videos 1A and 1B. Direct visualization of engineered HL-60 neutrophil migration up a steep CNO gradient in a micropipet assay. a-b, Cells visualized by differential interference contrast and fluorescence microscopy. CNO gradient shown in red, Alexa594 dye tracer mixed into CNO solution. These videos correspond to the still frames shown in **Figure 2A**. **a**, HL-60 neutrophils transfected with vector control do not respond to CNO gradient. **b**, HL-60 neutrophils transfected with Di and GFP migrate up CNO gradient.

Supplementary Video 2. Direct visualization of engineered HL-60 neutrophil migration up a precisely generated CNO gradient in a microfluidic chemotaxis assay device. Stable YFP and Di-expressing HL-60 neutrophils visualized by fluorescence microscopy (cells shown in green) migrate in a microfluidic chemotaxis assay device. Non-adherent cells are washed away at the beginning of the video. The CNO gradient is visualized by the presence of a red fluorescent Alexa594 dye tracer mixed into the chemoattractant solution. This video corresponds to the still frame images, tracks, and quantitation in **Figure 2B**.

Methods (for online) – (limit 1500 words) (*currently: 1,827 words*)

Gene constructs

The DREADD constructs hM3Dq, hM3(M2i3)Di, and hM4Di were a generous gift from Dr. Bryan Roth (University of North Carolina at Chapel Hill)²⁰. We refer to these constructs as Dq, Di3, and Di, respectively, in this manuscript. More information about these constructs can be found on Dr. Roth's online DREADD wiki resource at <http://pdsplit3.mml.unc.edu/projects/dreadd/wiki/WikiStart>. The enhanced firefly luciferase gene (effLuc) was a generous gift from Dr. Brian Rabinovich (M.D. Anderson Cancer Center)³⁰. Signal sequence - mCherry fusions to the DREADD genes were generated using PCR and a combinatorial cloning strategy based on the Type II restriction enzyme AarI developed by Peisajovich et al. and ligated into compatible pcDNA3.1(+), pHR'SIN:CSW lentiviral, and pMSCV retroviral plasmid backbones⁵². Similarly, an mCherry-Di fusion, an IRES2 element, and effLuc genes were inserted into the pMSCV retroviral plasmid backbone using the combinatorial cloning strategy.

Cell culture

HL-60 cells were cultured in suspension in RPMI-1640 + 10% FBS at a density of 0.15e6 - 1.5e6 cells/mL. For migration experiments, cells were differentiated into neutrophil-like cells by seeding at 0.15e6 cells/mL and treating with 1.3% DMSO (Sigma) for 5-6 days.

Human peripheral blood mononuclear cells were collected from normal donors and acquired as cell suspensions from flushed TRIMA leukoreduction chambers (Blood Centers of the Pacific, San Francisco, CA). Primary CD4+ T lymphocytes were purified by negative selection and Ficoll-Paque PLUS density medium separation (RosetteSep,

Stem Cell Technologies). Purified cells were cryopreserved and placed in liquid nitrogen storage. Cells were grown in the following growth medium: X-VIVO 15 (Lonza) + 5% human AB serum + 10mM N-acetylcysteine + 1X beta-mercaptoethanol + 1X Primocin supplemented every two days with 30 U/mL IL-2.

Mouse CD8⁺ T lymphocytes were isolated using negative magnetic selection beads (Stem Cell Technologies) from spleens harvested from C57BL/6J mice. Cells were grown in the following growth medium: X-VIVO 15 (Lonza) + 5% FBS + 10mM N-acetylcysteine + 1X beta-mercaptoethanol + 1X Primocin supplemented every two days with 30 U/mL human IL-2.

Neonatal human epidermal keratinocytes (Invitrogen) were cultured in EpiLife medium + HKGS supplement according to vendor recommendations.

Human umbilical vein endothelial cells (HUVECs) (Lonza) were cultured in EGM-2 media according to vendor recommendations on BD Biocoat Collagen I-coated tissue culture-treated plasticware.

Viral supernatant generation

Replication-incompetent retroviral particles were prepared in the Plat-E cell line (a 293T-based ecotropic retrovirus packaging cell line) (Cell Biolabs). Briefly, constructs of interest were cloned into the transfer vector pMSCV using standard molecular biology techniques and then co-transfected into the Plat-E cell line along with the packaging plasmid pCL-Eco using the transfection reagent FuGENE HD (Promega). Ecotropic envelope pseudotyped retroviral particles in the supernatant were collected 48 hours later.

Replication-incompetent lentiviral particles were prepared in 293T cells by standard methods. Briefly, constructs of interest were cloned into the transfer vector pHR^{SIN}:CSW using standard molecular biology techniques and then co-transfected into 293T cells along with the viral packaging plasmids pCMVdR8.91 and pMD2.G using the transfection reagent FuGENE HD (Promega). Amphotropic VSV-G pseudotyped lentiviral particles in the supernatant were collected 48 hours later.

Viral supernatants were titered by transducing 3T3 mouse fibroblast cells with serial dilutions of virus and determining the percentage of transduced cells via fluorescence microscopy and flow cytometry.

Transduction and stable cell line generation

Cells were transduced with viral vectors for stable expression of gene constructs of interest. HL-60 cells were incubated with amphotropic lentiviral supernatant at an MOI of 1-10 overnight and then washed and resuspended in normal growth medium. Human T lymphocytes were transduced with the same protocol except that the media was supplemented with 100 U/mL hIL-2 and the cells were activated 24 hours prior to transduction using CD3/CD28 Dynabeads (Invitrogen) following manufacturer recommendations. Human epidermal keratinocytes were transduced at an MOI of 10 and HUVECs were transduced at an MOI of 3 overnight by addition of lentiviral supernatants to cultures overnight before washing and resuspending in normal growth medium the next day.

Mouse T lymphocytes were transduced with ecotropic envelope-pseudotyped MSCV retrovirus by Retronectin binding and spinfection. Non-tissue culture-treated plates were

coated with Retronectin (Takara / Clontech) at a concentration of 32ug/mL in PBS for 2 hours. Following a 30 minute block in PBS + 2% BSA and a wash with PBS, retroviral supernatant was added to each well and the plate was spun in a swinging bucket centrifuge for 1.5 hours at 1200g. Following one additional rinse with PBS, T lymphocytes in growth medium supplemented with 100 U/mL hIL-2 were added to the wells and the plate was spun for an additional hour at 1200g at 32 C. T lymphocytes transduced in this way were activated 24 hours prior to spinfection using CD3/CD28 Dynabeads (Invitrogen) according to manufacturer recommendations.

Amaya transient electroporation

Differentiated HL-60 cells were electroporated with 2ug plasmid DNA using program Y-001 in Amaya transfection solution Kit V (Lonza) and allowed to recover for 6 hours in IMDM (Gibco) + 20% FBS + 2mM glutamine at 37 C prior to use in experiments.

xCELLigence impedance array-based cell spreading assay

We used the xCELLigence RTCA MP impedance array assay platform (ACEA Biosciences / Roche) as a screen to monitor cytoskeletal changes (adhesion / spreading) of HL-60 neutrophils in response to agonist. Wells were coated in human fibronectin (Sigma) at 100ug/mL in calcium/magnesium-free D-PBS for 1 hour and then blocked with mGey's buffer + 1% BSA (low endotoxin, Sigma) for 20 minutes. After washing the wells twice with mGey's buffer + 1% BSA, cells were plated and allowed to attach for 3 hours prior to stimulation. Measurements were taken in real-time during and after stimulation with CNO drug or positive control chemoattractant.

Boyden chamber assay

We used Boyden chamber assays to test the migration of cells through porous membranes. For HL-60 neutrophils (3×10^5 cells per insert), 24-well format BD Cell Culture Inserts (3 μ m pore size) or equivalent Fluoroblok format inserts were used. For T lymphocytes (1×10^5 cells per insert), 96-well format polycarbonate Transwells (5 μ m pore size, Corning) were used. For keratinocytes (4×10^4 cells per insert), 24-well format polycarbonate Transwells (8 μ m pore size, Corning) were used. For endothelial cells, 24-well HTS format BD Fluoroblok Cell Culture Inserts were used. Incubation times were 1 hour, 2 hours, 16 hours, and 16 hours respectively. Migrating cells were quantitated by flow cytometry (using Absolute Count standard beads (Bangs Laboratories)), luciferase assay (with luciferase-expressing cells), or fluorescence microscopy (imaging mCherry expressing-cells or staining cells post-experiment with Calcein AM (Molecular Probes)).

Transendothelial migration Boyden chamber assay

HUVECs were seeded at 200k/well in EGM-2 medium into BD fibronectin-coated 3.0 μ m pore size, 24-well HTS format Fluoroblok cell culture inserts. Endothelial monolayer integrity was measured by two methods: transendothelial electrical resistance (TEER) measurements using an EVOM2 Voltohmmeter and STX100F electrode (World Precision Instruments, Inc.) and via a standard FITC-dextran permeability assay. TEER measurements were performed daily according to manufacturer instructions. The permeability assay was performed as follows. FITC-dextran (MW 40,000) (Sigma) was added to the top insert of a HUVEC endothelial monolayer at a final concentration of

1mg/mL. Every 30 minutes for 2 hours, 100uL samples were taken from the bottom well for measurement and replaced with 100uL of medium. FITC content of samples was quantitated using a FlexStation 3 plate reader (Molecular Devices), 492nm/525nm excitation/emission wavelength with 515nm cutoff filter.

Micropipet gradient chemotaxis assay

Micropipet gradient chemotaxis assays were performed as described in Millius et al. 2009⁵³. Briefly, glass capillaries were pulled on a Sutter Model P-97 and backfilled with sterile-filtered chemoattractant solution mixed with 1uM Alexa 594 hydrazide dye (Molecular Probes / Invitrogen) as a fluorescent tracer. A micromanipulator (Narishige MM-89) was used to control flow rate by adjusting balance pressure.

CellASIC microfluidic chemotaxis assay

The ONIX microfluidic platform with M04G gradient generator plate (CellASIC / EMD Biosciences) was used to study HL-60 neutrophil migration.

Culture chambers were coated with 100ug/mL fibronectin in D-PBS (calcium/magnesium-free) for 30 minutes and then blocked in migration buffer (mHBSS + 0.25% BSA (low endotoxin)) for 30 minutes. HL-60 neutrophils at a density of 0.8e6/mL were flowed into the chamber and allowed to adhere for 20 minutes. Migration buffer was flowed through the chamber to wash away non-adherent and dead cells. A chemoattractant gradient was generated according to vendor recommendations, with a 1:10,000 dilution of Alexa594 hydrazide dye (Molecular Probes / Invitrogen) diluted into

chemoattractant solutions as a fluorescent tracer. Time lapse imaging was performed on a Nikon Ti-E inverted fluorescence microscope. Volocity software (Perkin Elmer) was used to track cells, generate cell traces, and calculate migration metrics. Track velocity is defined as total track length divided by time. Displacement rate is defined as track end-to-end distance divided by time. Directionality is defined as displacement divided by total track length.

PLGA bead fabrication

Biodegradable microspheres loaded with CNO were generated using a standard oil-in-water emulsion method⁵⁴ in a sterile environment using depyrogenated glassware, equipment, and water. Ester-terminated 50:50 Poly(DL-lactide-co-glycolide) (PLGA) (LACTEL) was dissolved in dichloromethane to make a 10% polymer solution. A 10mg/mL solution of CNO dissolved in methanol or methanol alone (vehicle control) was mixed with the PLGA polymer solution at a final concentration of 1mg/mL. The mixture was then slowly dispensed into a 0.5% polyvinyl alcohol (PVA) (Sigma) solution via glass syringe (Hamilton) with continuous homogenization at 4500 rpm (IKA Model S25N-18G) for 5 minutes. Additional 0.5% PVA was added to the beaker and the mixture was continuously stirred at 300rpm using an overhead propeller blade stirrer for four hours. Then the microspheres were collected by centrifuging at 1000g for 10min, washed twice in pyrogen-free water, flash frozen in liquid nitrogen, and lyophilized overnight.

Total drug encapsulation was determined by dissolving a pre-weighed quantity of microspheres overnight by agitating at 275 rpm at 37C in 0.1 N NaOH to accelerate hydrolysis. A time course of the release kinetics of the CNO-loaded microspheres in

PBS was taken by suspending a pre-weighed quantity of microspheres in PBS, incubating with agitation at 275rpm at 37C, removing aliquots at pre-determined time intervals, and replacing the buffer with an equivalent volume. The amount of CNO in solution was measured by two methods: LC/MS/MS (UCSF Drug Studies Unit) and by functional assay (quantitation of stable Di-expressing HL-60 neutrophil transwell migration to serial dilutions of CNO drug released into PBS solution by PLGA microspheres as compared to migration to serial dilutions of a known CNO standard).

Mouse T lymphocyte homing study

Animal studies were conducted with the UCSF Preclinical Therapeutics Core under a protocol approved by the UCSF Institutional Animal Care and Use Committee. PLGA microspheres were weighed, resuspended in PBS, vortexed, and bath sonicated for 30 seconds. The microspheres were injected subcutaneously (20uL) into the shaved flanks of albino C57BL/6J mice (Jackson Laboratory). Retrovirally transduced C57BL/6J mouse T lymphocytes expressing mCherry-tagged Di and an enhanced firefly luciferase (effLuc) were washed twice and resuspended in PBS prior to injection via lateral tail vein (2e6 per mouse). Bioluminescent imaging was performed using the IVIS 100 (Xenogen) pre-clinical imaging system at pre-determined time points with images taken 10 minutes following i.p. injection of 150mg/kg D-luciferin (Gold Biotechnology). Quantitation was performed using Living Image software.

FIGURE 1 Expression of engineered Gai-coupled GPCRs is sufficient to induce cytoskeletal changes and direct the chemotaxis of neutrophils up a gradient of a bio-inert small molecule drug CNO

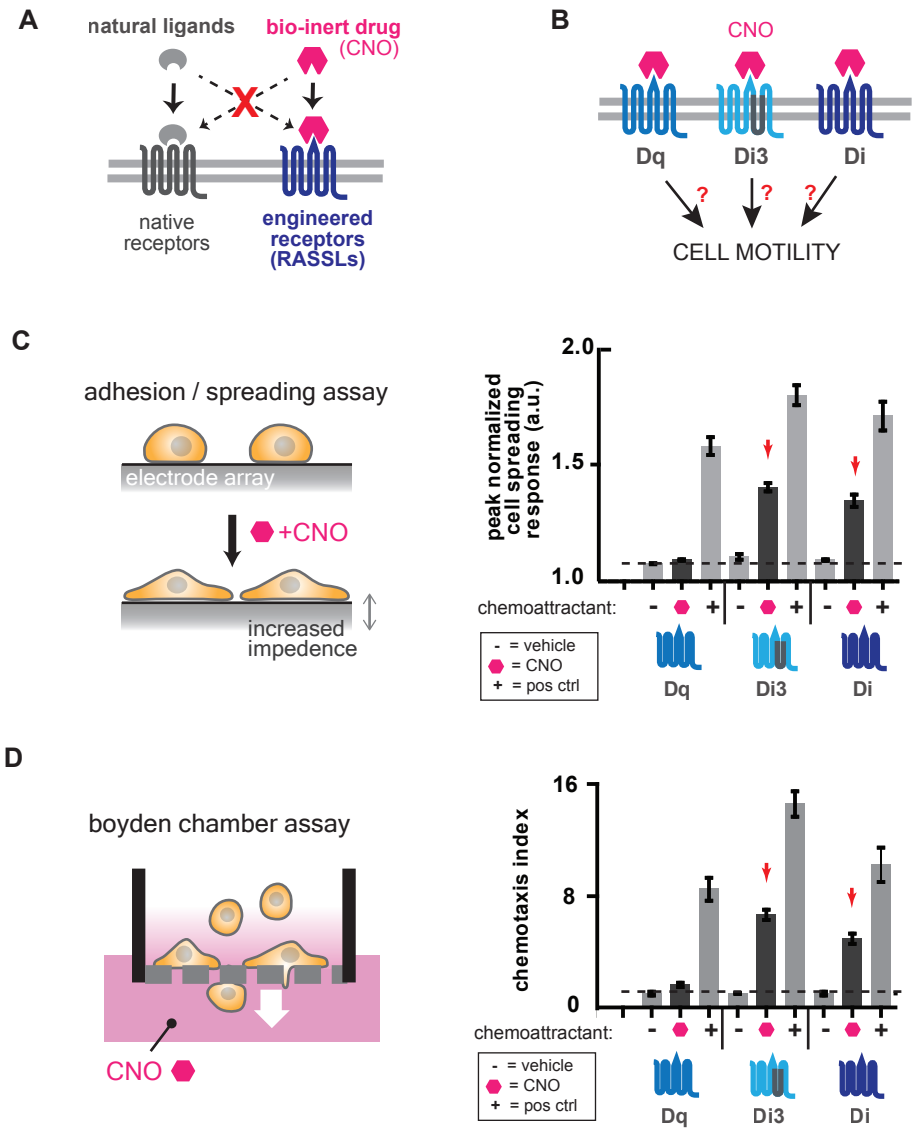


FIGURE 2 Microscopic analysis and quantitation of neutrophil cell migration in response to a gradient of CNO

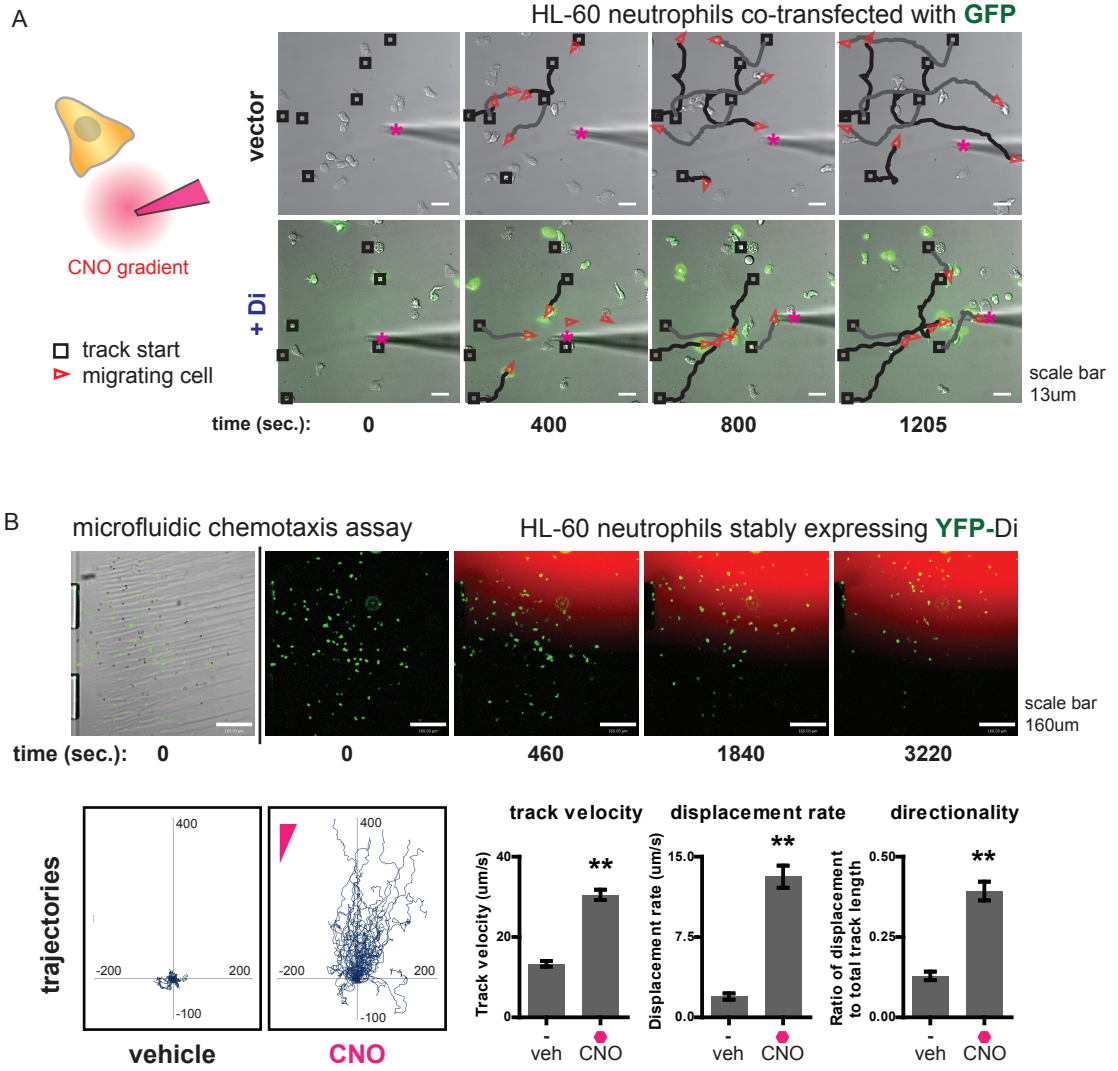


FIGURE 3 The engineered chemotaxis receptor Di is “portable” to a range of cell types and is sufficient to mediate both chemotaxis and transendothelial migration

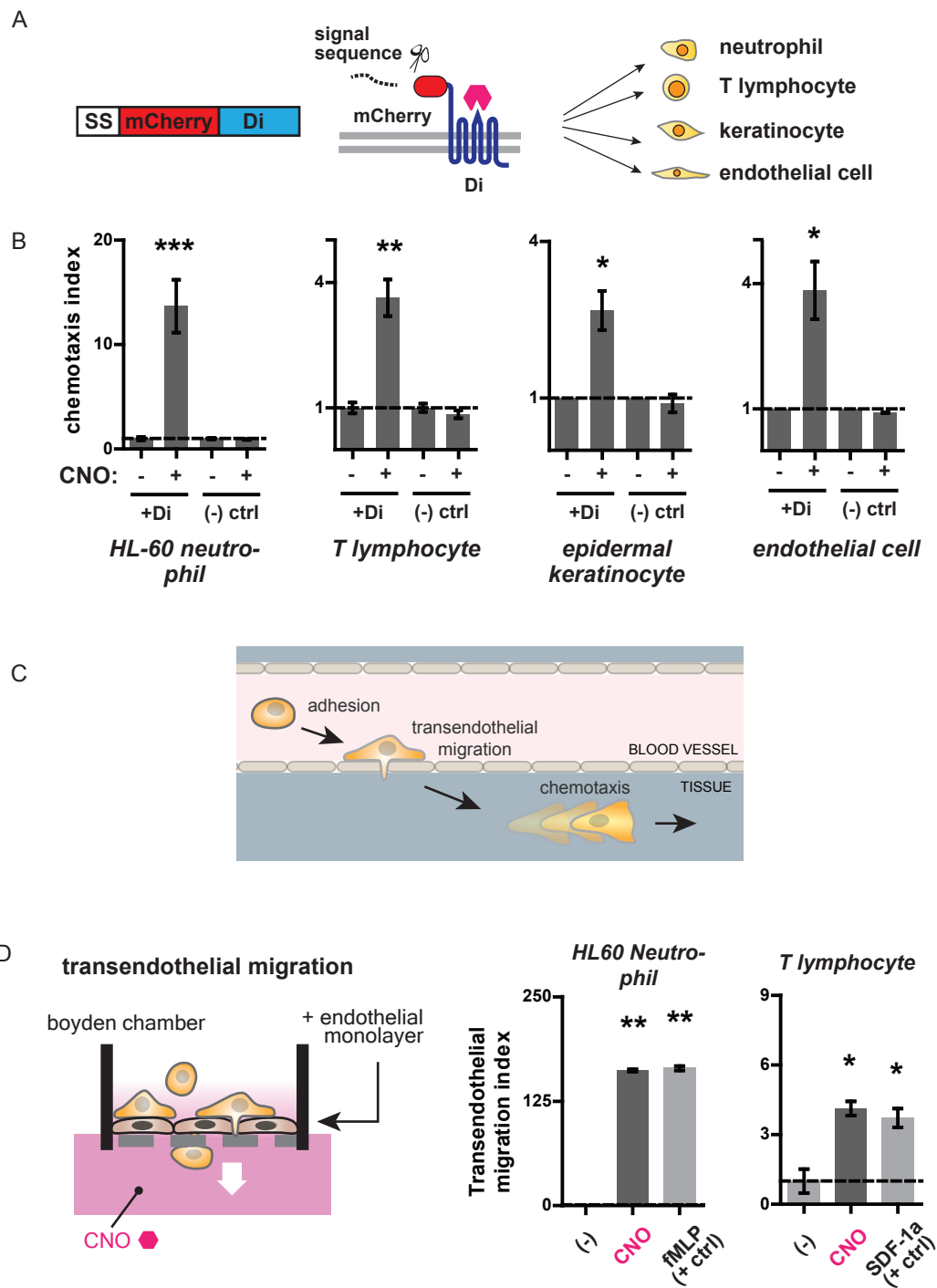
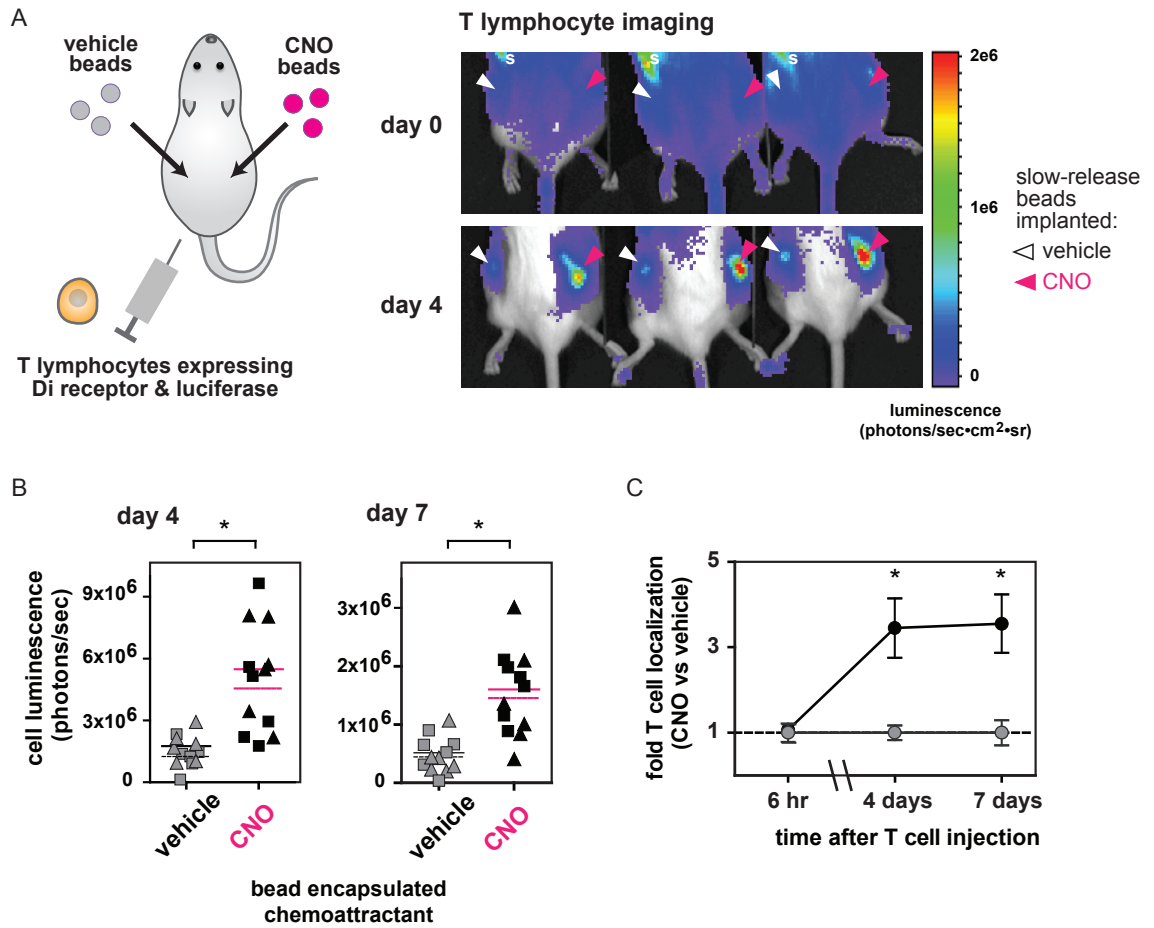
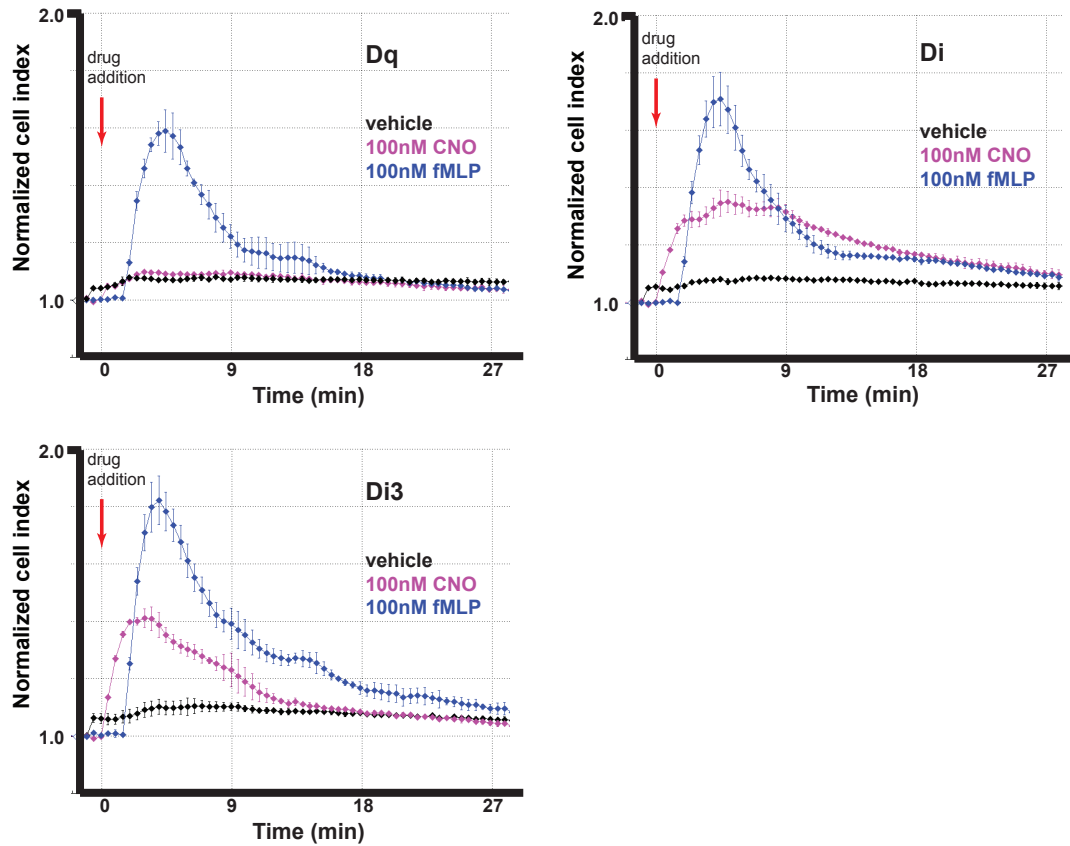


FIGURE 4 Intravenously administered primary T lymphocytes expressing Di specifically localize to a subcutaneously implanted depot of CNO slow-release biodegradable microspheres



CNO induces adhesion / spreading in engineered Gai-coupled GPCR-expressing HL-60 neutrophils, as determined using a real-time impedance-based assay



Supplementary Figure 1. CNO induces adhesion / spreading in engineered Gai-coupled GPCR-expressing HL-60 neutrophils, as determined using a real-time impedance-based assay.

Changes in electrical impedance as a result from cell spreading in response to drug or ligand are detected real-time by an electrode array. Expression of Di3 or Di causes HL-60 neutrophils to respond to CNO. All cells respond to the positive control chemoattractant fMLP. Mean +/- SEM for n=3 replicates is shown. Peak responses in this figure correspond to the bar graph in Figure 1C.

SUPPLEMENTARY VIDEOS 1A and 1B

Direct visualization of engineered HL-60 neutrophil migration up a steep CNO gradient in a micropipet assay.

a-b, Cells visualized by differential interference contrast and fluorescence microscopy. CNO gradient shown in red, Alexa594 dye tracer mixed into CNO solution. Videos correspond to the still frames shown in Figure 2A.

a, HL-60 neutrophils transfected with vector control do not respond to CNO gradient.

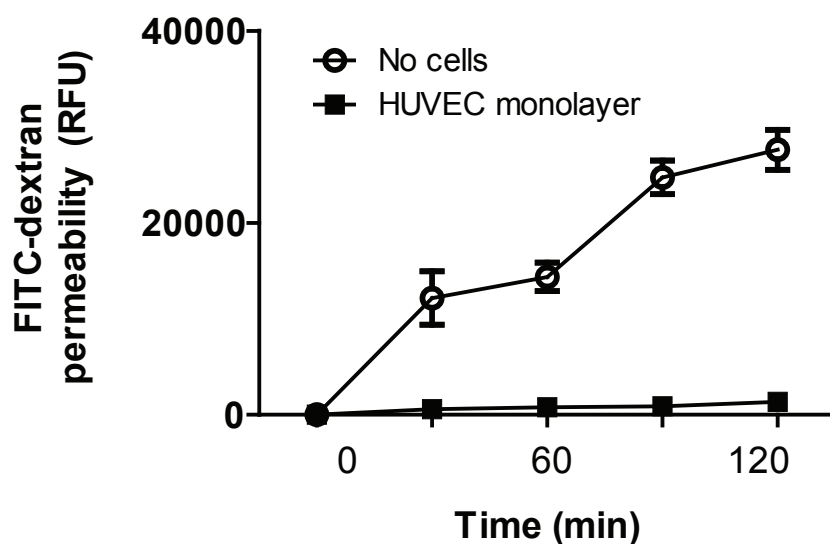
b, HL-60 neutrophils transfected with Di and GFP migrate up CNO gradient.

SUPPLEMENTARY VIDEO 2.

Direct visualization of engineered HL-60 neutrophil migration up a precisely generated CNO gradient in a microfluidic chemotaxis assay device.

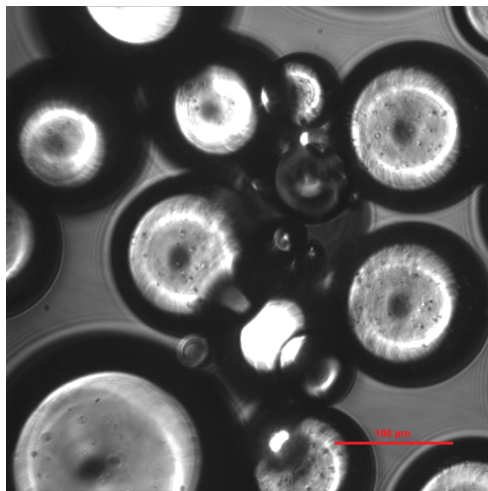
Stable YFP and Di-expressing HL-60 neutrophils (green) visualized by bright field and fluorescence microscopy migrate in a microfluidic chemotaxis assay device. Non-adherent cells are washed away at the beginning of the video. The CNO gradient (red) is visualized by the presence of a fluorescent Alexa594 dye tracer mixed into the chemoattractant solution. This video corresponds to the still frame images, tracks, and quantitation in Figure 2B.

Integrity of tight endothelial cell monolayers grown on porous inserts is demonstrated by blockage of FITC-dextran diffusion in a permeability assay



Supplementary Figure 2. Integrity of tight endothelial cell monolayers grown on porous inserts is demonstrated by blockage of FITC-dextran diffusion in a permeability assay. Human umbilical vein endothelial cells were seeded on fibronectin-coated porous transwell inserts to generate a tight monolayer, and monolayer integrity was assessed in a standard FITC-dextran permeability assay. Fluorescent dye diffusing through the porous inserts with or without endothelial cell monolayers was quantitated at 30 minute timepoints. Mean +/- SEM for n=4 replicates is shown.

Fabricated PLGA microspheres show typical morphology and size distribution suitable for subcutaneous injection



scale bar = 100um

Supplementary Figure 3. Fabricated PLGA microspheres show typical morphology and size distribution suitable for subcutaneous injection. Biodegradable PLGA microspheres loaded with CNO were generated using a standard oil-in-water emulsion method and visualized by standard bright field light microscopy.

Chapter 3. Use of an orthogonal cell migration tool to enhance the infiltration of tumors by adoptively transferred anti-tumor T cells

Introduction

T cell-based immunotherapy for cancer

T cell-based immunotherapies have shown impressive efficacy in recent clinical trials for cancer types ranging from metastatic melanoma to lymphomas and leukemias, even in heavily pre-treated and chemotherapy-resistant patients (1). Pioneering approaches involved the isolation of lymphocytes from patient tumor biopsies (so-called tumor infiltrating lymphocytes or TILs), expansion *ex vivo* in cell culture (generally with cytokine stimulation), and re-infusion into patients (2).

More recently, recombinant DNA technology has been used to overcome some of the disadvantages of TIL-based strategies, which include the difficulty of isolating sufficient T cell numbers from tumor biopsies, the length of time required to expand the T cell cultures *ex vivo* starting from small numbers, and the fact that TILs have in some cases been found to be anergic or defective in signaling, perhaps due to the immunosuppressive nature of tumor microenvironments (3–5). In these newer strategies, instead of isolating T cells from tumor biopsies, polyclonal T cells are easily collected and isolated from patient peripheral blood. Then recombinant vectors (including DNA, RNA, and viral vectors) are used to express in the cells either recombinant T cell receptor (TCR) chains cloned from tumor antigen-reactive T cells or chimeric antigen receptors (CARs), which are protein fusions of tumor antigen-specific single-chain antibody fragments (scFv) presented extracellularly and the transmembrane

and intracellular signaling domains of key components of immune cell activation signaling cascades. In the case of CARs, additional intracellular signaling domains from costimulatory receptors such as CD28 and 4-1BB can be attached to yield so-called 2nd and 3rd generation CARs that activate T cell signaling with greater potency. The generation, engineering, and use of recombinant TCRs and CARs is described in great detail elsewhere (6–12).

Thus, genetic modification strategies allow for the rapid generation of large numbers of patient T cells endowed with the ability to recognize and respond to cancer antigens by proliferating, secreting pro-inflammatory cytokines, and killing target cells. Further, especially in the case of CARs, these “designer” T cell therapeutic strategies open up the theoretical possibility to target T cells to any tumor cell surface antigen for which one can create an antibody (or other recognition domain).

Overcoming suboptimal infiltration of tumors by anti-tumor T cells

Efficient trafficking to and infiltration of tumors by tumor antigen-specific T cells is critical for effective anti-tumor activity. In mice and in humans, increased infiltration of tumors by lymphocytes correlates with better anti-tumor responses and prognoses in mouse studies and in human clinical trials (13–25). However, in many cases, trafficking of T cells into tumors can be quite inefficient – antigen-specific T cells can be undetectable in tumors despite the fact that they can be found circulating in peripheral blood (16, 26).

One determinant of effective trafficking of T cells into tumors in mouse models is the “matching” of the chemokine receptors expressed on T cells and the chemokines that are secreted by specific tumors. Chemokines and their receptors are involved in the homing of leukocytes (including T cells) to specific locations in the body in both normal

and inflammatory or disease settings (27–29). Work by a number of groups has shown that exogenous overexpression of pro-inflammatory chemokines in tumor cell lines enhances T cell infiltration and suppresses the growth of those tumors in mouse models (27, 28, 30). Further, expression in T cells of chemokine receptors specifically chosen to “match” the chemokines secreted by specific tumor types has been shown to be an effective strategy to augment T cell infiltration and anti-tumor efficacy, also in mouse tumor models.

Thus, augmenting anti-tumor T cell infiltration of tumors may enhance the efficacy T cell therapeutics in future applications. There are potential safety advantages to be had as well. By effectively increasing the therapeutic index of T cell treatments by decreasing the number of cells that must be administered for anti-tumor responses, enhanced tumor infiltration strategies may enable physicians to administer lower doses of cells to patients and minimize the risk of sometimes fatal “off-tumor” side effects (31, 32).

However, the use of the chemokine axis to direct anti-tumor T cell infiltration of tumors (such as through tumor-matched chemokine receptor expression) is not without its challenges. One complicating factor is that chemokine expression by tumors is highly variable. The types of chemokines expressed by tumors vary, as do their levels. It has been proposed that lack of expression of chemokines may be a mechanism of immune escape for tumors, as chemokine expression levels in metastatic melanoma has been found to be associated with CD8+ T cell recruitment (33). In support of this idea, it has been found that certain aggressive tumors such as MYCN-amplified tumors transcriptionally repress production of the chemokine CCL2. Also, high levels of chemokine expression do not necessarily lead to increased immune cell infiltration. Chemokines can also be repulsive for lymphocyte trafficking – for example, SDF-1

overexpression in B16 melanoma cells induces tumor cell-specific T cell chemorepulsion (34).

On the receptor side, one potential obstacle is that chemokine receptor expression on T cell subsets can vary according to growth and stimulation conditions in *ex vivo* culture (29, 33, 35). With forced expression of matched chemokine receptors, this is less of a concern. However, it is known that expression of chemokines by tumors can desensitize chemokine receptors on T cells (36).

Cross-reactivity is another potential obstacle for chemokine-based strategies. Chemokines that are frequently expressed in cancers are also commonly found on many non-cancer cells in both physiological and stress conditions in a variety of locations throughout the body. (37–41). Increased localization of T cells with forced expression of chemokine receptors at non-tumor sites theoretically increases the likelihood of off-target effects.

In Chapter 2, we demonstrated that expression of an engineered GPCR in a variety of cell types including T cells is sufficient to direct their chemotaxis toward a CNO source *in vitro* and their localization to a subcutaneously implanted depot of CNO-releasing microspheres in a mouse. We hypothesized that we could use this technology to increase the trafficking of CAR-expressing T cells into tumors, thereby enhancing the T cells' anti-tumor effect. This chapter discusses ongoing work in the lab in which we are expressing the previously described engineered chemotaxis receptor Di and an anti-CD19 chimeric antigen receptor in human CD4 and CD8 T cells, injecting established CD19+ tumors in mice with CNO-releasing microspheres, infusing the expanded T cells into the tumor-bearing mice, and tracking T cell trafficking and tumor growth over several weeks.

Results

Anti-CD19 CAR-expressing T cells respond to CD19-expressing target tumor cells in vitro

First, we generated T cells responsive to CD19-expressing tumor cells by expressing in them a second-generation anti-CD19 chimeric antigen receptor construct (**Fig. 3.1**). PCR fragments were cloned from a plasmid containing an anti-CD19 scFv – 4-1BB – CD3z CAR (acquired as a generous gift from Dr. Carl June and colleagues) to facilitate cloning using a combinatorial cloning strategy based on the Type II restriction enzyme AarI developed by Peisajovich et al (42). In addition, we fused a myc tag sequence to the N-terminus (extracellular) and, in some cases, GFP to the C-terminus (intracellular) to allow for sorting by fluorescent activated cell sorting (FACS) and visualization of receptor localization by microscopy. (This CAR construct is referred to simply as “the anti-CD19 CAR” throughout the remainder of this chapter). Constructs were cloned into a pHR'SIN:CSW lentiviral expression backbone and replication-incompetent VSV-G pseudotyped lentiviral supernatants were generated using standard methods in 293T cells by transfection of the lentiviral expression plasmid along with the packaging plasmids pCMVdR8.91 and pMD2.G using the transfection reagent FuGENE HD (Promega).

We tested the functionality of the anti-CD19 CAR construct in primary human T cells. Primary human CD4+ and CD8+ T cells were isolated from peripheral blood mononuclear cell suspensions from normal donors as described in Chapter 2. Cells were transduced with GFP-tagged anti-CD19 CAR lentiviral supernatants (transduction protocol as described in Chapter 2) and rested and maintained in growth medium in the

presence 30 U/mL of human IL-2 for greater than one week prior to their use in activation assays. Transduction efficiency was assessed by staining for myc and assaying for the percentage of CAR-expressing cells by flow cytometry (**Fig. 3.2**).

Transduced CD4⁺ T cells were stimulated with a K562 target cells expressing either CD19 or mesothelin (final ratio of T cells to K562 target cells: 5:2). After overnight incubation, cells were washed, surface stained with anti-CD69 antibody, and assessed by flow cytometry. Anti-CD19 CAR-expressing T cells showed an increase in CD69 surface expression when incubated with K562 cells expressing CD19 but not when incubated with K562 cells expressing the irrelevant antigen mesothelin. Untransduced T cells did not show an increase in CD69 surface expression with either K562 target cell type (**Fig. 3.3A**).

The cytotoxic activity of anti-CD19 CAR transduced CD8⁺ T cells was assessed using an *in vitro* killing assay. Briefly, CD8⁺ T cells were incubated with a 1:1 mixture of CD19 or mesothelin-expressing K562 target cells (final ratio of T cells to total K562 target cells: 5:2). To facilitate quantitation by flow cytometry, CD19-expressing K562 cells were also modified to express mCherry and mesothelin-expressing K562 cells were modified to express GFP. The ratio of surviving CD19-expressing versus mesothelin-expressing target K562 cells (as determined by flow cytometry by gating on and quantifying fluorescent cell populations) was used as a measurement of CD8⁺ T cell cytotoxic activity. Anti-CD19 CAR-expressing CD8⁺ T cells efficiently reduced the survival of CD19-expressing versus mesothelin-expressing K562 target cells. Untransduced T cells did not affect the ratio of surviving K562 target cells (**Fig. 3.3B**).

Establishment of a CD19+ Daudi subcutaneous tumor model to test CAR T cell efficacy

We next wanted to test the ability of anti-CD19 CAR transduced T cells to suppress the growth of CD19+ tumor xenografts in mice. First, we set out to establish an appropriate mouse tumor model. The Daudi cell line is a CD19+ Burkitt's lymphoma cell line to which T cells do not efficiently localize in *in vitro* Transwell assays or xenograft mouse models due to the tumor cell line's minimal secretion of chemokines such as MCP-1 (35). We reasoned that such a tumor, which is likely to be subject to less efficient immune surveillance in the body, would be a good model for testing the effects of increased tumor infiltration by adoptively transferred CAR-transduced T cells.

To facilitate sensitive, accurate, and quantitative measurement of Daudi tumor xenograft growth over time, we generated a stable line of Daudi tumor cells expressing a Renilla luciferase gene. To do this, we cloned an optimized red-shifted Renilla luciferase gene (rLuc8.6-535) into the pHR'SIN:CSW lentiviral expression plasmid, generated replication-deficient lentiviral particles as described previously, and established a stable line of Daudi cells expressing Renilla luciferase (hereafter referred to as rLuc/Daudi). (The rLuc8.6-535 gene was a generous gift of Dr. Sanjiv Sam Gambhir) (43).

We established tumor growth curves for the rLuc/Daudi cell line in the immunodeficient mouse strain NOD/SCID γ c- (also known as NSG). These mice allow for highly efficient engraftment of human cells including tumor xenografts and human T cells because they lack mature T cells, B cells, and functional NK cells, and are deficient in cytokine signaling (44, 45). Five million cells resuspended in PBS, mixed 1:1 with Matrigel (BD Biosciences) and injected subcutaneously into the shaved hind flanks of NSG mice in a final volume of 100 μ L. Tumor size was monitored by caliper measurements to estimate tumor volume (volume = 0.5 x Length x Width²) and

bioluminescent imaging using the Xenogen IVIS 100 system with intraperitoneal injections of Viviren Renilla luciferase *in vivo* imaging substrate (Promega) (**Fig. 3.4A-B**).

Anti-CD19 CAR T cells efficiently expand in vivo and treat subcutaneous Daudi xenograft tumors

Next we tested the anti-tumor efficacy of anti-CD19 CAR T cells infused into NSG mice bearing rLuc/Daudi subcutaneous tumors. CD4 and CD8 primary human T cells were each lentivirally transduced simultaneously with the previously described myc-tagged anti-CD19-41BB-CD3zeta CAR construct and a viral construct expressing a codon-optimized firefly luciferase gene for highly sensitive *in vivo* bioluminescent of infused T cells in living mice (a generous gift of Dr. Brian Rabinovich) (46). Transduction efficiency (70% CAR+ for CD4, 36% CAR+ for CD8) was assessed by staining the cells with fluorescent anti-myc antibody and determining the percentage of stained cells by flow cytometry (**Fig. 3.5A**).

The transduced CD4 and CD8 T cell cultures were rested until 9 days after Dynabead activation, counted, mixed together at a 1:1 ratio, resuspended in PBS, and injected intravenously via lateral tail vein into NSG mice bearing rLuc/Daudi tumors inoculated 11 days earlier. The tumors were tracked by caliper measurement and by bioluminescent imaging using the Xenogen IVIS 100 system (Caliper Life Sciences) following intraperitoneal injection of Viviren Renilla Luciferase *In Vivo* Imaging substrate (Promega). T cells were visualized in a similar manner, but following intraperitoneal injection of D-luciferin (GoldBio Technology).

Anti-CD19 CAR T cells expanded rapidly in rLuc/Daudi tumor-bearing mice and reduced the size of the subcutaneous tumors (**Fig. 3.5B-C**).

Use of an orthogonal cell migration tool augments the homing of CAR T cells to Daudi tumors

Having established that anti-CD19 CAR T cells are capable of treating subcutaneous rLuc/Daudi tumors, we hypothesized that we could augment the therapeutic effect of this T cell treatment by increasing tumor infiltration using an engineering approach to synthetic cell migration as described in Chapter 2. By expressing on T cells not only the anti-CD19 CAR but also the engineered chemotaxis receptor Di, we hoped to observe an increase in tumor-localized cells when CNO, the orthogonal small molecule ligand for the Di receptor, was injected into them. We would then expect a corresponding increase in anti-tumor activity with the greater quantity of T cells in the tumors.

We introduced the engineered chemotaxis receptor Di (fused to mCherry on its N-terminus), the myc-tagged anti-CD19 CAR construct, and the enhanced firefly luciferase gene into human primary CD4 and CD8 T cells using lentiviral transduction. Three days after transduction, the T cells were sorted for Di receptor expression to greater than 95% purity by fluorescence activated cell sorting (FACS), gating on mCherry-expressing cells. T cells were expanded in culture for an additional five days. The percentage of CAR-expressing cells was quantitated by myc-staining and flow cytometry (**Fig. 3.6A**).

Biodegradable PLGA microspheres loaded with CNO were generated using a standard oil-in-water emulsion method for use as a slow-release source of the drug *in vivo* (as described in Chapter 2). Vehicle microspheres were made by exclusion of CNO from the protocol. Microspheres were resuspended in PBS (10% w/v) and 20 μ L was directly injected into rLuc/Daudi tumors in NSG mice (11 days after tumor inoculation as described in the previous section). Immediately thereafter, transduced CD4 and CD8 T cells (mixed at a 1:1 ratio and resuspended in PBS) were injected into the mice intravenously via lateral tail vein injection.

In mice with bilateral subcutaneous rLuc/Daudi tumors where one tumor was injected with vehicle microspheres and the other with CNO microspheres, we observed that Di receptor-expressing T cells preferentially localized to the tumors injected with CNO microspheres (**Fig. 3.6B**). However, this preferential T cell localization dissipated by two weeks after T cell injection.

One possible explanation for the change in preferential localization at two weeks is that cells expanding in the CNO-injected tumor are able to leave and make their way to the other tumor over time (and vice versa), especially as the local T cell population is expanding beyond the “capacity” of a shrinking tumor. This would have an interesting therapeutic implication – driving greater infiltration of a primary tumor could in principle lead to an T cell activation and enhanced proliferation, and the cells could then survey the body to attack distant tumor sites or metastases.

However, for the purposes of this study, we chose to modify our study setup to more directly answer the experimental question: “Does increasing anti-tumor T cell localization to tumors lead to augmented anti-tumor effects?” To remove the possibility of a “crossover” effect of T cells leaving one tumor to go to the other, ongoing experiments in the lab will be conducted in mice bearing single tumors injected with either vehicle or CNO microspheres. As an additional optimization step to improve the reproducibility of future studies, T cells will be sorted for both Di receptor expression (as before) as well as anti-CD19 CAR (GFP) expression.

At the time of writing of this dissertation, the aforementioned experiments are ongoing but results are not yet available.

Discussion

Whether for the treatment of cancer or autoimmune disease or for regenerative medicine purposes, most cellular therapy approaches being employed in clinical trials and preclinical studies today rely solely on the endogenous homing capabilities of the therapeutic cell types being used. Unfortunately, the migratory capabilities of cells used for therapy can be variable due to heterogeneity of receptor expression and can also become highly compromised during *ex vivo* culture and expansion (e.g. due to the loss of adhesion molecule or homing receptor expression) (3, 29, 33, 35, 47).

This chapter described our initial work using an engineered orthogonal GPCR-based system to enhance the infiltration of tumors by anti-tumor T cells in a xenograft mouse tumor model. Work by other groups in the past have shown that by forcing the expression of specific chemokine receptors in anti-tumor T cells to “match” the chemokines secreted by specific tumor types, that one could enhance T cell localization to appropriate tumors and improve their treatment in mouse models (29, 31, 48, 49).

Our approach has two primary advantages over approaches such as chemokine receptor-matching: generalizability and orthogonality. The system we describe is generalizable because a single receptor, the Di RASSL, can be used in any T cell to guide its migration to any tumor in which the drug CNO is present. The term orthogonality refers to the fact that the Di receptor and small molecule drug CNO make up an exclusive pair – the receptor binds only to the small molecule and not to any known endogenous ligands, while the small molecule binds only to the engineered receptor and not to any known endogenous receptors. From a therapeutic perspective, an orthogonal system is advantageous because: 1) the drug should not have off-target effects in the body, which allows for its use without concern for adverse events due to drug toxicities, 2) the receptor responds specifically only to a single drug and vice versa,

and 3) the drug is present only where it is delivered (and wherever it distributes thereafter).

These last two points above are in stark contrast with the case in the ever-complex chemokine - chemokine receptor axis. Chemokine receptors respond to multiple chemokines (and vice versa) and most chemokines are known to be present in various locations throughout the body on normal tissues as well as in specific tumor types ((29, 31, 48–50). Further, some tumors express very low levels of chemokines; this has been proposed as a means of immune escape by tumors (33). Finally, species differences in the expression, diversity, cell type-specificity of expression, and selectivity of chemokines for chemokine receptors make it such that mouse models are likely to be poor predictors for any off-target effects of human chemokine receptor-matching strategies in human xenograft mouse tumor models (50).

On the other hand, a weakness of our current approach is that the drug CNO is a synthetic molecule that cannot be genetically encoded and produced by a cell. An orthogonal system in which both receptor and ligand are proteins that can be encoded as genes would be valuable for future work, and the development of such systems is ongoing in the lab. In our experiments, CNO is directly delivered to tumors as a slow-release formulation of biodegradable polymer particles by intratumoral injection, but a promising future approach would be to deliver the drug through targeted drug delivery technologies such as “smart liposomes” that accumulate at tumors or other sites of disease.

One final caveat is that the drug CNO can be back-metabolized to the active anti-psychotic drug clozapine in humans (but not in mice), though this occurs at a low percentage, the half-life of CNO in circulation is on the order of tens of minutes, and the

levels of CNO necessary for activation of the Di receptor are about 100-fold lower than the minimum plasma levels necessary for therapeutic effects in anti-psychotic patients (51, 52). Nevertheless, the development of new agonists for orthogonal receptors that cannot be metabolized to active drugs would be a useful development for the field.

In conclusion, the use of an orthogonal receptor to control mammalian cell homing may be a useful strategy for enhancing the efficacy of an anti-tumor T cell therapeutic agent. Preliminary work shows proof-of-principle that we can enhance the homing of engineered T cells into tumors, and the results of ongoing experiments should give us further data on the degree to which this enhances the therapeutic effect of T cell administration.

Figures

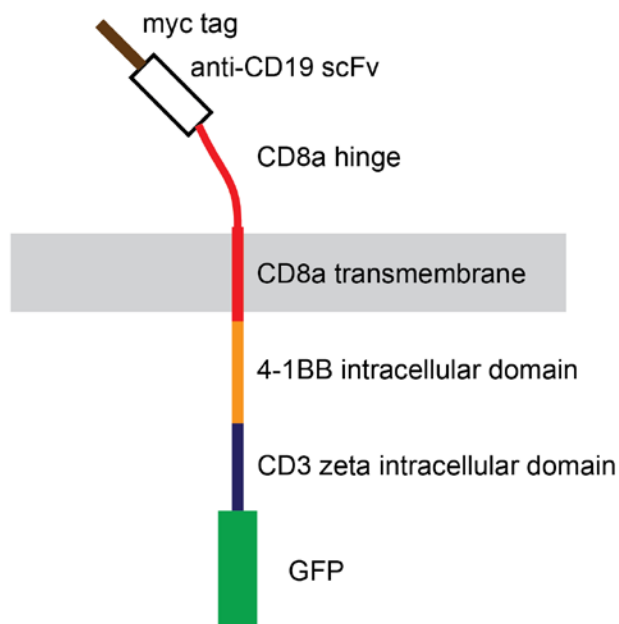


Figure 3.1. Anti-CD19 chimeric antigen receptor design. The construct consists of an anti-CD19 scFv for antigen recognition fused to the CD8a Hentgen transmembrane domains, the intracellular signaling domain from 4-1BB, and the intracellular signaling domain of the CD3 zeta chain. A myc tag was fused to the N-terminus and GFP fused to the C-terminus of the construct to facilitate surface staining and fluorescence activated cell sorting procedures, respectively.

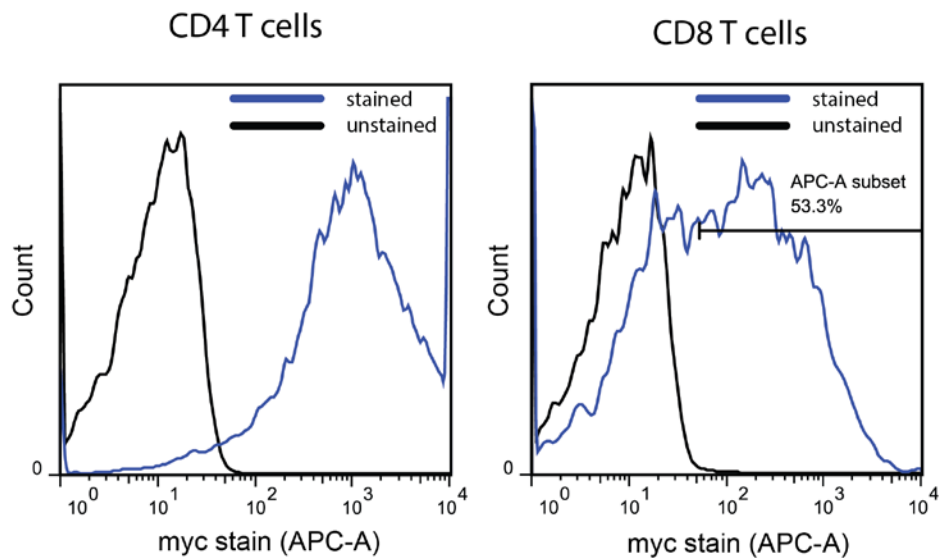


Figure 3.2. Anti-CD19 CAR-transduced primary T cells express CAR on cell surface. Primary human CD4 and CD8 T cells lentivirally transduced with myc-tagged chimeric antigen receptor construct were stained with fluorescent anti-myc antibody and assayed by flow cytometry. Nearly 100% of CD4 T cells and over 50% of CD8 T cells stained positive for the receptor.

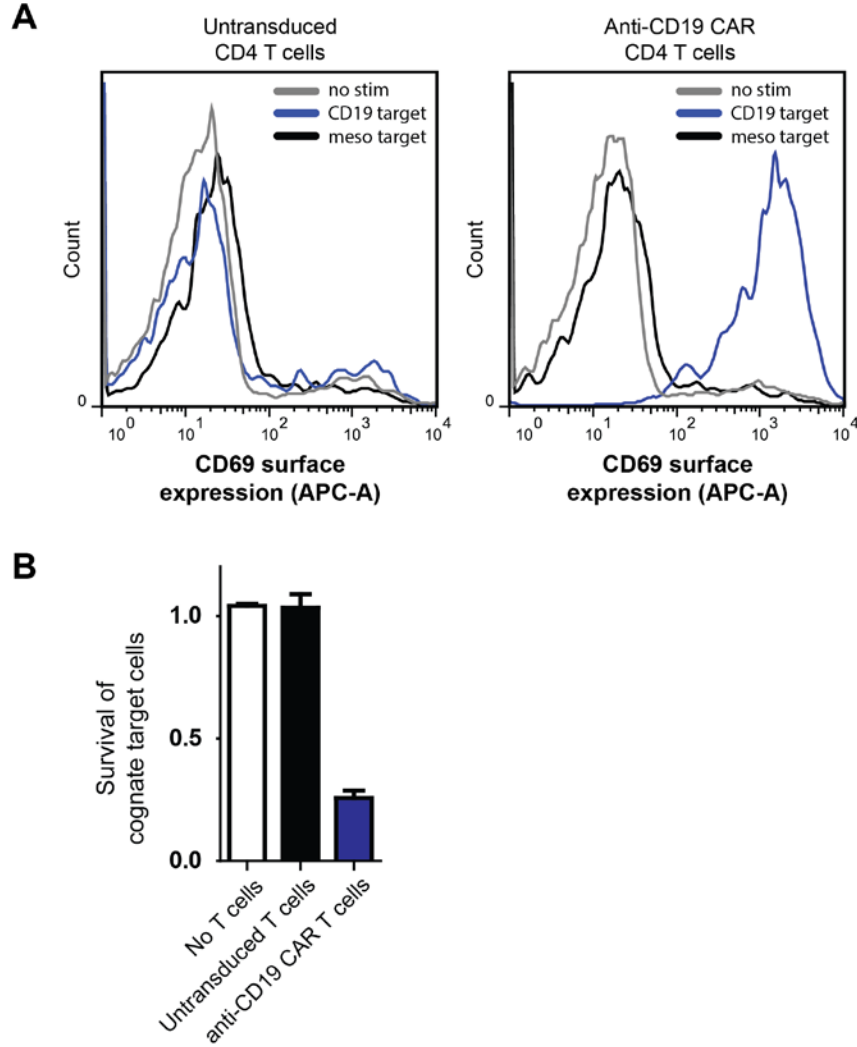


Figure 3.3. Anti-CD19 CAR T cells are functional against a CD19-expressing tumor cell line *in vitro*. A) Anti-CD19 CAR-transduced CD4 T cells upregulate surface expression of CD69, an activation marker, after stimulation with cognate CD19-expressing tumor cells (blue traces) but not with tumor cells expressing the irrelevant antigen mesothelin (black traces). Untransduced CD4 T cells did not respond to tumor cells expressing either antigen. B) Anti-CD19 CAR-transduced CD8 T cells decreased the survival of CD19-expressing target tumor cells relative to mesothelin (irrelevant antigen)-expressing target tumor cells. Untransduced CD8 T cells had no effect on the relative survival of antigen-expressing target tumor cells.

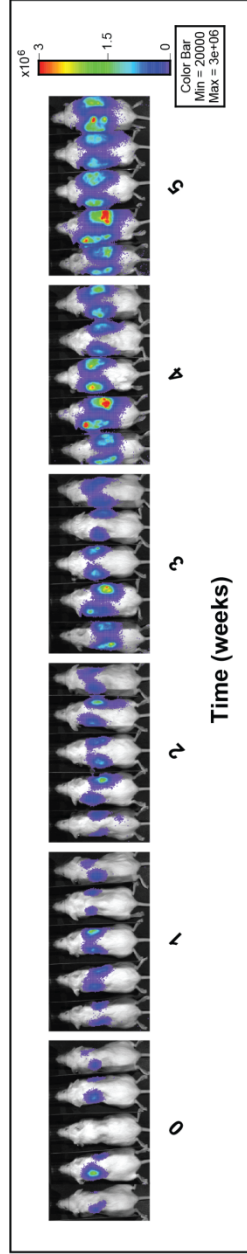
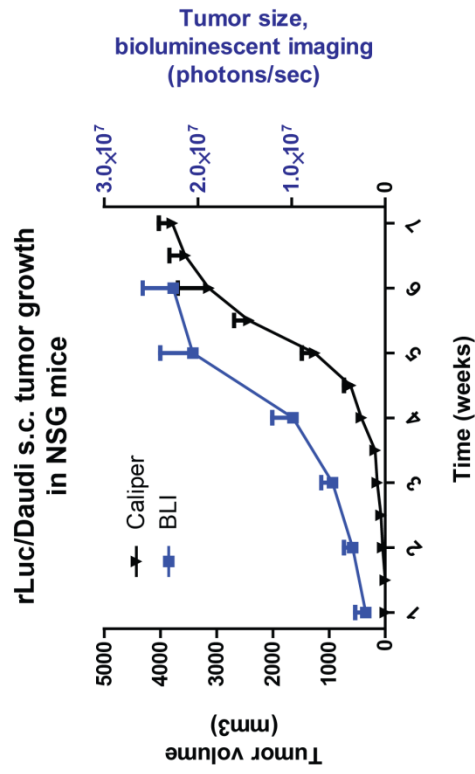


Figure 3.4. rLuc/Daudi tumor cell lines grow robustly as subcutaneous tumors in immunodeficient NSG mice. A) Tumor growth is tracked by two measures: caliper measurements (tumor volume = $0.5 \times \text{length} \times \text{width}^2$) (left axis) and bioluminescent imaging using VividRen imaging substrate with Xenogen IVIS imaging system (right axis). B) Imaging of rLuc-expressing tumors is an accurate and sensitive means of tracking tumor growth.

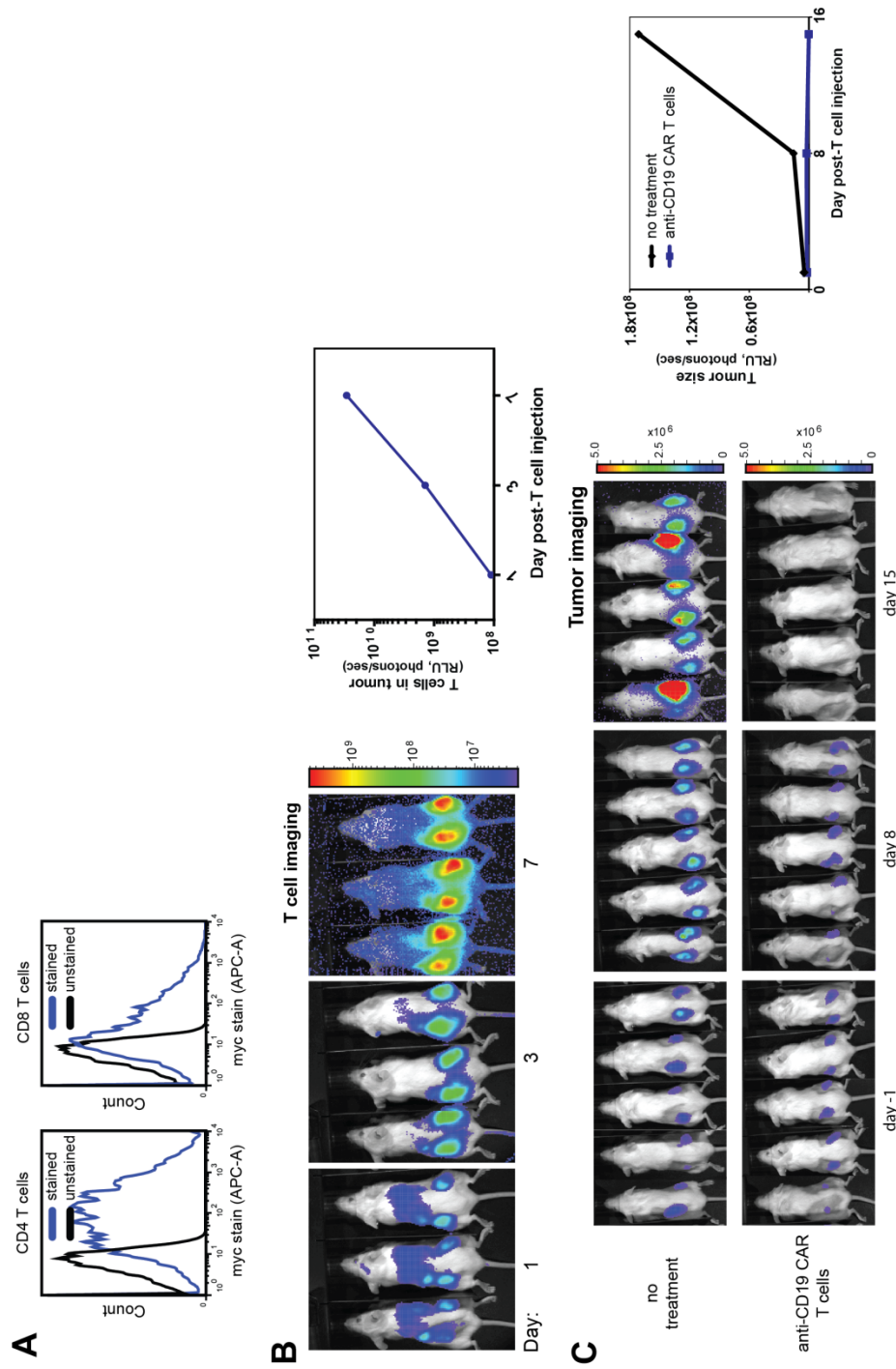


Figure 3.5. Anti-CD19 CAR-transduced primary T cells expand in rLuc/Daudi tumor-bearing NSG mice and reduce the size of subcutaneous tumors. A) Primary human CD4 and CD8 T cells lentivirally transduced with firefly luciferase and myc-tagged chimeric antigen receptor constructs were stained with fluorescent anti-myc antibody and assayed by flow cytometry. B) T cells expand in rLuc/Daudi tumor-bearing mice (visualized by bioluminescent imaging with D-luciferin substrate). C) Tumor burden is efficiently reduced by anti-CD19 CAR T cell administration (visualized by bioluminescent imaging with Viviren substrate).

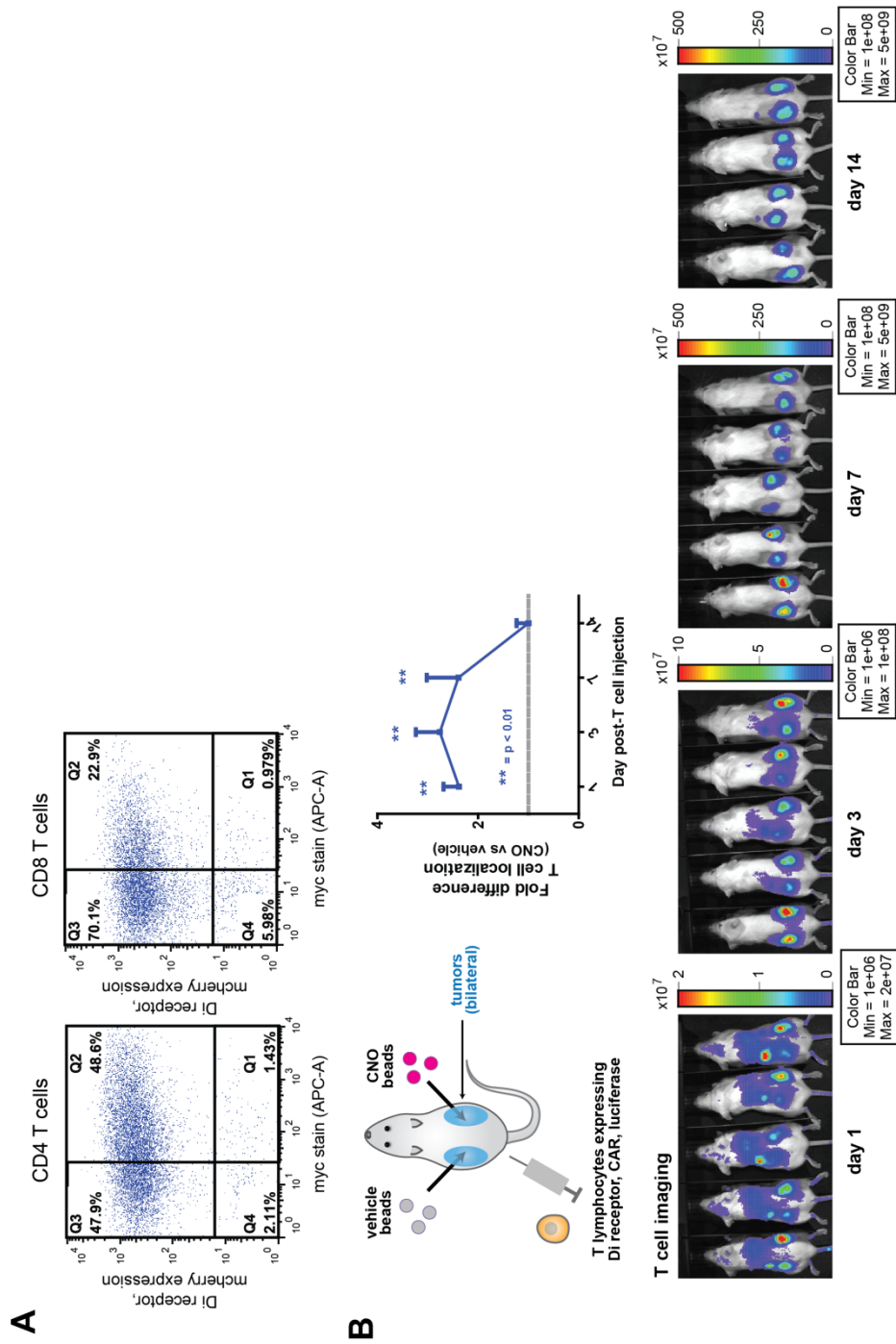


Figure 3.6. Anti-CD19 CAR- and Di receptor-transduced primary T cells preferentially localize to rLuc/Daudi tumors (right flank) injected with CNO microspheres relative to tumors in the contralateral flank (left) injected vehicle control microspheres. A) Primary human CD4 and CD8 T cells lentivirally transduced with firefly luciferase, mCherry-tagged Di receptor, and myc-tagged chimeric antigen receptor constructs were stained with fluorescent anti-myc antibody and assayed by flow cytometry. B) T cells visualized by bioluminescent imaging (D-luciferin substrate)

References

1. S. A. Rosenberg, Raising the bar: the curative potential of human cancer immunotherapy., *Science translational medicine* **4**, 127ps8 (2012).
2. M. E. Dudley, J. R. Wunderlich, T. E. Shelton, J. Even, S. A. Rosenberg, Generation of tumor-infiltrating lymphocyte cultures for use in adoptive transfer therapy for melanoma patients., *Journal of immunotherapy (Hagerstown, Md. : 1997)* **26**, 332–42 (2003).
3. T. L. Whiteside, Signaling defects in T lymphocytes of patients with malignancy., *Cancer immunology, immunotherapy : CII* **48**, 346–52 (1999).
4. N. Monu, A. B. Frey, Suppression of proximal T cell receptor signaling and lytic function in CD8+ tumor-infiltrating T cells., *Cancer research* **67**, 11447–54 (2007).
5. N. Demotte *et al.*, Restoring the association of the T cell receptor with CD8 reverses anergy in human tumor-infiltrating lymphocytes., *Immunity* **28**, 414–24 (2008).
6. T. M. Clay *et al.*, Efficient Transfer of a Tumor Antigen-Reactive TCR to Human Peripheral Blood Lymphocytes Confers Anti-Tumor Reactivity, *J. Immunol.* **163**, 507–513 (1999).
7. Z. Eshhar, T. Waks, G. Gross, D. G. Schindler, Specific activation and targeting of cytotoxic lymphocytes through chimeric single chains consisting of antibody-binding domains and the gamma or zeta subunits of the immunoglobulin and T-cell receptors., *Proceedings of the National Academy of Sciences of the United States of America* **90**, 720–4 (1993).
8. B. Irving, A. Weiss, The cytoplasmic domain of the T cell receptor chain is sufficient to couple to receptor-associated signal transduction pathways, *Cell* **64**, 891–901 (1991).
9. C. J. Turtle, M. Hudecek, M. C. Jensen, S. R. Riddell, Engineered T cells for anti-cancer therapy., *Current opinion in immunology* **24**, 633–9 (2012).
10. K. J. Curran, H. J. Pegram, R. J. Brentjens, Chimeric antigen receptors for T cell immunotherapy: current understanding and future direction, *The Journal of Gene Medicine* (2012) (available at <http://onlinelibrary.wiley.com/doi/10.1002/jgm.2604/abstract>).
11. M. Kalos, Muscle CARs and TcRs: turbo-charged technologies for the (T cell) masses., *Cancer immunology, immunotherapy : CII* , 127–135 (2011).
12. T. S. Park, S. a Rosenberg, R. a Morgan, Treating cancer with genetically engineered T cells., *Trends in biotechnology* **29**, 550–557 (2011).
13. P. J. Cohen, M. T. Lotze, J. R. Roberts, S. A. Rosenberg, E. S. Jaffe, The immunopathology of sequential tumor biopsies in patients treated with interleukin-2.

- Correlation of response with T-cell infiltration and HLA-DR expression., *The American journal of pathology* **129**, 208–16 (1987).
14. J. T. Rubin, L. J. Elwood, S. A. Rosenberg, M. T. Lotze, Immunohistochemical correlates of response to recombinant interleukin-2-based immunotherapy in humans., *Cancer research* **49**, 7086–92 (1989).
 15. D. J. Cole *et al.*, Histopathological analysis of metastatic melanoma deposits in patients receiving adoptive immunotherapy with tumor-infiltrating lymphocytes., *Cancer immunology, immunotherapy: CII* **38**, 299–303 (1994).
 16. B. A. Pockaj *et al.*, Localization of 111indium-labeled tumor infiltrating lymphocytes to tumor in patients receiving adoptive immunotherapy. Augmentation with cyclophosphamide and correlation with response., *Cancer* **73**, 1731–7 (1994).
 17. M. Ogawa *et al.*, Enhanced induction of very late antigen 4/lymphocyte function-associated antigen 1-dependent T-cell migration to tumor sites following administration of interleukin 12., *Cancer research* **57**, 2216–22 (1997).
 18. M. Erreni *et al.*, Expression of chemokines and chemokine receptors in human colon cancer., *Methods in enzymology* **460**, 105–21 (2009).
 19. J. Galon *et al.*, Type, density, and location of immune cells within human colorectal tumors predict clinical outcome., *Science (New York, N.Y.)* **313**, 1960–4 (2006).
 20. F. Pagès *et al.*, Effector memory T cells, early metastasis, and survival in colorectal cancer., *The New England journal of medicine* **353**, 2654–66 (2005).
 21. H. Musha *et al.*, Selective infiltration of CCR5(+)CXCR3(+) T lymphocytes in human colorectal carcinoma., *International journal of cancer. Journal international du cancer* **116**, 949–56 (2005).
 22. M. Ohta *et al.*, The high expression of Fractalkine results in a better prognosis for colorectal cancer patients., *International journal of oncology* **26**, 41–7 (2005).
 23. M. Tosolini *et al.*, Clinical impact of different classes of infiltrating T cytotoxic and helper cells (Th1, th2, treg, th17) in patients with colorectal cancer., *Cancer research* **71**, 1263–71 (2011).
 24. M. S. Mitchell *et al.*, Phase I trial of adoptive immunotherapy with cytolytic T lymphocytes immunized against a tyrosinase epitope., *Journal of clinical oncology: official journal of the American Society of Clinical Oncology* **20**, 1075–86 (2002).
 25. R. J. Buckanovich *et al.*, Endothelin B receptor mediates the endothelial barrier to T cell homing to tumors and disables immune therapy., *Nature medicine* **14**, 28–36 (2008).
 26. S. A. Rosenberg *et al.*, Treatment of Patients With Metastatic Melanoma With Autologous Tumor-Infiltrating Lymphocytes and Interleukin 2, *JNCI Journal of the National Cancer Institute* **86**, 1159–1166 (1994).

27. B. Homey, A. Müller, A. Zlotnik, Chemokines: agents for the immunotherapy of cancer?, *Nature reviews. Immunology* **2**, 175–84 (2002).
28. S. Chada, R. Ramesh, A. M. Mhashilkar, Cytokine- and chemokine-based gene therapy for cancer., *Current opinion in molecular therapeutics* **5**, 463–74 (2003).
29. M. H. Kershaw *et al.*, Redirecting migration of T cells to chemokine secreted from tumors by genetic modification with CXCR2., *Human gene therapy* **13**, 1971–80 (2002).
30. X. Yang, Y. Chu, Y. Wang, R. Zhang, S. Xiong, Targeted in vivo expression of IFN-gamma-inducible protein 10 induces specific antitumor activity., *Journal of leukocyte biology* **80**, 1434–44 (2006).
31. E. K. Moon *et al.*, Expression of a functional CCR2 receptor enhances tumor localization and tumor eradication by retargeted human T cells expressing a mesothelin-specific chimeric antibody receptor., *Clinical cancer research : an official journal of the American Association for Cancer Research* **17**, 4719–30 (2011).
32. H. E. Heslop, Safer CARs., *Molecular therapy : the journal of the American Society of Gene Therapy* **18**, 661–2 (2010).
33. H. Harlin *et al.*, Chemokine expression in melanoma metastases associated with CD8+ T-cell recruitment., *Cancer research* **69**, 3077–85 (2009).
34. F. Vianello *et al.*, Murine B16 melanomas expressing high levels of the chemokine stromal-derived factor-1/CXCL12 induce tumor-specific T cell chemorepulsion and escape from immune control., *Journal of immunology (Baltimore, Md. : 1950)* **176**, 2902–14 (2006).
35. C. E. Brown *et al.*, Tumor-derived chemokine MCP-1/CCL2 is sufficient for mediating tumor tropism of adoptively transferred T cells., *Journal of immunology (Baltimore, Md. : 1950)* **179**, 3332–41 (2007).
36. R. A. Kurt, A. Baher, K. P. Wisner, S. Tackitt, W. J. Urba, Chemokine receptor desensitization in tumor-bearing mice., *Cellular immunology* **207**, 81–8 (2001).
37. B. P. Barna *et al.*, Regulation of monocyte chemoattractant protein-1 expression in adult human non-neoplastic astrocytes is sensitive to tumor necrosis factor (TNF) or antibody to the 55-kDa TNF receptor, *Journal of Neuroimmunology* **50**, 101–107 (1994).
38. Z. Brown *et al.*, IL-1 receptor antagonist inhibits monocyte chemotactic peptide 1 generation by human mesangial cells, *Kidney International* **42**, 95–101 (1992).
39. S. D. Cushing, Minimally Modified Low Density Lipoprotein Induces Monocyte Chemotactic Protein 1 in Human Endothelial Cells and Smooth Muscle Cells, *Proceedings of the National Academy of Sciences* **87**, 5134–5138 (1990).
40. T. J. Standiford, S. L. Kunkel, S. H. Phan, B. J. Rollins, R. M. Strieter, Alveolar macrophage-derived cytokines induce monocyte chemoattractant protein-1 expression

from human pulmonary type II-like epithelial cells., *J. Biol. Chem.* **266**, 9912–9918 (1991).

41. S. L. Deshmane, S. Kremlev, S. Amini, B. E. Sawaya, Monocyte Chemoattractant Protein-1 (MCP-1): An Overview, (2010) (available at <http://online.liebertpub.com/doi/abs/10.1089/jir.2008.0027>).

42. S. G. Peisajovich, J. E. Garbarino, P. Wei, W. A. Lim, Rapid diversification of cell signaling phenotypes by modular domain recombination., *Science (New York, N.Y.)* **328**, 368–72 (2010).

43. A. M. Loening, A. M. Wu, S. S. Gambhir, Red-shifted Renilla reniformis luciferase variants for imaging in living subjects., *Nature methods* **4**, 641–3 (2007).

44. L. D. Shultz *et al.*, Human lymphoid and myeloid cell development in NOD/LtSz-scid IL2R gamma null mice engrafted with mobilized human hemopoietic stem cells., *Journal of immunology (Baltimore, Md. : 1950)* **174**, 6477–89 (2005).

45. L. D. Shultz, F. Ishikawa, D. L. Greiner, Humanized mice in translational biomedical research., *Nature reviews. Immunology* **7**, 118–30 (2007).

46. B. A. Rabinovich *et al.*, Visualizing fewer than 10 mouse T cells with an enhanced firefly luciferase in immunocompetent mouse models of cancer., *Proceedings of the National Academy of Sciences of the United States of America* **105**, 14342–6 (2008).

47. J. M. Karp, G. S. Leng Teo, Mesenchymal stem cell homing: the devil is in the details., *Cell stem cell* **4**, 206–16 (2009).

48. J. A. Craddock *et al.*, Enhanced tumor trafficking of GD2 chimeric antigen receptor T cells by expression of the chemokine receptor CCR2b., *Journal of immunotherapy (Hagerstown, Md. : 1997)* **33**, 780–8 (2010).

49. A. Di Stasi *et al.*, T lymphocytes coexpressing CCR4 and a chimeric antigen receptor targeting CD30 have improved homing and antitumor activity in a Hodgkin tumor model., *Blood* **113**, 6392–402 (2009).

50. J. J. Onuffer, R. Horuk, Chemokines, chemokine receptors and small-molecule antagonists: recent developments., *Trends in pharmacological sciences* **23**, 459–67 (2002).

51. J.-M. Guettier *et al.*, A chemical-genetic approach to study G protein regulation of beta cell function in vivo., *Proceedings of the National Academy of Sciences of the United States of America* **106**, 19197–202 (2009).

52. W.-H. Chang *et al.*, Reversible metabolism of clozapine and clozapine N-oxide in schizophrenic patients, *Progress in Neuro-Psychopharmacology and Biological Psychiatry* **22**, 723–739 (1998).

Chapter 4. Building a “pause” safety switch for safer T cell therapeutics

Introduction

Bacterial pathogens and their mechanisms of virulence are of growing interest, both because of emerging infectious disease and biosecurity threats. However, we realize that pathogens could also actually be very useful tools for beneficial synthetic biology applications. For example, many proteins from type III secretion system bacterial pathogens interface with MAP kinase pathways as a mechanisms to suppress and evade the immune response (these bacteria are essentially naturally evolved synthetic biologists). While these pathogen effector proteins are important for virulence, it also seems logical that these proteins could be very useful for synthetic biology - particularly for interfacing with and precisely modulating MAPK signaling in various organisms, ranging from biotechnological cells like yeast, to biomedical cells, such as immune cells engineered for adoptive immunotherapy. Pathways like MAPK cascades, which are the targets of many pathogen factors, are widespread in all eukaryotes and control critical growth, differentiation, immune, and stress responses.

In the manuscript that comprises this chapter, we explored the usage of two bacterial pathogen proteins, OspF from *Shigella*, and YopH from *Yersinia Pestis*, as reagents to precisely modulate MAPK signaling, both in yeast and human immune cells. We showed that:

- The effector proteins can be used to block specific steps in a pathway (akin to using small molecular inhibitors as analytical tools).

- The effector proteins can be artificially targeted to distinct signaling complexes, thereby controlling the selectivity of the physiological MAPK pathways that they modulate
- Unique properties of the effector proteins can be used to engineer new cellular behaviors - e.g. frequency dependent signaling. For example, we show that because of the irreversible nature of the reaction catalyzed by OspF, synthetic negative feedback loops built with this protein can result in strong frequency dependent input filtering.
- These bacterial effector proteins can be used to precisely modulate T cell activation. They can block it (like an inhibitor) if constitutively expressed; they can limit the amplitude of T cell activation if used in synthetic negative feedback control loops; and they can transiently pause T cell activation, if they are inducibly expressed. All of these properties could be useful tools in engineering precisely controlled therapeutic T cells used in adoptive immunotherapy, where a classic problem is being able to balance the targeted immune response (e.g. towards tumor or chronic infection) with non-specific autoimmune-like side effects.

This work was published in *Nature* in 2012.

Ping Wei, Wilson W. Wong, Jason S. Park, Ethan E. Corcoran, Sergio G. Peisajovich, James J. Onuffer, Arthur Weiss, and Wendell A. Lim. Bacterial virulence proteins as tools to rewire kinase pathways in yeast and immune cells. *Nature*, 488(7411), 384-388 (2012).

Bacterial Virulence Proteins as Tools to Rewire Kinase Pathways in Yeast and Immune Cells

Ping Wei^{1,2*}, Wilson W. Wong^{1,2,3*}, Jason S. Park^{1,2,3}, Ethan E. Corcoran^{2,3,4}, Sergio G. Peisajovich^{1,2}, James J. Onuffer^{1,3}, Arthur Weiss^{2,3,4}, Wendell A. Lim^{1,2,3‡}

¹Department of Cellular & Molecular Pharmacology

²Howard Hughes Medical Institute

³The Cell Propulsion Lab

⁴Department of Medicine

University of California San Francisco

San Francisco, CA 94158

* These authors contributed equally to this manuscript

‡To whom correspondence should be addressed: lim@cmp.ucsf.edu

Current Addresses

W.W. Wong – Department of Biomedical Engineering, Boston University.
wilwong@bu.edu

E.E. Corcoran – Department of Pulmonology and Critical Care Medicine, Northwest Permanente PC. Ethan.E.Corcoran@kp.org

S.G. Peisajovich – Department of Cell & Systems Biology, University of Toronto.
sergio.peisajovich@utoronto.ca

ABSTRACT

Bacterial pathogens have evolved specific effector proteins that, by interfacing with host kinase signaling pathways, provide a mechanism to evade immune responses during infection^{1,2}. Although these effectors are responsible for pathogen virulence, we realized that they might also serve as valuable synthetic biology reagents for engineering cellular behavior. Here, we have exploited two effector proteins, the *Shigella flexneri* OspF protein³ and *Yersinia pestis* YopH protein⁴, to systematically rewire kinase-mediated responses in both yeast and mammalian immune cells. Bacterial effector proteins can be directed to selectively inhibit specific mitogen activated protein kinase (MAPK) pathways in yeast by artificially targeting them to pathway specific complexes. Moreover, we show that unique properties of the effectors generate novel pathway behaviors: OspF, which irreversibly inactivates MAPKs⁴, was used to construct a synthetic feedback circuit that displays novel frequency-dependent input filtering. Finally, we show that effectors can be used in T cells, either as feedback modulators to precisely tune the T cell response amplitude, or as an inducible pause switch that can temporarily disable T cell activation. These studies demonstrate how pathogens could provide a rich toolkit of parts to engineer cells for therapeutic or biotechnological applications.

Many bacterial pathogens have developed an array of effector proteins to rewire host signaling networks and down-regulate the immune response ²(**Fig. 1a**). Some effectors mimic host activities, such as the *Yersinia pestis* effector YopH, which is a highly active phosphotyrosine phosphatase³. Other effectors utilize unusual mechanisms, such as the *Shigella flexneri* OspF protein, which irreversibly inactivates MAP kinases by catalyzing a β -elimination reaction that removes the hydroxyl group of the key phospho-threonine side chain⁴.

MAPK pathways play a central role in diverse eukaryotic responses, ranging from immune response to cell fate decisions^{5,6}. Thus, the ability to tune MAPK response would facilitate engineering cells for diverse therapeutic and biotechnological applications^{7,8}. Recent work has shown that MAPK signaling dynamics in yeast can be reshaped with synthetic feedback loops that involve controlled expression and targeting of pathway modulators to appropriate signaling complexes⁹. Identifying effective pathway modulators is challenging, and thus we hypothesized that pathogen effector proteins may have untapped utility as components for predictably and systematically engineering signaling pathways. Here, we use the effector proteins OspF and YopH to modulate kinase signaling pathways in yeast and in human primary T cells.

We first introduced OspF into yeast. As reported¹⁰, overexpression of OspF led to growth inhibition under standard conditions, hyperosmotic stress conditions (**Fig. 1b**), and cell wall damaging conditions (**Supplementary Fig. 1a**). OspF contains a

canonical docking peptide at its N-terminus that allows it to bind multiple MAPK's in yeast¹¹. We found that expression of an OspF mutant lacking its native docking peptide (Δ N-OspF) yielded normal growth behavior under all conditions (**Fig. 1b**, **Supplementary Fig. 1a**). Next we tested whether Δ N-OspF could be redirected to a specific pathway by tagging the protein with a leucine zipper heterodimerization motif, and fusing the complementary interacting motif to Pbs2, the scaffold protein that organizes the osmolarity MAPK pathway. This targeted version of Δ N-OspF only displayed a growth defect under high salt conditions, showing that OspF activity could be engineered to inhibit a specific MAPK (**Fig. 1b**).

To further explore re-targeting OspF to specific pathways, we engineered yeast strains in which Δ N-OspF was selectively targeted to either the osmolarity MAPK complex or the mating MAPK complex (by targeting it to the mating pathway scaffold protein, Ste5) (**Fig. 1c**). Targeting of Δ N-OspF to the Pbs2 inhibited the osmolarity response but not the mating response. Conversely, when Δ N-OspF was targeted to Ste5, only the mating response was inhibited. Thus, the inhibitory activity of this effector could be selectively aimed at one of several MAPK pathways in the same cell.

One of the unique aspects of OspF is that it catalyzes an irreversible inactivation of MAPKs (unlike reversible dephosphorylation by a phosphatase). Thus MAPK activity can only be restored through new protein synthesis, which has a much slower timescale than re-phosphorylation (**Fig. 2a and Fig. 2b**). This longer timescale would

be expected to lead to an extended refractory period after OspF action, during which the targeted MAPK pathway could no longer respond to subsequent stimuli.

Computational simulations indicated that a long refractory period could result in significant changes to the frequency-dependent behavior of pathway response (**Supplementary Fig. 2**). There is growing evidence that cells use frequency modulation of diverse molecular events to encode and transmit information^{12,13}. Our models indicated that with a negative feedback loop (i.e. MAPK activity induced expression of OspF) to “filter out” pathway activation, pathway output would be dampened when input periods are long enough to accumulate significant amounts of the negative effector but shorter than the refractory period (**Supplementary Fig. 2**).

To test if OspF could be used to filter frequency dependent inputs, we constructed a synthetic negative feedback loop in the yeast osmo-response pathway by expressing OspF targeted to the osmo-response signaling complex (Δ N-OspF-zipper) from the Hog1 responsive promoter, *pSTL1* (**Fig. 2c**). As a comparison, we also engineered an analogous synthetic feedback loop using a reversible Hog1 MAPK inhibitory protein -- the yeast MAPK phosphatase, PTP2. Phospho-Hog1 translocation to the nucleus was used as a fast-timescale output reporter (**Supplementary Fig. 3**)¹⁴⁻¹⁶. To measure integrated output over a longer timescale, we also measured a slower timescale transcriptional reporter -- expression of mCherry from the *pSTL1* promoter.

We found that the OspF-mediated negative feedback circuit altered the osmostress pathway response to intermediate frequency stimulation, but not to continuous stress or to high frequency stimulation (**Fig. 2d, Supplementary Fig. 4a**). Furthermore, in the course of stimulating cells with pulses of KCl of varying length, we discovered that an input period of ~16 minutes (intermediate frequency) leads to highly divergent transcriptional responses (**Fig. 2d**). Examination of Hog1 nuclear import in the OspF feedback strain shows that after 3 pulses, the amount of Hog1 competent for nuclear localization has decreased to near zero, consistent with a model in which - in this timeframe - there is sufficient OspF to inactivate the bulk of the Hog1 population and to now render the cells refractory to further pulses of stimulation. The cells containing a PTP2 negative feedback circuit do not show this dramatic filtering at this frequency. With higher frequency stimulation (2 min period), the three strains also do not significantly differ from each other in response, presumably because there is inadequate activation time with each pulse to build up a sufficient concentration of effector¹⁷.

A broad frequency dependence analysis shows that the wild-type osmo-response pathway functions as a band pass filter, with maximal response at intermediate frequencies, while the engineered pathway more closely resembles a low pass filter, with maximal responses at low frequency (**Fig. 2e**). These distinct frequency filtering behaviors fit those predicted by computational simulations (**Supplementary Fig. 2d**).

We then sought to test whether these bacterial effectors could be used to rewire signaling in immune cells. Human T cells are an attractive synthetic biology platform because they can be isolated from patients, genetically engineered *ex vivo*, and then transferred back into patients to treat cancer and chronic infection^{18,19}. While promising, the therapeutic application of engineered T cells carry risks of adverse side effects including inadvertent autoimmune-like attack of off-target host tissues^{20,21}. Thus mechanisms to control the specificity, amplitude and timing of T cell function are critical to balance therapeutic action against off-target toxicity.

Both OspF and YopH can modify the T cell receptor (TCR) pathway (**Fig. 3a**). OspF inactivates the MAPK ERK, which is a central component of TCR signaling^{4,22}, while YopH dephosphorylates phospho-tyrosine, including the T cell scaffold proteins LAT and SLP-76²³. Constitutive expression of YopH and OspF in *Jurkat* T cells leads to severe inhibition of TCR activation, as measured by an NFAT transcriptional reporter²⁴ (**Fig. 3a**) (as well as other reporters of T cell activation –**Supplementary Fig. 5a**). Expression of the catalytic dead versions of YopH and OspF had no effect on the TCR activation (**Supplementary Fig. 5b**). In addition, we showed that these two effectors clearly target distinct steps of the T cell activation pathway, since induction of the T cells with the combination of phorbol 12-myristate 13-acetate (PMA) and ionomycin, which activates the T cell downstream of the PLC γ 1-LAT/SLP76 dependent response, bypassed YopH inhibition²⁵, but was sensitive to OspF inhibition (**Fig. 3a**,

Supplementary Fig. 5a). Thus, distinct pathogen effector proteins can be used to block this pathway at particular steps, much like a specific small molecule inhibitor.

Given the ability of OspF and YopH to modulate T cell responses, we sought to use these proteins to build circuits that could, in principle, improve the safety of therapeutic T cells. In adoptive T cell therapy, a challenge is to limit over-activation or off-target activation of T cells that could lead to killing of host cells or to cytokine storm – a life-threatening immune response. One approach is to incorporate a safety “kill switch”²⁶⁻²⁸ into the T cells, such as the herpes simplex virus thymidine kinase (HSV TK) gene. This protein converts the pro-drug ganciclovir into an inhibitor of replication, thus killing cells expressing the gene. While HSV TK is currently being tested in a phase III clinical trial for the treatment of graft vs. host disease in bone marrow transplants, this strategy irreversibly destroys the engineered, adoptively transferred cells²⁹. Thus instead of killing the engineered cells, we sought to design circuits that would limit the amplitude of the T cell response or to temporarily pause T cell activity.

We first tested whether bacterial effectors could be used to limit the response amplitude of *Jurkat* T cells. Negative feedback loops can act to limit the maximal amplitude of a response³⁰, so we engineered a library of negative feedback loops in which the OspF and YopH were expressed from a series of TCR responsive promoters of varying strength (AP1 and NFAT) (**Fig. 3b, Supplementary Fig. 7**). For further tuning of feedback parameters, we also tagged effectors with degradation sequences (PEST

motif) that reduce half-life of the effectors. This series of negative feedback loops led to controlled reduction of the maximal response amplitude of T cell activation (**Fig. 3b**). Moreover, the amplitude could be tuned systematically by varying feedback promoter strength and effector stability (**Supplementary Fig. 7b**). For example, expression of OspF from the strong feedback (*pNFAT*) promoter leads to a very low maximal response amplitude, but this effect could be systematically tuned by destabilizing the OspF effector with a PEST tag.

We also tested whether the bacterial effectors could be used to construct pause switches, which could transiently and reversibly, disable T cells. We placed the effectors under the control of a tetracycline inducible promoter (*pTRE*), which allowed external control of the timing of effector expression with the addition of doxycycline. Effectors were fused to a destabilization domain so that they would be rapidly degraded once doxycycline is removed. Using this system, we first showed that transient expression of bacterial effectors can inhibit TCR signaling after the pathway is activated in *Jurkat* T cells (**Fig. 3c**). TCR signaling can be inhibited up to 6 hours after activation using this approach (**Supplementary Fig. 8b**). Finally, we showed that engineered T cells can be subjected to cycles of TCR activation, pausing with a short period of induced expression of the bacterial effector, and then reactivated after this pause (**Supplementary Fig. 8c**).

We then tested the pause switch in a clinically important cell type for adoptive immunotherapy - primary human CD4⁺ T cells (in contrast to the *Jurkat* T cell line, which does not require cytokine or TCR activation to stimulate proliferation). We showed that when OspF is induced by the addition of doxycycline, both IL-2 release and cell proliferation were inhibited in a dose-dependent manner (**Fig. 4b, 4c**). Activation of the TCR by anti-CD3/CD28 and antigen presenting cells can also be inhibited by expression of OspF (**Supplementary Fig. 9a**). Moreover, after dox is removed, IL-2 release and cell division recovers within 6-18 hours (**Fig. 4d, 4e**). Sustained dox exposure can inhibit T cell activity over the course of several days (**Fig. 4e**) without having any significant effect on cell viability (**Supplementary Fig. 9c**). Thus this work provides a proof of principle for the design of a simple “pause” switch that could allow external control over the timing and level of T cell activation and cytokine release, in order to minimize adverse events associated with adoptive immunotherapy such as cytokine storm.

Most work on bacterial pathogen effector proteins has the long-term aim of neutralizing the pathogens’ infectious capabilities. We have shown, however, that bacterial effectors can also be valuable synthetic biology tools, because of their unique biochemical properties. We have employed bacterial effectors to modulate MAPK signaling in yeast to generate novel time-dependent dynamics. We also showed that bacterial effectors

can be used to flexibly tune human T cell receptor signaling dynamics, with potential application as safety switches for adoptive immunotherapy. The vast array of bacterial pathogen effector proteins, beyond those studied here, holds promise as a rich and important source of parts for the cellular engineering toolkit.

METHODS SUMMARY

Flow cytometry experiments

Analysis of the pathway-dependent fluorescent proteins (GFP and mCherry) expression in yeast cells and phosphorylated ERK in *Jurkat* T cells were performed with the BD LSRII flow cytometer (BD Biosciences) equipped with a high-throughput sampler. 1.5 μ M of α -factor (GenScript) or 0.4 M of KCl were added into yeast cultures to induce separately the mating-specific or osmo-specific pathway response. For staining of phosphorylated ERK in *Jurkat* T cell, cells were fixed, made permeable by incubation with ice-cold 90% methanol on ice for 30 minutes and stained with primary antibody to phosphorylated ERK (Cell Signaling) and anti-rabbit APC secondary antibody (Jackson Immunoresearch).

Microfluidics and fluorescent microscopy

Mircofluidic yeast cell culture was performed in Y04C plate with ONIX flow control system (Cellasic Corp). Cells were loaded into the flow chamber pre-coated with concanavalin A. Pulse stimulation with salt media was performed by ONIX FG flow control software (Cellasic Corp) with the flow pressure of 8 psi. Image acquisition was performed with a TE2000-E automated inverted microscope (Nikon) with Perfect Focus and 100x oil immersion lens. The image analysis for both nuclear Hog1-GFP import

and *pSTLL1*-mCherry expression was performed with custom Matlab (Mathworks) software.

Human T cell activation assay

Resting human primary CD4⁺ cells (transduced with the pause switch constructs or untransduced) were pretreated with 200 ng/ml doxycycline for 6 hours. 50,000 cells were placed in a 96-well plate with 200 μ L human growth media with activation agents added (10 ng/mL PMA + 0.5 μ M ionomycin, magnetic Dynabeads coated with anti-CD3/anti-CD28 (beads/cells ratio, 0.3:1)). After 24 hours of incubation at 37°C, the released IL-2 in the supernatant was measured with the human IL-2 ELISA kit II (BD Biosciences). Cells labeled with CellTrace Violet dye (Invitrogen) were assayed by flow cytometry after 4 days incubation to quantitate cell proliferation.

Full Methods and any associated references are available in the online version of the paper at www.nature.com/nature.

References

- 1 Ribet, D. & Cossart, P., Pathogen-mediated posttranslational modifications: A re-emerging field. *Cell* 143 (5), 694-702 (2010).
- 2 Broberg, C.A. & Orth, K., Tipping the balance by manipulating post-translational modifications. *Curr Opin Microbiol* 13 (1), 34-40 (2010).
- 3 Zhang, Z.Y. *et al.*, Expression, purification, and physicochemical characterization of a recombinant Yersinia protein tyrosine phosphatase. *J Biol Chem* 267 (33), 23759-23766 (1992).
- 4 Li, H. *et al.*, The phosphothreonine lyase activity of a bacterial type III effector family. *Science* 315 (5814), 1000-1003 (2007).
- 5 Shaw, A.S. & Filbert, E.L., Scaffold proteins and immune-cell signalling. *Nat Rev Immunol* 9 (1), 47-56 (2009).
- 6 Dong, C., Davis, R.J., & Flavell, R.A., MAP kinases in the immune response. *Annu Rev Immunol* 20, 55-72 (2002).
- 7 Khalil, A.S. & Collins, J.J., Synthetic biology: applications come of age. *Nat Rev Genet* 11 (5), 367-379 (2010).
- 8 Purnick, P.E. & Weiss, R., The second wave of synthetic biology: from modules to systems. *Nat Rev Mol Cell Biol* 10 (6), 410-422 (2009).
- 9 Bashor, C.J., Helman, N.C., Yan, S., & Lim, W.A., Using engineered scaffold interactions to reshape MAP kinase pathway signaling dynamics. *Science* 319 (5869), 1539-1543 (2008).
- 10 Kramer, R.W. *et al.*, Yeast functional genomic screens lead to identification of a role for a bacterial effector in innate immunity regulation. *PLoS pathogens* 3 (2), e21 (2007).
- 11 Zhu, Y. *et al.*, Structural insights into the enzymatic mechanism of the pathogenic MAPK phosphothreonine lyase. *Molecular cell* 28 (5), 899-913 (2007).
- 12 Nelson, D.E. *et al.*, Oscillations in NF-kappaB signaling control the dynamics of gene expression. *Science* 306 (5696), 704-708 (2004).
- 13 Cai, L., Dalal, C.K., & Elowitz, M.B., Frequency-modulated nuclear localization bursts coordinate gene regulation. *Nature* 455 (7212), 485-490 (2008).
- 14 Muzzey, D., Gomez-Uribe, C.A., Mettetal, J.T., & van Oudenaarden, A., A systems-level analysis of perfect adaptation in yeast osmoregulation. *Cell* 138 (1), 160-171 (2009).
- 15 Mettetal, J.T., Muzzey, D., Gomez-Uribe, C., & van Oudenaarden, A., The frequency dependence of osmo-adaptation in *Saccharomyces cerevisiae*. *Science* 319 (5862), 482-484 (2008).

- 16 Hersen, P., McClean, M.N., Mahadevan, L., & Ramanathan, S., Signal processing
by the HOG MAP kinase pathway. *Proc Natl Acad Sci U S A* 105 (20),
7165-7170 (2008).
- 17 Pelet, S. *et al.*, Transient activation of the HOG MAPK pathway regulates
bimodal gene expression. *Science* 332 (6030), 732-735 (2011).
- 18 Morgan, R.A., Dudley, M.E., & Rosenberg, S.A., Adoptive cell therapy: genetic
modification to redirect effector cell specificity. *Cancer J* 16 (4), 336-341 (2010).
- 19 June, C.H., Blazar, B.R., & Riley, J.L., Engineering lymphocyte subsets: tools,
trials and tribulations. *Nat Rev Immunol* 9 (10), 704-716 (2009).
- 20 Morgan, R.A. *et al.*, Case report of a serious adverse event following the
administration of T cells transduced with a chimeric antigen receptor recognizing
ERBB2. *Mol Ther* 18 (4), 843-851 (2010).
- 21 Brentjens, R., Yeh, R., Bernal, Y., Riviere, I., & Sadelain, M., Treatment of
chronic lymphocytic leukemia with genetically targeted autologous T cells: case
report of an unforeseen adverse event in a phase I clinical trial. *Mol Ther* 18 (4),
666-668 (2010).
- 22 Arbibe, L. *et al.*, An injected bacterial effector targets chromatin access for
transcription factor NF-kappaB to alter transcription of host genes involved in
immune responses. *Nat Immunol* 8 (1), 47-56 (2007).
- 23 Gerke, C., Falkow, S., & Chien, Y.H., The adaptor molecules LAT and SLP-76
are specifically targeted by *Yersinia* to inhibit T cell activation. *J Exp Med* 201
(3), 361-371 (2005).
- 24 Lin, J. & Weiss, A., The tyrosine phosphatase CD148 is excluded from the
immunologic synapse and down-regulates prolonged T cell signaling. *J Cell Biol*
162 (4), 673-682 (2003).
- 25 Yao, T., Mecsas, J., Healy, J.I., Falkow, S., & Chien, Y., Suppression of T and B
lymphocyte activation by a *Yersinia pseudotuberculosis* virulence factor, yopH. *J*
Exp Med 190 (9), 1343-1350 (1999).
- 26 Kieback, E., Charo, J., Sommermeyer, D., Blankenstein, T., & Uckert, W., A
safeguard eliminates T cell receptor gene-modified autoreactive T cells after
adoptive transfer. *Proc Natl Acad Sci U S A* 105 (2), 623-628 (2008).
- 27 de Witte, M.A. *et al.*, An inducible caspase 9 safety switch can halt cell
therapy-induced autoimmune disease. *J Immunol* 180 (9), 6365-6373 (2008).
- 28 Bonini, C. *et al.*, The suicide gene therapy challenge: how to improve a successful
gene therapy approach. *Mol Ther* 15 (7), 1248-1252 (2007).
- 29 Ciceri, F. *et al.*, Infusion of suicide-gene-engineered donor lymphocytes after
family haploidentical haemopoietic stem-cell transplantation for leukaemia (the
TK007 trial): a non-randomised phase I-II study. *Lancet Oncol* 10 (5), 489-500
(2009).

³⁰ Brandman, O. *et al.*, Feedback loops shape cellular signals in space and time. *Science* 322 (5900), 390-395 (2008).

Supplementary Information is linked to the online version of the paper at www.nature.com/nature.

Acknowledgements

We thank K. Orth for the YopH plasmid; K. McNally and S. Neou for tissue culture support; H. El-Samad, C. Voigt, C. Tang and the Lim lab for helpful discussions. We acknowledge the 2007 UCSF iGEM team (M. Chen, E. Chou, J. Huang, L. Jann, E. Meltzer, A. Ng, and R. Ovadia) for their initial work on bacterial effectors in yeast.

Supported by an American Cancer Society fellowship (W.W.W), a Li Foundation Fellowship (P.W.), a California Institute for Regenerative Medicine fellowship (Grant Number TG2-01153) (J.S.P.), NIH grants PN2EY016546, RO1GM055040, RO1GM062583, and P50GM081879 (W.A.L.), the NSF Synthetic Biology and Engineering Research Center (W.A.L.), the Packard Foundation (W.A.L.), and the Howard Hughes Medical Institute (A.W. and W.A.L.).

Author Contributions

P.W., S.P. and W.L. initiated project in yeast. W.W, E.C. A.W, and W.L initiated the project in T cells. P.W., W.W. and W.L wrote the paper. P.W. and S.P. performed the

experiments in yeast. W.W, P.W., E.C., J.O. and J.P performed the experiment in T cells.

Author Information

Reprints and permissions information is available at www.nature.com/reprints. The authors declare no competing financial interests. Readers are welcome to comment on the online version of this article at www.nature.com/nature. Correspondence and requests for materials should be addressed to W.L. (lim@cmp.ucsf.edu).

Figure Legends

Figure 1. Bacterial effector OspF can block selective MAP kinase pathways in yeast. **a**, Type III secretion effectors that modulate host kinase signaling. **b**, Targeting of OspF to yeast osmolarity pathway. Wild-type OspF impairs growth on rich media, but is rescued by docking motif deletion (Δ N-OspF). Recruitment of Δ N-OspF to osmolarity scaffold Pbs2 via leucine zipper selectively blocks growth on 1 M KCl (zipper* - mutant leucine zipper; K134A - catalytic dead mutant of OspF). **c**, Δ N-OspF selectively inhibits mating or osmolarity if targeted to appropriate scaffold complex, assayed using pathway specific transcriptional reporters. Average fluorescence and standard deviation of three experiments is shown.

Figure 2. Tuning frequency dependent response of yeast osmolarity pathway using synthetic OspF feedback loop. **a**, OspF, is MAP kinase phosphothreonine lyase. **b**, OspF irreversibly inhibits MAP kinase activity. **c**, Synthetic negative feedback loop was built by expressing OspF from osmo-inducible *pSTL1* promoter. Hog1-GFP nuclear accumulation (Nuc:Tot ratio) was measured as a fast output reporter. *pSTL1*-mCherry served as a slower, gene expression reporter. **d**, Cells were stimulated with variable frequency inputs: low (constant), high (period = 2 min) and intermediate (period = 16 min). Significant difference in response to intermediate frequency stimulation is observed. **e**, frequency-response curves for wild-type and OspF feedback strains (arrow: period = 16 min). Each point is average of 50-100 cells; standard deviation from three repeats is shown. More detail on the frequency analysis is given in Supplementary Figs. 2-4.

Figure 3. OspF can be used to precisely control T cell activation amplitude and duration in *Jurkat* T cells. **a**, Constitutively expressed OspF and YopH inhibit specific steps in the T-cell receptor pathway. Activation of NFAT transcription by anti-TCR antibody vs. PMA/ionomycin is shown. **b**, Synthetic amplitude limiters were constructed using negative feedback loops with different effectors, promoters, and degrons. Dose-response curves of the *pNFAT*-OspF circuit, with or without degron are shown. **c**, Synthetic pause switch was built by expressing OspF from a doxycycline inducible promoter, *pTRE*. A four-hour pulse induction disabled T cell response when initiated at 0 or 2 hours after T cell stimulation. Standard deviation from three samples is shown.

Figure 4. OspF can be used as a synthetic pause switch to control human primary CD4+ T cell activation. **a**, Off-target activation of transplanted T cells can induce cytokine storm in adoptive immunotherapy. A pause switch could prevent this adverse response. **b**, Six-hour pre-induction of OspF by doxycycline inhibited IL-2 release and proliferation of activated CD4+ T cells. **c**, Six-hour pre-treatment with different doses of doxycycline can tune IL-2 release. **d**, Cells treated with six-hour dox pulse were sampled at different times after the pulse, then subjected to a 24 hr IL-2 release assay or a four-day proliferation assay. **e**, IL-2 release can be inhibited either transiently or in a sustained manner by varying the duration of dox treatment. Average and standard deviation of three experimental repeats are shown.

METHODS

Yeast constructs and strains

All yeast constructs used in this study (**Supplementary Table 1**) were cloned using a combinatorial cloning strategy based on the Type II restriction enzyme AarI developed by Peisajovich et al.³¹. For the MAPK pathway specific inhibitory experiments, strains WP022 and WP116 were constructed from the W303-derived strain SP147 (**Supplementary Table 2**) by tagging the C-terminal of endogenous Pbs2 or Ste5 with leucine zipper respectively. To construct WP039 for measuring the nuclear Hog1 accumulation, the C-terminal of endogenous Hog1 in wild type W303 strain was tagged with GFP using standard integration technique. For the visualization of the nucleus, a histone protein Htb2 was C-terminally tagged with mCherry, expressed from the *ADHI* promoter, and integrated at *TRP1* locus. Endogenous Pbs2 was tagged with a leucine zipper by PCR integration and was used in synthetic feedback loops. Synthetic effector gene cassettes were integrated at the *LEU2* locus. Yeast promoters, terminator, and the PTP2 gene were PCR amplified from *Saccharomyces cerevisiae* genomic DNA (Invitrogen). YopH gene was a kind gift from Kim Orth. The OspF gene was synthesized by Integrated DNA Technologies, Inc. All yeast genomic integrations were confirmed by yeast colony PCR.

Yeast flow cytometry experiments

Analysis of the pathway-dependent fluorescent proteins (GFP and mCherry) expression in yeast cells was performed with the BD LSRII flow cytometer (BD Biosciences) equipped with a high-throughput sampler. For each experiment, triplicate cultures were grown in synthetic complete media to early log phase ($OD_{600} = 0.1 - 0.2$). At time = 0, 1.5 μ M of α -factor (GenScript) or 0.4 M of KCl were added into parallel cultures to induce separately the mating- specific or osmo-specific pathway response. For mating response, 100 μ L aliquots were taken at time = 0 and after 2 hours of induction; for osmotic response, 100 μ L aliquots were taken at time = 0 and after 1 hour of induction. Each 100 μ L sample aliquot was immediately mixed with 100 μ L of cycloheximide (10 μ g/mL) in 96-well plates to stop the protein synthesis. After incubating the samples at room temperature for 30 minutes in the dark to allow for the maturation of fluorescent proteins, the levels of fluorescence protein were determined by flow cytometry. For each read, 10,000 cells were counted, and the mean fluorescent density was calculated by Flowjo software (BD Biosciences) as the pathway output value and the standard deviation from triplicate experiments was indicated as the error bar.

Yeast microfluidics, fluorescent microscopy, and image processing

Mircofluidic yeast cell culture was performed in Y04C plate with ONIX flow control system (Cellasic Corp)³². Cultures were grown to mid-log phase ($OD_{600} = 0.2 - 0.8$) in synthetic complete media. Cells were diluted to $OD_{600} = 0.01$ in 600 μ L of fresh media and sonicated at a minimum set of 11% for 1 sec using Fisher Scientific model 500 sonicator with a 2 mm tip. Cells were loaded into the flow chamber pre-coated with concanavalin A and flowed over by synthetic complete media for more than 20 min before applying the square pulse sequence. Pulse stimulation with salt media was performed by ONIX FG flow control software (Cellasic Corp) with the flow pressure of 8 psi. Image acquisition was performed with a TE2000-E automated inverted microscope (Nikon) with Perfect Focus and 100x oil immersion lens.

Background subtraction was performed first on all fluorescence images using ImageJ (<http://imagej.nih.gov>). The subsequent image analysis for both nuclear Hog1-GFP import and *pSTL1*-mCherry expression was performed with custom Matlab (Mathworks) software (developed by Kai-Yeung Lau from Chao Tang's lab at UCSF). For Hog1-GFP import analysis, cell boundaries were first determined from the bright field DIC images. Cell nuclei were segmented by mCherry labeled nuclear images. The nuclear and total cell GFP densities were calculated from the GFP fluorescent images. For *pSTL1*-mCherry expression, cell boundaries were determined the same way Hog1-GFP localization and mCherry densities were determined from the mCherry

fluorescent images. For all frequency responses, 210 min long time course of pulse stimulation was performed and the maximum value of each time course was taken as the output of the stimulation frequency. The population average of over 50 - 100 cells was determined for each single measurement, and each experiment was repeated at least three times (see also **Supplemental Fig. 3c and 3d**) and the standard deviation was calculated with the three repeats.

***Jurkat* T cell lines, plasmids, and transfection**

Jurkat T cell with *pNFAT-EGFP* (Neomycin resistant) stably integrated into the chromosome is a Weiss lab stock strain. All plasmids were made by using standard cloning techniques, AarI combinatorial cloning technique³¹ and Gateway cloning technique (Invitrogen). See **Supplementary Tables** for more cloning detail. *Jurkat* cells were maintained in RPMI 1640 supplemented with 10% heat inactivated (HI) FBS (Invitrogen), extra L-glutamine (2 mM), penicillin, streptomycin, and G418 (2mg/mL, Invitrogen).

For transfection, *Jurkat* T cells were cultured in RPMI 1640 supplemented with 10% heat inactivated fetal bovine serum (FBS) and glutamine (10G RPMI) for at least 1 day. 20 million cells were spun down, washed once with 10G RPMI, and resuspended in 300ul of 10G RPMI. 15µg of each plasmid was added to each transfection, vortexed briefly, and

incubated at room temperature for 15 minutes. The cell/DNA mixture was then subject to electroporation (BioRad, square pulse, 300V, 10ms pulse, 0.4 cm cuvette). The cells were rested at room temperature for 10 minutes before resuspending in 10mL of 10G RPMI. The cells were allowed to recover overnight before performing further experiment. For transfection with plasmids that contain the *pTRE* promoter, the serum was switched to Tet-free serum (Clontech).

T cell activation and doxycycline induction

T cell receptor was activated with a *Jurkat* specific anti-TCR antibody, C305 (ascites, UCSF antibody core) at 1:2000 dilution unless stated other wise at the cell density of 2.5million cell/mL (for most experiment) or 0.5 million cells/mL (for Dox inducible expression (100nM) of effectors experiment). Phorbol 12-myristate 13-acetate

(25ng/mL) and ionomycin (1 μ M) was also used to activate T cell in some experiment.

For the dose response curve, the highest dose of C305 is 1:600 and serially diluted 3 fold to generate 8 doses total.

T cell antibody staining and flow cytometry analysis

For staining of cell surface expression of CD69, cells were fixed, and stained with

anti-CD69-APC (BD). For staining of phosphorylated ERK, cells were fixed, made

permeable by incubation with ice-cold 90% methanol on ice for 30 minutes and stained

with primary antibody to phosphorylated ERK (4370 Cell Signaling) and anti-rabbit APC secondary antibody (711-136-152, Jackson Immunoresearch). All samples were analyzed with BD LSRII equipped with high throughput sampler. Live cells were determined from forward and side scattering. Transfected cells were determined by comparing cells without mCherry to cells transfected with *pEF-mCherry*. Only transfected and live cells were included in the analysis. Error bar represents the standard deviation from three samples.

Western blot to determine protein expression level

1 million live cells were quickly spun down and lysed on ice for 30min. The supernatant were then spun down at 4°C for 30 min. The lysates were then mixed with DTT and SDS sample loading buffer and boiled for 3 minutes. Samples were separated with SDS PAGE gel (4-12% Bis-Tris) and then transferred to nitrocellulose blot. The blot were stained with primary anti-HA antibody (Santa Cruz Biotechnology) and Li-Cor anti-mouse 680 LT secondary antibody. The blot was imaged with the Li-Cor Odyssey.

Human primary CD4+ T cell transduction

Human peripheral blood mononuclear cells were collected from normal donors and acquired as cell suspensions from flushed TRIMA leukoreduction chambers (Blood

Centers of the Pacific, San Francisco, CA). Primary CD4⁺ T cells were purified by negative selection and Ficoll-Paque PLUS density medium separation (RosetteSep, Stem Cell Technologies). Purified cells were cryopreserved and placed in liquid nitrogen storage.

Replication-incompetent lentiviral particles were prepared in 293T cells by standard methods. Briefly, constructs of interest were cloned into the transfer vector pHR⁺SIN:CSW using standard molecular biology techniques and then co-transfected into 293T cells along with the viral packaging plasmids pCMVdr8.91 and pMD2.G using the transfection reagent FuGENE HD (Roche). Amphotropic VSV-G pseudotyped lentiviral particles in the supernatant were collected 48 hours later.

Prior to use, human primary CD4⁺ T cells were thawed and cultured overnight in growth medium (X-VIVO 15 + 5% human AB serum + 10mM N-acetylcysteine + 1X beta-mercaptoethanol + 1X Primocin) supplemented with 30U/mL IL-2. The next day, cells were activated with Dynabeads human T-Activator CD3/CD28 (Invitrogen) at a 3:1 beads-to-cells ratio. After 24 hours of activation, the cells were transduced with lentiviral particles. In some cases, transduction was performed on RetroNectin-coated tissue culture plates to enhance viability and transduction efficiency. Briefly, non-tissue culture treated plates were coated with RetroNectin (32µg/mL) and then blocked with

PBS + 2% BSA. Viral supernatant was loaded into the wells and the plate was centrifuged at 1,200g for 1.5 hours at room temperature. Finally, wells were washed once with PBS, activated T cells were loaded into the wells, and the plate was once again centrifuged at 1,200g for 1 hour with reduced braking speed. T cells were then placed into the 37°C incubator.

IL-2 release assay

Transduced cells were rested by culturing them for greater than 10 days in the presence of 30U/mL IL-2 added every other day for maintenance. Doxycycline (200 ng/mL) was added to the cells and the cells were incubated for 6 hours. Cells were washed and 5e4 human primary CD4+ cells (transduced with the pause switch constructs or untransduced) were placed in a 96-well plate with 200 µL human growth media with activation agents added (10 ng/mL PMA + 0.5 µM ionomycin, magnetic Dynabeads coated with anti-CD3/anti-CD28 (beads/cells ratio, 0.3:1), or Raji B cells loaded with a superantigen cocktail). Doxycycline (200ng/mL) was added into appropriate wells. After 24 hours of incubation at 37C, the released IL-2 in the supernatant was measured with the human IL-2 ELISA kit II (BD Biosciences).

Human primary CD4+ T cell proliferation assay

Resting primary CD4⁺ T cells were pretreated with 200 ng/ml doxycycline for 6 hours and then labeled with CellTrace Violet dye (Invitrogen). 5x10⁴ dye-labeled human CD4⁺ T cells were placed in a 96-well plate with 200 μL human growth media in the presence or absence of doxycycline (200ng/mL) and Dynabeads coated with anti-CD3/anti-CD28 (beads/cells ratio, 0.3:1) to induce proliferation. After incubation at 37C for 4 days, the cells were assayed by flow cytometry. FlowJo curve fitting software was used to quantitate cell proliferation as indicated by dilution of the CellTrace Violet dye in proliferating cells.

- ³¹ Peisajovich, S.G., Garbarino, J.E., Wei, P., & Lim, W.A., Rapid diversification of cell signaling phenotypes by modular domain recombination. *Science* 328 (5976), 368-372 (2010).
- ³² Lee, P.J., Helman, N.C., Lim, W.A., & Hung, P.J., A microfluidic system for dynamic yeast cell imaging. *BioTechniques* 44 (1), 91-95 (2008).

Figure 1

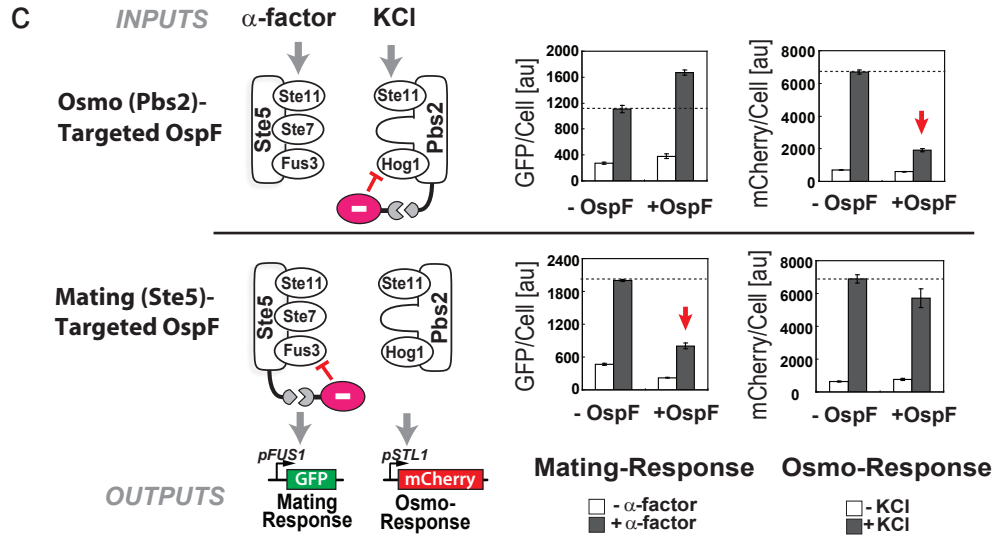
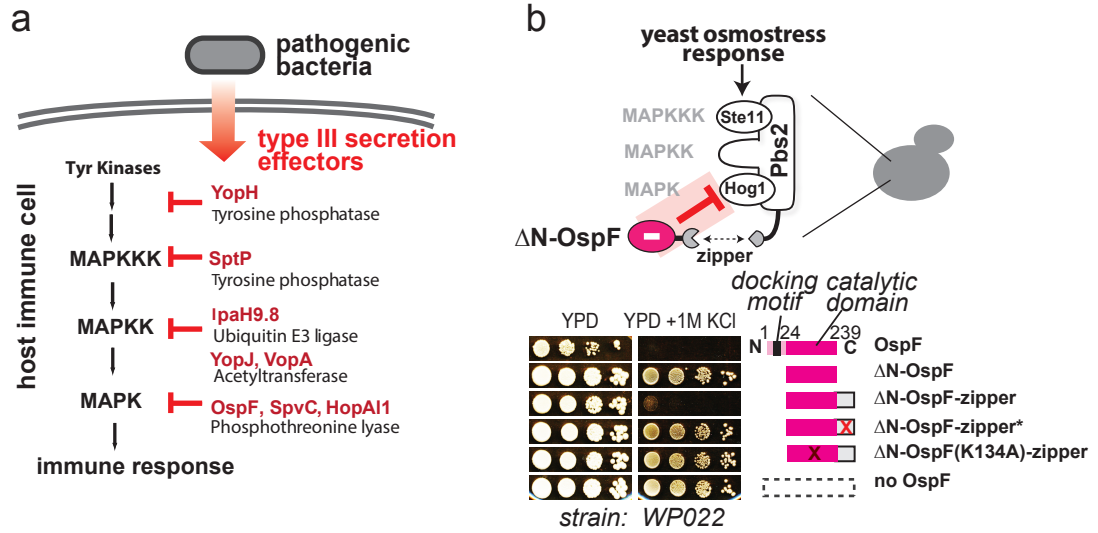


Figure 2

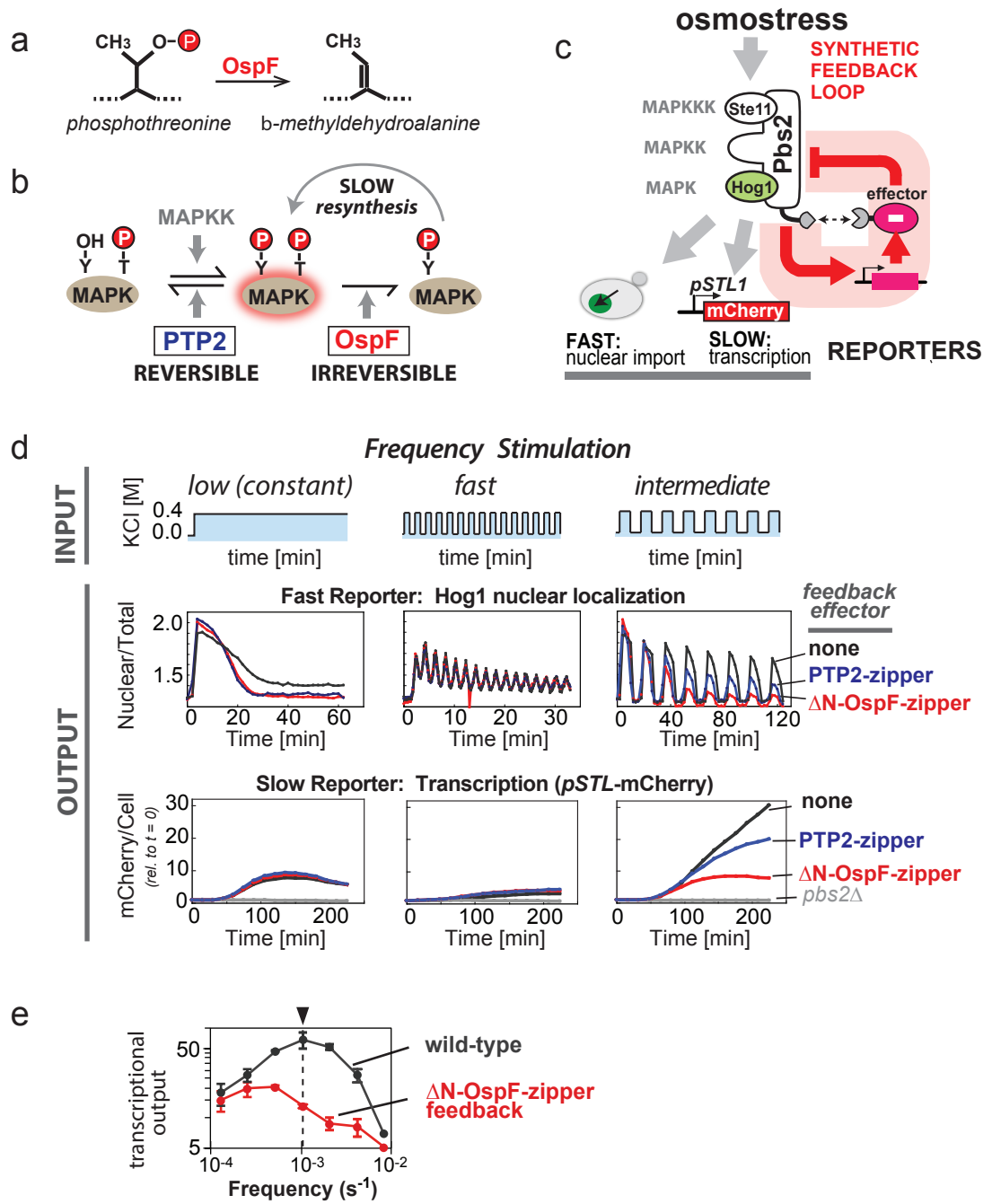


Figure 3

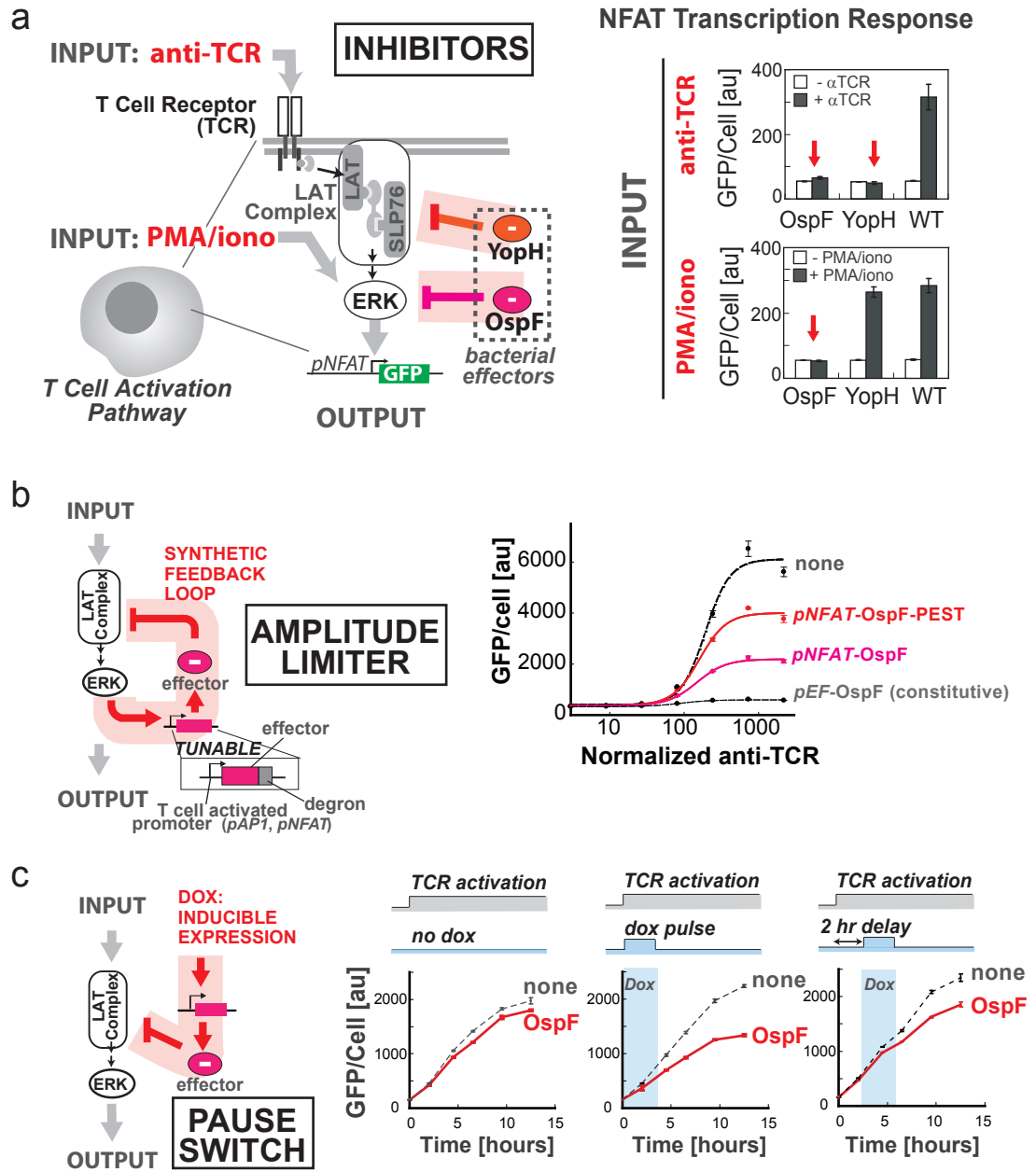
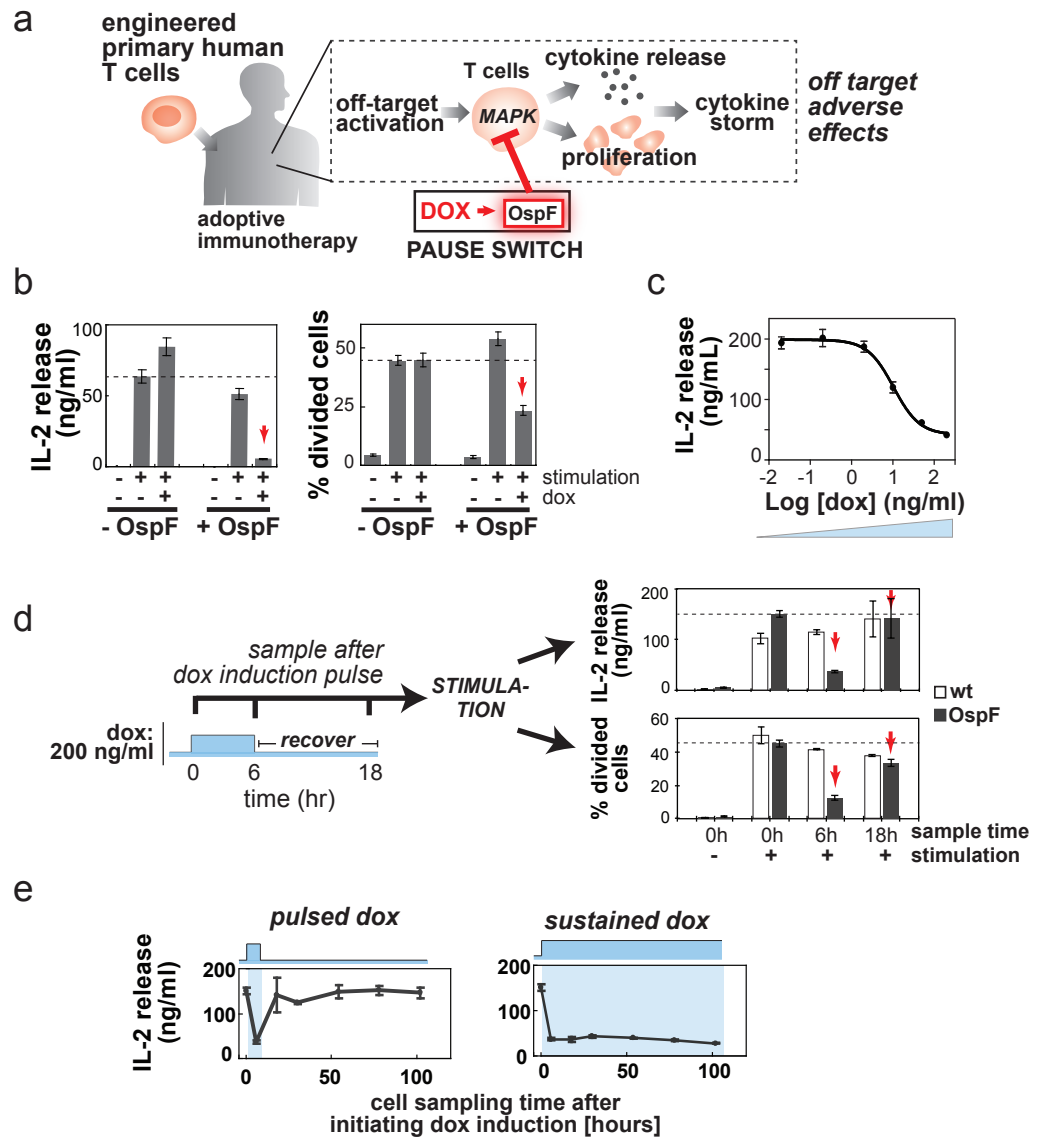


Figure 4



Supplementary Information For:

**Bacterial Virulence Proteins as Tools to Rewire Kinase Pathways in
Yeast and Immune Cells**

Ping Wei^{1,2*}, Wilson W. Wong^{1,2,3*}, Jason S. Park^{1,2,3}, Ethan E. Corcoran^{2,3,4},
Sergio G. Peisajovich^{1,2}, James J. Onuffer^{1,3}, Arthur Weiss^{2,3,4}, Wendell A. Lim^{1,2,3‡}

‡To whom correspondence should be addressed: lim@cmp.ucsf.edu

The PDF file includes:

Materials and Methods

Supplementary Computation Model

Supplementary Tables 1 – 8

Supplementary Figures 1 – 9

Materials and Methods

Yeast experiment

Constructs and strains

All constructs used in this study (Supplementary Table 1) were cloned using a combinatorial cloning strategy based on the Type II restriction enzyme AarI developed by Peisajovich et al¹. For the MAPK pathway specific inhibitory experiments, strain WP022 and WP116 were constructed from the W303-derived strain SP147 (Supplementary Table 2) by tagging the C-terminal of endogenous Pbs2 or Ste5 with leucine zipper respectively. To construct WP039 for measuring the nuclear Hog1 accumulation, the C-terminal of endogenous Hog1 in wild type W303 strain was tagged with GFP using standard integration technique. A histone protein Htb2 was C-terminally tagged with mCherry and the expression was driven by *ADHI* promoter. This Htb2-mCherry fusion protein was integrated at *TRP1* locus for the visualization of the nucleus. Endogenous Pbs2 was tagged with a leucine zipper by PCR integration and was used in synthetic feedback loops. Synthetic effector gene cassettes were integrated at the *LEU2* locus. Yeast promoters, terminator, and the *PTP2* gene were PCR amplified from *Saccharomyces cerevisiae* genomic DNA (Invitrogen). YopH gene was a kind gift from Kim Orth. The OspF gene was synthesized by Integrated DNA Technologies, Inc. All yeast genomic integrations were confirmed by yeast colony PCR.

Flow cytometry experiments

Analysis of the pathway-dependent fluorescent proteins (GFP and mCherry) expression in yeast cells was performed with the BD LSRII flow cytometer (BD Biosciences) equipped with a high-throughput sampler. For each experiment, triplicate cultures were grown in synthetic complete media to early log phase ($OD_{600} = 0.1 - 0.2$). At time = 0, 1.5 μ M of α -factor (GenScript) or 0.4 M of KCl were added into parallel cultures to induce separately the mating- specific or osmo-specific pathway response. For mating response, 100 μ L aliquots were taken at time = 0 and after 2 hours of induction; for osmotic response, 100 μ L aliquots were taken at time = 0 and after 1 hour of induction. Each 100 μ L sample aliquot was immediately mixed with 100 μ L of cycloheximide (10 μ g/mL) in 96-well plates to stop the protein synthesis. After incubating the samples at room temperature for 30 minutes in the dark to allow for the maturation of fluorescent proteins, the levels of fluorescence protein were determined by flow cytometry. For each read, 10,000 cells were counted, and the mean fluorescent density was calculated by Flowjo software (BD Biosciences) as the pathway output value and the standard deviation from triplicate experiments was indicated as the error bar.

Microfluidics, fluorescent microscopy, and image processing

Microfluidic yeast cell culture was performed in Y04C plate with ONIX flow control system (CellASIC Corp)². Cultures were grown to mid-log phase ($OD_{600} = 0.2 - 0.8$) in synthetic complete media. Cells were diluted to $OD_{600} = 0.01$ in 600 μ L of fresh media and sonicated at a minimum set of 11% for 1 sec using Fisher Scientific model 500 sonicator with a 2 mm tip. Cells were loaded into the flow chamber pre-coated with

concanavalin A and flowed over by synthetic complete media for more than 20 min before applying the square pulse sequence. Pulse stimulation with salt media was performed by ONIX FG flow control software (Cellasic Corp) with the flow pressure of 8 psi. Image acquisition was performed with a TE2000-E automated inverted microscope (Nikon) with Perfect Focus and 100x oil immersion lens.

Background subtraction was performed first on all fluorescence images using ImageJ (<http://imagej.nih.gov>). The subsequent image analysis for both nuclear Hog1-GFP import and *pSTL1*-mCherry expression was performed with custom Matlab (Mathworks) software (developed by Kai-Yeung Lau from Chao Tang's lab at UCSF). For Hog1-GFP import analysis, cell boundaries were first determined from the bright field DIC images. Cell nuclei were segmented by mCherry labeled nuclear images. The nuclear and total cell GFP densities were calculated from the GFP fluorescent images. For *pSTL1*-mCherry expression, cell boundaries were determined the same way Hog1-GFP localization and mCherry densities were determined from the mCherry fluorescent images. For all frequency responses, 210 min long time course of pulse stimulation was performed and the maximum value of each time course was taken as the output of the stimulation frequency. The population average of over 50 - 100 cells was determined for each single measurement, and each experiment was repeated at least three times (see also **Supplementary Fig. 3c and 3d**) and the standard deviation was calculated with the three experimental repeats.

***Jurkat* T cell experiments**

Cell line and plasmids

Jurkat T cell with *pNFAT-EGFP* (Neomycin resistant) stably integrated into the chromosome is a Weiss lab stock strain. All plasmids were made by using standard cloning techniques, AarI combinatorial cloning technique¹ and Gateway cloning technique (Invitrogen). See **Supplementary Tables** below for more cloning detail.

Culture condition

Jurkat was maintained in RPMI 1640 supplemented with 10% heat inactivated (HI) FBS (Invitrogen), extra L-glutamine (2 mM), penicillin, streptomycin, and G418 (2mg/mL, Invitrogen).

Transfection

Before transfection, *Jurkat* T cells were cultured in RPMI 1640 supplemented with 10% Heat inactivated fetal bovine serum (FBS) and glutamine (10G RPMI) for at least 1 day. For each transfection, 20 million cells were spun down, washed once with 10G RPMI, and resuspended in 300ul of 10G RPMI. 15µg of each plasmid was added to each transfection, vortexed briefly, and incubated at room temperature for 15 minutes. The cell/DNA mixture was then subject to electroporation (BioRad, square pulse, 300V, 10ms pulse, 0.4 cm cuvette). The cells were rested at room temperature for 10 minutes before resuspending in 10mL of 10G RPMI. The cells were allowed to recover overnight before performing further experiment. For transfection with plasmids that contain the *pTRE* promoter, the serum was switched to Tet-free serum.

T cell activation and doxycycline induction

T cell receptor was activated with a *Jurkat* specific anti-TCR antibody, C305 (ascites, UCSF antibody core) at 1:2000 dilution unless stated otherwise at the cell density of 2.5 million cells/mL (for most experiment) or 0.5 million cells/mL (for Dox inducible expression (100nM) of effectors experiment). Phorbol 12-myristate 13-acetate (25ng/mL) and ionomycin (1 μ M) was also used to activate T cell in some experiment. For the dose response curve, the highest dose of C305 is 1:600 and serially diluted 3 fold to generate 8 doses total.

Antibody staining and flow cytometry analysis

For staining of cell surface expression of CD69, cells were fixed, and stained with anti-CD69-APC (BD). For staining of phosphorylated ERK, cells were fixed, made permeable by incubation with ice-cold 90% methanol on ice for 30 minutes and stained with primary antibody to phosphorylated ERK (197G2; Cell Signaling) and anti-rabbit APC secondary antibody (711-136-152, Jackson Immunoresearch). All samples were analyzed with BD LSRII equipped with high throughput sampler. Live cells were determined from forward and side scattering. Transfected cells were determined by comparing cells without mCherry to cells transfected with *pEF-mCherry*. Only transfected and live cells were included in the analysis. Error bar represents the standard deviation from three samples.

Western blot to determine protein expression level

1 million live cells were quickly spun down and lysed on ice for 30min. The supernatant were then spun down at 4°C for 30 min. The lysates were then mixed with DTT and SDS sample loading buffer and boiled for 3 minutes. Samples were separated with SDS PAGE gel (4-12% Bis-Tris) and then transferred to nitrocellulose blot. The blot were stained with primary anti-HA antibody (Santa Cruz Biotechnology) and Li-Cor anti-mouse 680 LT secondary antibody. The blot was imaged with the Li-Cor Odyssey.

Human primary CD4+ T cell experiments

Human primary CD4+ T cell transduction

Human peripheral blood mononuclear cells were collected from normal donors and acquired as cell suspensions from flushed TRIMA leukoreduction chambers (Blood Centers of the Pacific, San Francisco, CA). Primary CD4+ T cells were purified by negative selection and Ficoll-Paque PLUS density medium separation (RosetteSep, Stem Cell Technologies). Purified cells were cryopreserved and placed in liquid nitrogen storage.

Replication-incompetent lentiviral particles were prepared in 293T cells by standard methods. Briefly, constructs of interest were cloned into the transfer vector pHR'SIN:CSW using standard molecular biology techniques and then co-transfected into 293T cells along with the viral packaging plasmids pCMVdR8.91 and pMD2.G using the transfection reagent FuGENE HD (Roche). Amphotropic VSV-G pseudotyped lentiviral particles in the supernatant were collected 48 hours later.

Prior to use, human primary CD4+ T cells were thawed and cultured overnight in growth medium (X-VIVO 15 + 5% human AB serum + 10mM N-acetylcysteine + 1X beta-mercaptoethanol + 1X Primocin) supplemented with 30U/mL IL-2. The next day, cells were activated with Dynabeads human T-Activator CD3/CD28 (Invitrogen) at a 3:1

beads-to-cells ratio. After 24 hours of activation, the cells were transduced with lentiviral particles. In some cases, transduction was performed on RetroNectin-coated tissue culture plates to enhance viability and transduction efficiency. Briefly, non-tissue culture treated plates were coated with RetroNectin (32 μ g/mL) and then blocked with PBS + 2% BSA. Viral supernatant was loaded into the wells and the plate was centrifuged at 1200g for 1.5 hours at room temperature. Finally, wells were washed once with PBS, activated T cells were loaded into the wells, and the plate was once again centrifuged at 1200g for 1 hour with reduced braking speed. T cells were then placed into the 37°C incubator.

Human primary CD4+ T cell IL-2 release assay

Transduced cells were rested by culturing them for greater than 10 days in the presence of 30U/mL IL-2 added every other day for maintenance. Doxycycline (200 ng/ml) was added to the cells and the cells were incubated for 6 hours. Cells were washed and 5e4 human primary CD4+ cells (transduced with the pause switch constructs or untransduced) were placed in a 96-well plate with 200 μ L human growth media with activation agents added (10 ng/ml PMA + 0.5 μ M ionomycin, magnetic Dynabeads coated with anti-CD3/anti-CD28 (beads/cells ratio, 0.3:1), or Raji B cells loaded with a superantigen cocktail). Doxycycline (200ng/mL) was added into appropriate wells. After 24 hours of incubation at 37°C, the released IL-2 in the supernatant was measured with the human IL-2 ELISA kit II (BD Biosciences).

Human primary CD4+ T cell proliferation assay

Resting primary CD4+ T cells were pretreated with 200 ng/ml doxycycline for 6 hours and then labeled with CellTrace Violet dye (Invitrogen). 5e4 dye-labeled human CD4+ T cells were placed in a 96-well plate with 200 μ L human growth media in the presence or absence of doxycycline (200ng/mL) and Dynabeads coated with anti-CD3/anti-CD28 (beads/cells ratio, 0.3:1) to induce proliferation. After incubation at 37°C for 4 days, the cells were assayed by flow cytometry. FlowJo curve fitting software was used to quantitate cell proliferation as indicated by dilution of the CellTrace Violet dye in proliferating cells.

Supplementary Computation Model

The simulation results shown in Supplementary Figure 2 and 3 are based on the computation model developed by Zi et al³. The following are the equations used for the wild type model (same as Zi et al). All the kinetic parameters are also the same as the model by Zi et al. The simulation were solved in MATLAB.

$$\frac{d[Pbs2]}{dt} = -\frac{K_{pho}^{Pbs2} \cdot [Pbs2]}{1 + \left(\frac{PI_t}{\alpha}\right)^8} + K_{depho}^{Pbs2} \cdot [Pbs2PP] - [Pbs2] \cdot V_{ratio} \quad (1)$$

$$\frac{d[Pbs2PP]}{dt} = \frac{K_{pho}^{Pbs2} \cdot [Pbs2]}{1 + \left(\frac{PI_t}{\alpha}\right)^8} - K_{depho}^{Pbs2} \cdot [Pbs2PP] - [Pbs2PP] \cdot V_{ratio} \quad (2)$$

$$\begin{aligned} \frac{d[Hog1c]}{dt} = & -K_{pho}^{Hog1} \cdot [Pbs2PP] \cdot [Hog1c] + K_{depho}^{Hog1PPc} \cdot [Hog1PPc] \\ & - K_{imp}^{Hog1c} \cdot [Hog1c] + \frac{K_{exp}^{Hog1n} \cdot [Hog1n] \cdot V_{nuc}}{V_{cyt}} - [Hog1c] \cdot V_{ratio} \end{aligned} \quad (3)$$

$$\begin{aligned} \frac{d[Hog1PPc]}{dt} = & K_{pho}^{Hog1} \cdot [Pbs2PP] \cdot [Hog1c] - K_{depho}^{Hog1PPc} \cdot [Hog1PPc] \\ & - K_{imp}^{Hog1PPc} \cdot [Hog1PPc] + \frac{K_{exp}^{Hog1PPn} \cdot [Hog1PPn] \cdot V_{nuc}}{V_{cyt}} \\ & - [Hog1PPc] \cdot V_{ratio} \end{aligned} \quad (4)$$

$$\begin{aligned} \frac{d[Hog1n]}{dt} = & \frac{K_{imp}^{Hog1c} \cdot [Hog1c] \cdot V_{cyt}}{V_{nuc}} - K_{exp}^{Hog1n} \cdot [Hog1n] + K_{depho}^{Hog1PPn} \cdot [Hog1PPn] \\ & - [Hog1n] \cdot V_{ratio} \end{aligned} \quad (5)$$

$$\frac{d[Hog1PPn]}{dt} = \frac{K_{imp}^{Hog1PPc} \cdot [Hog1PPc] \cdot V_{cyt}}{V_{nuc}} - K_{exp}^{Hog1PPn} \cdot [Hog1PPn] - K_{depho}^{Hog1PPn} \cdot [Hog1PPn] - [Hog1PPn] \cdot V_{ratio} \quad (6)$$

$$\begin{aligned} \frac{d[Glyc_in]}{dt} = & K_{s0}^{Glyc} + \frac{K_{s1}^{Glyc} \cdot (totalHog1PP)^4}{\beta^4 + (totalHog1PP)^4} + K_{s2}^{Glyc} \cdot [Yt] \\ & - \left(K_{exp0}^{Glyc} + \frac{K_{exp1}^{Glyc} \cdot (PI_t)^{12}}{(\gamma)^{12} + (PI_t)^{12}} \right) \cdot ([Glyc_in] - [Glyc_ex]) \\ & - [Glyc_in] \cdot V_{ratio} \end{aligned} \quad (7)$$

$$\frac{d[Yt]}{dt} = K_{s0}^{Yt} + K_{s1}^{Yt} \cdot [z4] - K_t^{Yt} \cdot [Yt] - [Yt] \cdot V_{ratio} \quad (8)$$

$$\frac{d[z1]}{dt} = \frac{4 \cdot ([Hog1PPn] - [z1])}{\tau} \quad (9)$$

$$\frac{d[z2]}{dt} = \frac{4 \cdot ([z1] - [z2])}{\tau} \quad (10)$$

$$\frac{d[z3]}{dt} = \frac{4 \cdot ([z2] - [z3])}{\tau} \quad (11)$$

$$\frac{d[z4]}{dt} = \frac{4 \cdot ([z3] - [z4])}{\tau} \quad (12)$$

$$\frac{d(V_{os})}{dt} = -G \cdot Lp \cdot (PI_e + PI_t - PI_i) \quad (13)$$

$$PI_e = PI_e^0 + w \cdot [NaCl] \quad (14)$$

$$PI_t = \begin{cases} \frac{PI_t^0 \cdot (V_{os} - V_{os}^{PI_t=0})}{(V_{os}^0 - V_{os}^{PI_t=0})} & \text{if } V_{os}^0 > V_{os}^{PI_t=0} \\ 0 & \text{if } V_{os}^0 \leq V_{os}^{PI_t=0} \end{cases} \quad (15)$$

$$V_{cell} = V_{os} + V_b \quad (16)$$

$$V_{cyt} = f^{V_{cyt}} \cdot V_{cell} = 0.5 \cdot V_{cell} \quad (17)$$

$$V_{nuc} = f^{V_{nuc}} \cdot V_{cell} = 0.07 \cdot V_{cell} \quad (18)$$

$$\begin{aligned} PI_i &= \frac{n \cdot R \cdot T}{V_{os}} = \frac{n_0 + n_{Glyc}}{V_{os}} \cdot R \cdot T = \frac{n_0 + [Glyc_in] \cdot V_{cyt}}{V_{os}} \cdot R \cdot T \\ &= \frac{n_0 + [Glyc_in] \cdot V_{cyt}}{V_{os}} \cdot 10^{-9} \cdot 8.314 \cdot 303.15 \end{aligned} \quad (19)$$

$$totalHog1PP = \frac{([Hog1PPc] \cdot V_{cyt} + [Hog1PPn] \cdot V_{nuc}) \cdot 602}{6780} \quad (20)$$

$$\begin{aligned} V_{ratio} &= \frac{1}{V_{cell}} \cdot \frac{d(V_{cell})}{dt} = \frac{1}{V_{cell}} \cdot \frac{d(V_{os} + V_b)}{dt} = \frac{1}{V_{cell}} \cdot \frac{d(V_{os})}{dt} \\ &= \frac{-G \cdot Lp \cdot (PI_e + PI_t - PI_i)}{V_{cell}} \end{aligned} \quad (21)$$

$$\begin{aligned} Rt &= \frac{[Hog1n] + [Hog1PPn]}{\left(\frac{N_{Hog1}^{total}}{N_a} \right)} \\ &= \frac{([Hog1n] + [Hog1PPn]) \cdot 0.8 \cdot (V_{os} + V_b) \cdot 602}{6780} \end{aligned} \quad (22)$$

(note: $[Hog1n]$ and $[Hog1PPn]$ have unit of 10^{-6} M; V_{cell} has unit of 10^{-15} L)

For the computation model that contains the reversible feedback loop, equations involving the cytoplasmic Hog1 were changed to account for the modification of Hog1 by the effector. Only cytoplasmic Hog1 is affected directly by the effector. Another equation was added to account for the expression of the effector by nuclear phosphorylated Hog1.

$$\begin{aligned}
\frac{d[Hog1c]}{dt} = & -K_{pho}^{Hog1} \cdot [Pbs2PP] \cdot [Hog1c] + K_{depho}^{Hog1PPc} \cdot [Hog1PPc] \\
& - K_{imp}^{Hog1c} \cdot [Hog1c] + \frac{K_{exp}^{Hog1n} \cdot [Hog1n] \cdot V_{nuc}}{V_{cyt}} - [Hog1c] \cdot V_{ratio} \\
& + \alpha_1 \cdot [Hog1PPc] \cdot [Effector]
\end{aligned} \tag{23}$$

$$\begin{aligned}
\frac{d[Hog1PPc]}{dt} = & K_{pho}^{Hog1} \cdot [Pbs2PP] \cdot [Hog1c] - K_{depho}^{Hog1PPc} \cdot [Hog1PPc] \\
& - K_{imp}^{Hog1PPc} \cdot [Hog1PPc] + \frac{K_{exp}^{Hog1PPn} \cdot [Hog1PPn] \cdot V_{nuc}}{V_{cyt}} \\
& - [Hog1PPc] \cdot V_{ratio} - \alpha_1 \cdot [Hog1PPc] \cdot [Effector]
\end{aligned} \tag{24}$$

$$\frac{d[Effector]}{dt} = \frac{\alpha_{14} [Hog1PPn]^n}{K_{14}^n + [Hog1PPn]^n} - [Effector] \cdot V_{ratio} \tag{25}$$

For the model that contains the irreversible feedback loop, the equations involving the cytoplasmic phosphorylated Hog1 were changed, but not the non-phosphorylated Hog1. Instead, a new specie of dead Hog1 (Hog1Dead) appears and a new equation was added to describe the dynamics of this specie of Hog1. Furthermore, even though Hog1Dead cannot participate in transcription response and be phosphorylated again, it is still fluorescence and may be translocated into nucleus similar to non-phosphorylated Hog1. Therefore the equation that describe the level of total nuclear Hog1 was modified to include new Hog1Dead.

$$\frac{d[Hog1PPc]}{dt} = K_{pho}^{Hog1} \cdot [Pbs2PP] \cdot [Hog1c] - K_{depho}^{Hog1PPc} \cdot [Hog1PPc] \quad (26)$$

$$- K_{imp}^{Hog1PPc} \cdot [Hog1PPc] + \frac{K_{exp}^{Hog1PPn} \cdot [Hog1PPn] \cdot V_{nuc}}{V_{cyt}} \\ - [Hog1PPc] \cdot V_{ratio} - \alpha_1 \cdot [Hog1PPc] \cdot [Effector]$$

$$\frac{d[Hog1Deadc]}{dt} = -K_{imp}^{Hog1c} \cdot [Hog1Deadc] + \frac{K_{exp}^{Hog1n} \cdot [Hog1Deadn] \cdot V_{nuc}}{V_{cyt}} \quad (27)$$

$$- [Hog1Deadc] \cdot V_{ratio} + \alpha_1 \cdot [Hog1PPc] \cdot [Effector]$$

$$\frac{d[Hog1Deadn]}{dt} = +K_{imp}^{Hog1c} \cdot [Hog1Deadc] - \frac{K_{exp}^{Hog1n} \cdot [Hog1Deadn] \cdot V_{nuc}}{V_{cyt}} \quad (28)$$

$$- [Hog1Deadn] \cdot V_{ratio}$$

$$\frac{d[Effector]}{dt} = \frac{\alpha_{14} [Hog1PPn]^n}{K_{14}^n + [Hog1PPn]^n} - [Effector] \cdot V_{ratio} \quad (29)$$

$$Rt = \frac{[Hog1n] + [Hog1PPn] + [Hog1Deadn]}{\left(\frac{N_{Hog1}^{total}}{N_a} \right) (V_{cell} - V_{cell}^{wall})} \quad (30)$$

$$= \frac{([Hog1n] + [Hog1PPn] + [Hog1Deadn]) \cdot 0.8 \cdot (Vos + Vb) \cdot 602}{6780}$$

The goal of this model is to compare the outcome of reversible modification to irreversible modification, therefore the parameters for the enzyme kinetics and gene express dynamics are the same for both the reversible and irreversible effectors. The parameters were chosen to qualitatively match experimental results.

For figure S2, the parameters are

$$\alpha_1 = 0.1, \alpha_{14} = 0.3, K_{14} = 0.08, n=10, \mu=0.01.$$

For **Supplementary Figure 2**, the heat map parameters ranges are

Effector (maximum) enzyme activity: $\alpha_1 = 0.01-10$,

Effector (maximum) gene expression rate: $\alpha_{14} = 0.05 - 10$,

Effector degradation rate $\mu = 0.0005 - 0.5$

Supplementary Table 1 Plasmids used in yeast experiments

Plasmid	Parent vector	Promoter	Epitope	Gene	Leucine zipper ⁴
WP201	pNH605	<i>pCYC1</i>	3xFlag	OspF	adapter
WP202	pNH605	<i>pCYC1</i>	3xFlag	OspF (K134A)	adapter
WP203	pNH605	<i>pCYC1</i>	3xFlag	ΔN-OspF	adapter
WP204	pNH605	<i>pCYC1</i>	3xFlag	ΔN-OspF	EE
WP205	pNH605	<i>pCYC1</i>	3xFlag	ΔN-OspF	RR
WP206	pNH605	<i>pCYC1</i>	3xFlag	ΔN-OspF(K134A)	EE
WP207	pNH605	<i>pSTL1</i>	3xFlag	ΔN-OspF	EE
WP208	pNH605	<i>pSTL1</i>	3xFlag	PTP2	EE

Supplementary Table 2 Yeast strains used in this study

Strain	Description
SP147	<i>W303 MATa, bar1::NatR, far1Δ, mfa2::pFUS1-GFP, HO::pSTL1-mCherry, his3, trp1, leu2, ura3</i>
WP020	<i>W303 MATa, bar1::NatR, far1Δ, mfa2::pFUS1-GFP, HO::pSTL1-mCherry, pbs2::URA3, his3, trp1, leu2, ura3</i>
WP022	<i>W303 MATa, bar1::NatR, far1Δ, mfa2::pFUS1-GFP, HO::pSTL1-mCherry, Pbs2::Pbs2-zipper(RR), his3, trp1, leu2, ura3</i>
WP116	<i>W303 MATa, bar1::NatR, far1Δ, mfa2::pFUS1-GFP, HO::pSTL1-mCherry, Ste5::Ste5-zipper(EE), his3, trp1, leu2, ura3</i>
WP038	<i>W303 MATa, Trp1::pADH1-Htb2-mCherry, Hog1::Hog1-GFP, pbs2::URA3, his3, trp1, leu2, ura3</i>
WP039	<i>W303 MATa, Trp1::pADH1-Htb2-mCherry, Hog1::Hog1-GFP, Pbs2::Pbs2-zipper(RR), his3, trp1, leu2, ura3</i>

Supplementary Table 3. Expression vectors used in the study with *Jurkat* T cell

Expression Vectors						
Vector	Vector Name	Vector Source	Promoter	Gene	Cloning methods	
1	pEF-HA-OspF	pEF/FRT/V5/DEST	Invitrogen	EF1-alpha	HA-OspF	Invitrogen's gateway recombination (LR clonase II) with pEF/FRT/V5/DEST and pENTR HA-OspF
2	pEF-HA-YopH	pEF/FRT/V5/DEST	Invitrogen	EF1-alpha	HA-YopH	Invitrogen's gateway recombination (LR clonase II) with pEF/FRT/V5/DEST and pENTR HA-YopH
3	pEF-HA-SHP-1	pEF/FRT/V5/DEST	Invitrogen	EF1-alpha	HA-SHP-1	Invitrogen's gateway recombination (LR clonase II) with pEF/FRT/V5/DEST and pENTR HA-SHP1
4	pNFAT-HA-OspF	p4XNFAT DEST	Arthur Weiss	4XNFAT	HA-OspF	Invitrogen's gateway recombination (LR clonase II) with pNFAT-DEST and pENTR HA-OspF
5	pNFAT-HA-YopH	p4XNFAT DEST	Arthur Weiss	4XNFAT	HA-YopH	Invitrogen's gateway recombination (LR clonase II) with pNFAT-DEST and pENTR HA-YopH
6	pAPI-HA-OspF	pAPI-DEST	Clontech	3XAP-1	HA-OspF	Invitrogen's gateway recombination (LR clonase II) with pAPI-DEST and pENTR HA-OspF
7	pAPI-HA-YopH	pAPI-DEST	Clontech	3XAP-1	HA-YopH	Invitrogen's gateway recombination (LR clonase II) with pAPI-DEST and pENTR HA-YopH
8	pNFAT-HA-OspF-PEST	p4XNFAT DEST	Arthur Weiss	4XNFAT	HA-OspF-PEST	Invitrogen's gateway recombination (LR clonase II) with pNFAT-DEST and pENTR HA-OspF-PEST
9	pNFAT-HA-YopH-PEST	p4XNFAT DEST	Arthur Weiss	4XNFAT	HA-YopH-PEST	Invitrogen's gateway recombination (LR clonase II) with pNFAT-DEST and pENTR HA-YopH-PEST
10	pAPI-HA-OspF-PEST	pAPI-DEST	Clontech	3XAP-1	HA-OspF-PEST	Invitrogen's gateway recombination (LR clonase II) with pAPI-DEST and pENTR HA-OspF-PEST
11	pAPI-HA-YopH-PEST	pAPI-DEST	Clontech	3XAP-1	HA-YopH-PEST	Invitrogen's gateway recombination (LR clonase II) with pAPI-DEST and pENTR HA-YopH-PEST
12	pTRE-DD-OspF	pTRE-DEST	Clontech	TRE	DD-OspF	Invitrogen's gateway recombination (LR clonase II) with pTRE-DEST and pENTR DD-OspF
13	pTRE-DD-YopH	pTRE-DEST	Clontech	TRE	DD-YopH	Invitrogen's gateway recombination (LR clonase II) with pAPI-DEST and pENTR DD-YopH
14	pEF-mCherry	pEF/FRT/V5/DEST	Invitrogen	EF1-alpha	mCherry	Invitrogen's gateway recombination (LR clonase II) with pEF/FRT/V5/DEST and pENTR-mCherry
15	pEF-HA-GST	pEF/FRT/V5/DEST	Invitrogen	EF1-alpha	GST-HA	Invitrogen's gateway recombination (LR clonase II) with pEF/FRT/V5/DEST and pENTR-GST-HA
16	pEF/pTetON	pEF/FRT/V5/DEST	Invitrogen	CMV	Tet-ON Advanced (rtTA)	The expression cassette of pCMV-Tet-ON Advanced was PCR amplified from pTet-ON Advanced. The amplified fragment was then cloned into pEF/FRT/V5 DEST between the restriction site Acc65I and SphI
17	pEF-HA-OspF K134A	pEF/FRT/V5/DEST	Invitrogen	EF1-alpha	HA-OspFK134A	Invitrogen's gateway recombination (LR clonase II) with pEF/FRT/V5/DEST and pENTR HA-OspFK134A
18	pEF-HA-YopH C403A	pEF/FRT/V5/DEST	Invitrogen	EF1-alpha	HA-YopHC403A	Invitrogen's gateway recombination (LR clonase II) with pEF/FRT/V5/DEST and pENTR HA-YopHC403A

The DD in plasmid 12 and 13 is a destabilization domain based described by Banaszynski et al⁵. This domain was chosen because of its low basal expression level.

Supplementary Table 4. Gateway donor vector used to generate the expression vector

Donor Vectors Vector Name	Vector Source	Promoter	Gene	Cloning methods
pENTR-HA-OspF	pENTR (pDONR221)	Invitrogen	-	HA-OspF
pENTR-HA-YopH	pENTR (pDONR221)	Invitrogen	-	HA-YopH
pENTR-HA-SHP-1	pENTR (pDONR221)	Invitrogen	-	HA-SHP-1
pENTR-HA-OspFK134A	pENTR (pDONR221)	Invitrogen	-	HA-OspFK134A
pENTR-HA-YopHC403A	pENTR (pDONR221)	Invitrogen	-	HA-YopHC403A
pENTR-HA-OspF-PEST	pENTR (pDONR221)	Invitrogen	-	HA-OspF-PEST
pENTR-HA-YopH-PEST	pENTR (pDONR221)	Invitrogen	-	HA-YopH-PEST
pENTR-DD-OspF	pENTR (pDONR221)	Invitrogen	-	DD-OspF
pENTR-DD-YopH	pENTR (pDONR221)	Invitrogen	-	DD-YopH
pENTR-GST-HA	pENTR (pDONR221)	Invitrogen	-	GST-HA
pENTR-mCherry	pENTR (pDONR221)	Invitrogen	-	mCherry

All fusion proteins were constructed using the AarI cloning method described in Peisajovich et al. Briefly, the pDONR221 is modified to include the AarI cloning sites between the attB1 and attB2 recombination sites. After digestion with AarI, fragments are ligated using standard cloning technique.

This construct was made using the gateway cloning strategy

Supplementary Table 5. Gateway destination vector used to generate the expression vector

Destination Vectors Vector Name	Vector Source
pNFAT(d2)-DEST	pNFAT-GFP
pAPI-DEST	pAPI-Luc
pEF/FRT/V5/DEST	pEF/FRT/V5/DEST
pTRE-DEST	pTRE-Tight

Supplementary Table 6. Other vectors used to generate the expression vector

Other Vectors Vector Name	Vector Source	Promoter	Gene	Cloning methods
pTuner-OspF	pTuner	Clontech	CMV	OspF
pTuner-YopH	pTuner	Clontech	CMV	YopH
pTet-ON Advanced	pTet-ON Advanced	Clontech	CMV	Tet-ON Advanced

Using standard cloning technique, OspF was cloned between the XhoI and BamHI site

Using standard cloning technique, OspF was cloned between the XhoI and BamHI site

No modification made

Supplementary Table 7. Plasmids used in the transfection*

Figure #	Sample	Plasmid A	Plasmid B
Figure 3A	pEF-HA-YopH	2	-
	pEF-HA-OspF	1	-
	WT	15	-
Figure 3B	pNFAT-HA-OspF	4	-
	pNFAT-HA-OspF-PEST	8	-
	pEF-HA-OspF	1	-
	WT	15	-
Figure 3C, S8	pTRE-DD-Yop	13	16
	pTRE-DD-OspF	12	16
	WT	15	16
Figure S5A, S5C	pEF-YopH	2	-
	pEF-OspF	1	-
	pEF-SHP-1	3	-
	WT	14	-
Figure S7	pNFAT-HA-OspF	4	-
	pNFAT-HA-OspF-PEST	8	-
	pAP1-HA-OspF	6	-
	pAP1-HA-OspF-PEST	10	-
	pNFAT-HA-YopH	5	-
	pNFAT-HA-YopH-PEST	9	-
	pAP1-HA-YopH	7	-
	pAP1-HA-YopH-PEST	11	-
	pEF-HA-YopH	2	-
	pEF-HA-OspF	1	-
	WT	15	-
Figure S5B	pEF-YopH	1	-
	pEF-YopHC403A	18	-
	pEF-OspF	2	-
	pEF-OspFK134A	17	-
	WT	15	-

- A *pEF*-mCherry plasmid (13) is used in all transfection as transfection efficiency marker. The identity of plasmid number can be found in Supplementary Table 3.

Supplementary Table 8. Plasmids used in the human primary CD4+ T cell experiments

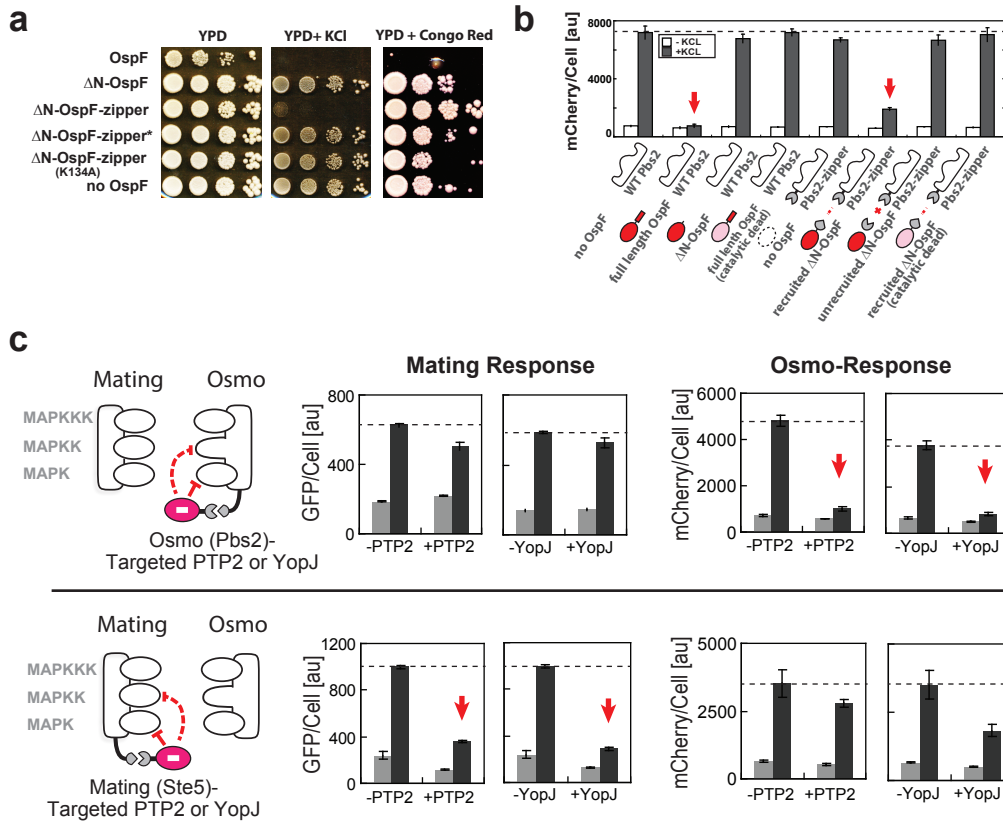
Plasmid	Parent vector	Gene
pHR-rtTA	pHR'SIN:CSW	Tet-ON Advanced
pHR-TRE-DD-OspF	pHR'SIN:CSW	Tet-inducible OspF

Supplemental References

1. Peisajovich, S. G., Garbarino, J. E., Wei, P. & Lim, W. A. Rapid diversification of cell signaling phenotypes by modular domain recombination. *Science* **328**, 368-72 (2010).
2. Lee, P. J., Helman, N. C., Lim, W. A. & Hung, P. J. A microfluidic system for dynamic yeast cell imaging. *BioTechniques* **44**, 91-5 (2008).
3. Zi, Z., Liebermeister, W. & Klipp, E. A quantitative study of the Hog1 MAPK response to fluctuating osmotic stress in *Saccharomyces cerevisiae*. *PloS one* **5**, e9522 (2010).
4. Bashor, C. J., Helman, N. C., Yan, S. & Lim, W. A. Using engineered scaffold interactions to reshape MAP kinase pathway signaling dynamics. *Science* **319**, 1539-43 (2008).
5. Banaszynski, L. A., Chen, L. C., Maynard-Smith, L. A., Ooi, A. G. & Wandless, T. J. A rapid, reversible, and tunable method to regulate protein function in living cells using synthetic small molecules. *Cell* **126**, 995-1004 (2006).

Supplementary Figure 1

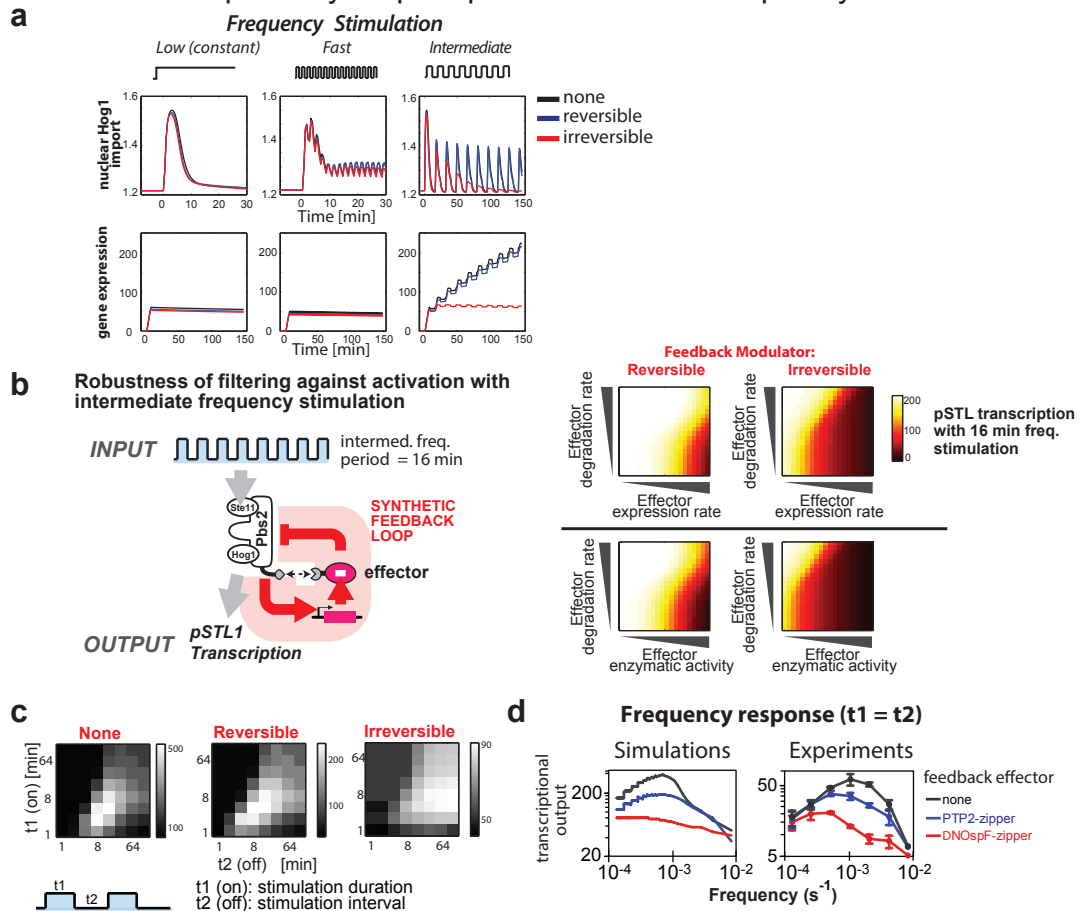
Pathogen effectors can be harnessed to inhibit specific MAPKs through scaffold protein recruitment with leucine zippers in yeast



Supplementary Figure 1. Engineering effectors that specifically block the MAPK pathways. **a**, Yeast cells with variants of OspF were plated on YPD (left), YPD with 1 M KCl (middle), and YPD with 30 μ g/ml congo red (right) plates. Variants include wild type OspF, Δ N-OspF, Δ N-OspF with zipper, Δ N-OspF with nonbinding zipper (zipper*), catalytic dead Δ N-OspF (K134A) with zipper and cells without OspF (No OspF). **b**, The transcriptional osmo-responses (as reported by *pSTL1*-mCherry) were measured at 1 hour after stimulated with 0.4 M KCl. All variant of OspFs were expressed by the *pCYC1* promoter and integrated into yeast genome; Pbs2 variants were integrated and expressed from endogenous Pbs2 locus. Only the OspF variants that are recruited to Hog1/Pbs2 display selective inhibition. Catalytic activity of OspF and functional zippers are required for inhibition using Δ N-OspF (no docking motif). **c**, PTP2, a yeast endogenous protein tyrosine phosphatase, and YopJ, a *Yersinia* MAPKK acetyltransferase, were engineered to selectively inhibit mating or osmo-MAPK pathway with leucine zipper based MAPK pathway recruitment. *pAHD1* promoter was used to constitutively express PTP2-zipper, while *pCYC1*-promoter was used to drive the constitutive expression of YopJ.

Supplementary Figure 2

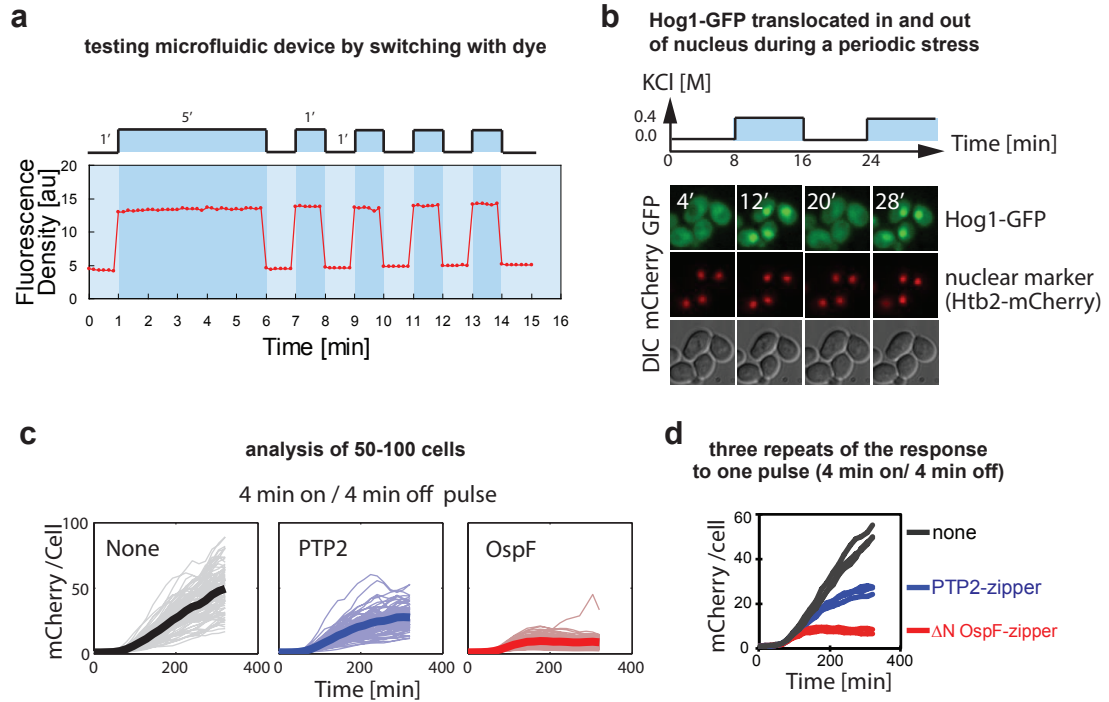
Simulations indicate that irreversible effector feedback loop will more robustly filter HOG MAPK pathway output upon intermediate frequency stimulation



Supplementary Figure 2. Simulation indicates that synthetic negative feedback loops can alter the frequency dependent activation of the HOG MAPK pathway. **a**, Hog1 translocation into the nucleus and *pSTL1* transcription activity with feedback loops under periodic stimulation. The simulation for control cells (black line) is based on the model by Zi et. al. and described in supplemental data. The model with a reversible feedback loop (blue line) uses the WT model with an additional transcription feedback loops expressing effectors that convert activated Hog1 into inactive form. The model with an irreversible feedback loop (red line) is the same as the reversible feedback loop, except the effectors modifies activated Hog1 into a dead Hog1 that cannot be phosphorylated again. See Supplementary Model for more details. Simulations are shown for constant stimulation, stimulation at high frequency (2 min period) and intermediate frequency (16 min period). **b**, The gene expression from an osmostress pathway transcriptional reporter upon stimulation with 16 minute period input was calculated. Plots show the dependence of reporter gene expression as a function of the properties of the negative feedback effector, i.e. effector expression rate, degradation rate, and enzymatic activity. Both reversible and irreversible enzyme can filter out this frequency input, but an irreversible effector can perform the task over much wider parameter range than a reversible effector. **c**, The model simulation suggested irreversible regulated cells introduced novel transcriptional response pattern with varying stimulation duration (on, t_1) and interval time (off, t_2). **d**, The model simulated the frequency dependent transcriptional response ($t_1 = t_2$) of the cells with no effector control (dark grey), with PTP2-zipper feedback (blue), and with OspF feedback (red). The transcriptional frequency response was also measured by experiments.

Supplementary Figure 3

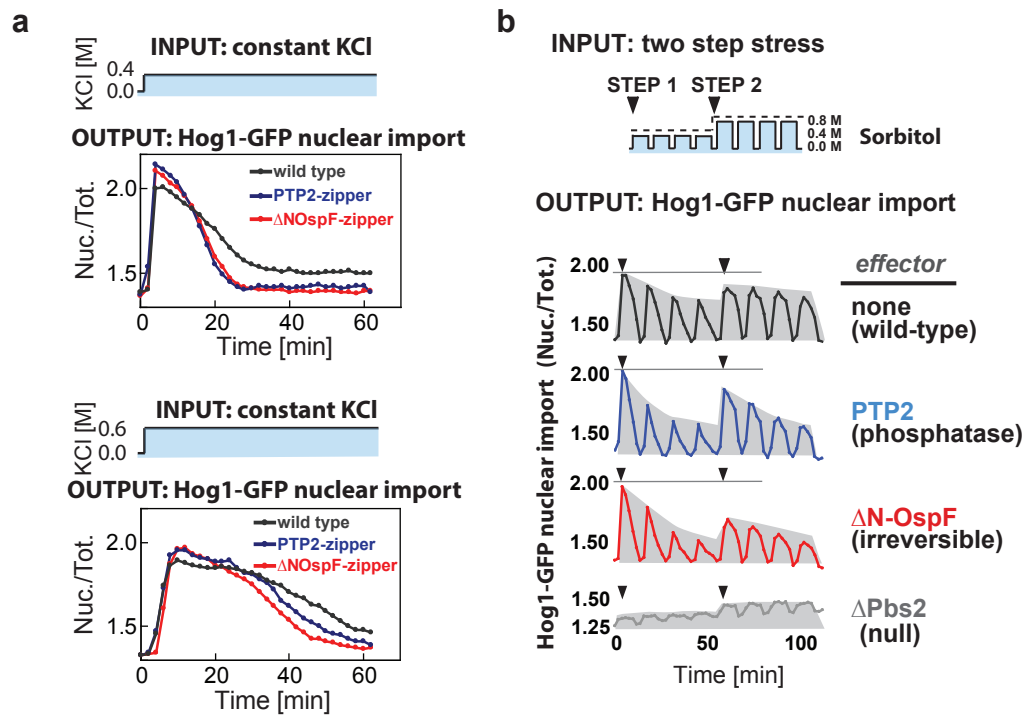
Characterization of the single cell fluorescence microscopy assay and the microfluidic control



Supplementary Figure 3. Single cell assaying with microfluidic device. **a**, CellASIC microfluidic device can switch media effectively within 10 seconds. The fluorescent dye, Texas Red, was added into the SD-complete media with 0.4 M KCl (on) to visualize the flow-switching. The SD-complete media with no KCl was as "off". A 5 min "on" followed by 4 cycles of 1 min "on" and 1 min "off" pulses was performed in a CellASIC Y04C plate with the flow-control pressure of 8 psi. The fluorescence density was calculated with ImageJ. **b**, Hog1 fused with GFP at the C-terminus is imported into nucleus when exposed to synthetic complete media with 0.4 M KCl and exported out of the nucleus following exposure to media without KCl. Htb2 fused with mCherry at C-terminus constitutively expressed by *pADH1* was used to visualize the nucleus. Automated analysis of fractional import of Hog1 is described in Methods. **c**, For transcriptional activity assay, an average of 50 - 100 live cells was calculated. **d**, Each frequency data set was measured at least 3 times separately to calculate the standard deviation. An example frequency point, 4 min on/4 min off is shown.

Supplementary Figure 4

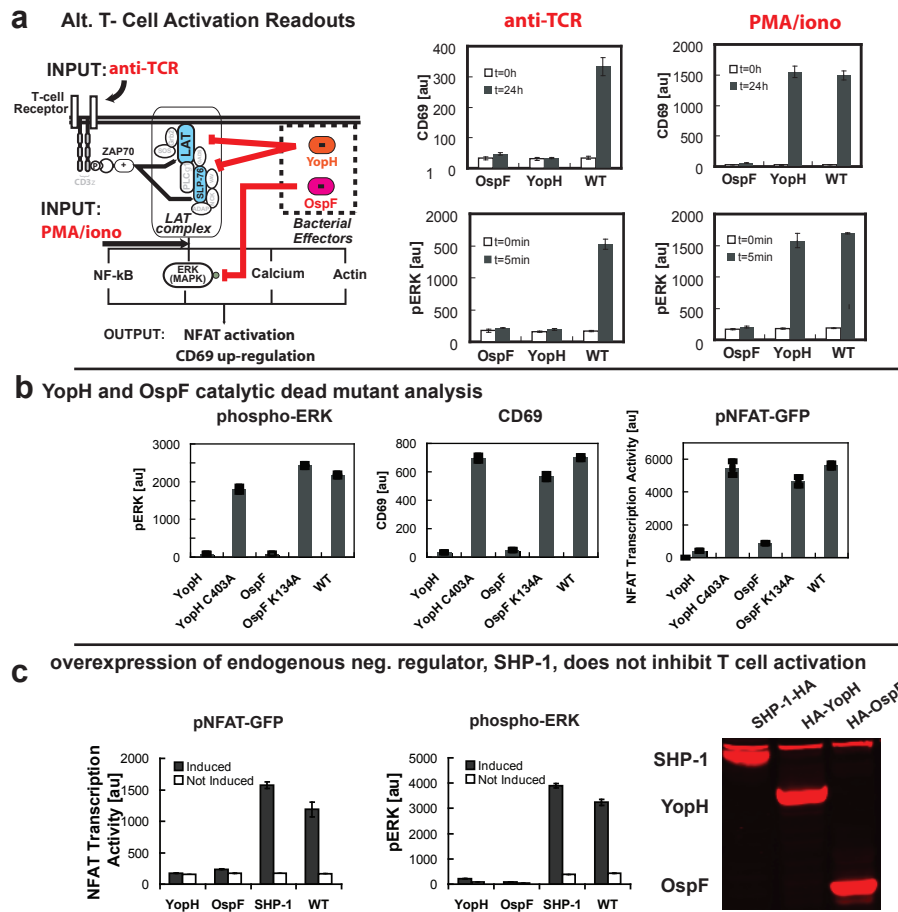
Negative feedback regulation slightly accelerated the osmo-adaptation at both low and high stress, and feedback loop with OspF rendered the cell less responsive to a second step of osmstress.



Supplementary Figure 4. OspF mediated feedback renders the cell less responsive to a second step of osmstress stimulation. **a**, Wild type (grey), PTP2 (blue) and Δ N-OspF (red) cells were stimulated with constant KCl (0.4M or 0.6M). The Hog1-GFP nuclear import was measured as the output of the activation of osmotic response. **b**, Cells were stimulated with 0.4 M sorbitol for 10 min with 4 min interval for four cycles, followed by a subsequent simulation with 0.8 M sorbitol for another four cycles. A time course of nuclear Hog1-GFP accumulation was recorded. We found that after four pulses of 0.4 M sorbitol, both the PTP2 and OspF negative feedback strains showed a dramatic decrease in Hog1 that could be imported to the nucleus (indicative of similar deactivation of phospho-Hog1 by both effectors). However, upon a second step up to higher osmolarity (0.8 M sorbitol), the PTP2 feedback strain was able to re-elicited a high level of Hog1 import, while the OspF feedback strain was not. These results are consistent with PTP2 converting phospho-Hog1 into dephosphorylated Hog1, which still remains competent for re-phosphorylation upon a further increase in MAPKK activity. In contrast, very little of the Hog1 population in the OspF strain was competent for rapid reactivation. These results are consistent with the OspF irreversibly depleting the pool of activatable Hog1 (except for new synthesis).

Supplementary Figure 5

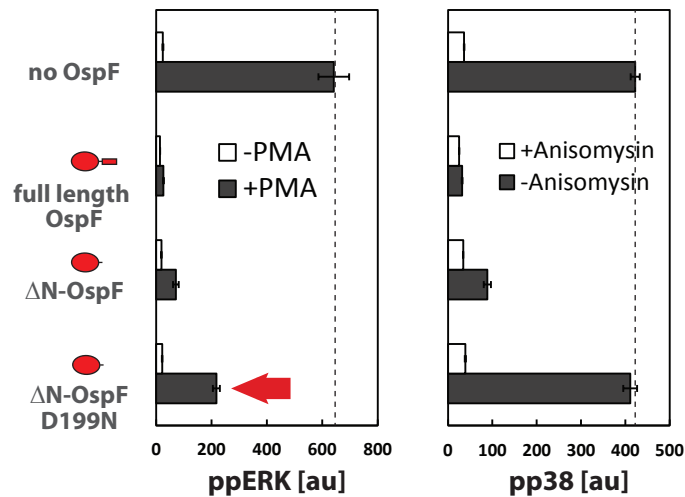
YopH and OspF inhibits T cell activation when induced with an anti-TCR antibody, while overexpression of mammalian SHP-1 phosphatase does not inhibit T cell response.



Supplementary Figure 5. Other TCR responses - ERK activation and CD69 expression - were also inhibited by YopH and OspF when cells are induced with an anti-TCR antibody (C305), while overexpression of mammalian SHP-1 phosphatase does not inhibit T cell response. a, Similar to the responses observed with NFAT transcription activation, YopH has no effect on phospho-ERK and CD69 upregulation when T cells were induced with PMA/ionomycin. b, Catalytic dead mutant of YopH (YopH C403A) and OspF (OspF K134A) have no effect on TCR activation (induced with C305) as measured by phospho-ERK, CD69 and NFAT transcription activation. c, Comparison of the effect of SHP-1 overexpression to YopH and OspF on TCR activation, as measured by NFAT transcription activity and phospho-ERK. (right) Expression level of proteins measured by Western blot against the HA epitope tag. Overexpression the mammalian phosphatase SHP-1, did not inhibit TCR activation most likely because SHP-1 is autoinhibited and subjected to complex regulation. This regulatory complexity is one of the challenges of using endogenous pathway modulators. In general, bacterial effectors may be easier to use as synthetic biology reagents for rewiring mammalian signaling.

Supplementary Figure 6

Specific OspF mutant can be used to derive negative regulator that is specific for pERK vs pp38 MAPK inhibition in Jurkat T cells.

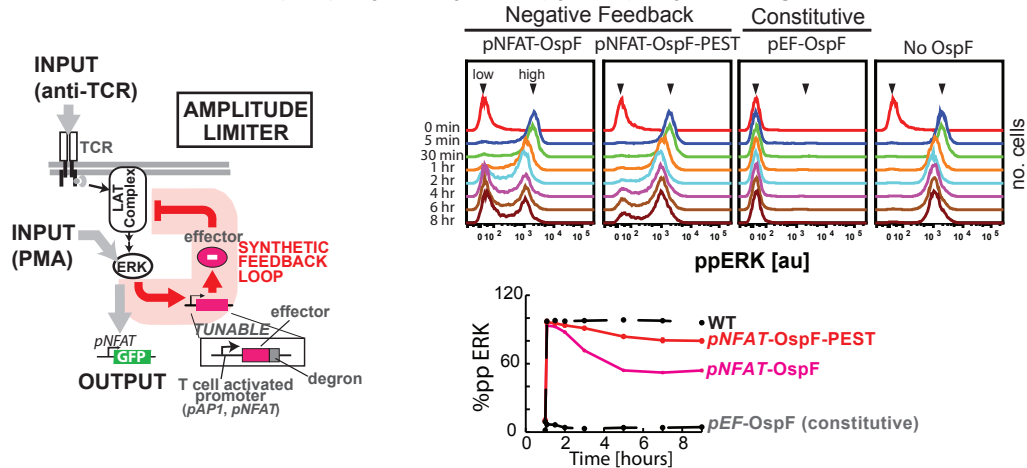


Supplementary Figure 6: Specific OspF mutant can be used to derive negative regulator that is specific for pERK vs pp38 MAPK inhibition in Jurkat T cells. Jurkat T cells were transfected with OspF and various mutants (all fused to mCherry at the N terminus). The ERK pathway was induced with PMA while the p38 pathway was induced with anisomycin. The level of pERK (left) and pp38 (right) was measured by phosphoflow with antibody against ppERK (Cell Signaling 4370) or pp38 (Cell Signaling 4511). Only cells with low OspF expression level (as determined by mCherry level) were included in the analysis. Full length wild type OspF and ΔN-OspF are very active toward both ERK and p38. The D199N mutant, however, is biased toward ERK when expressed at low level.

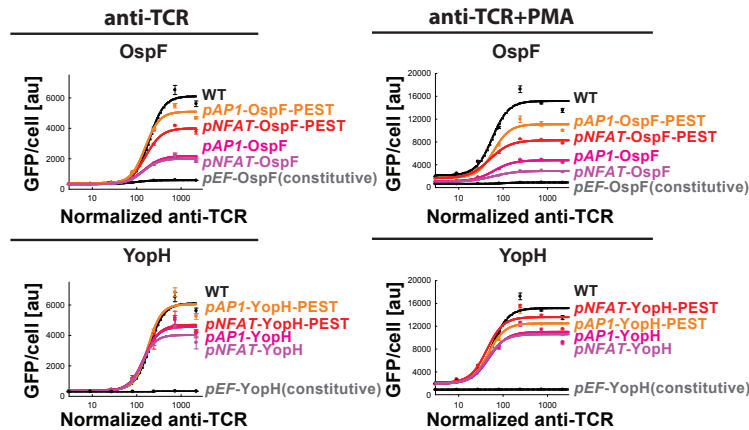
Supplementary Figure 7

Mechanism of amplitude limiter circuit: Introduction of OspF negative feedback loop causes transient Erk activation (instead of sustained), leading to lower steady pathway output amplitude

a Direct observation of Erk phosphorylation dynamics (by FACS) in synthetic negative feedback T cell circuits



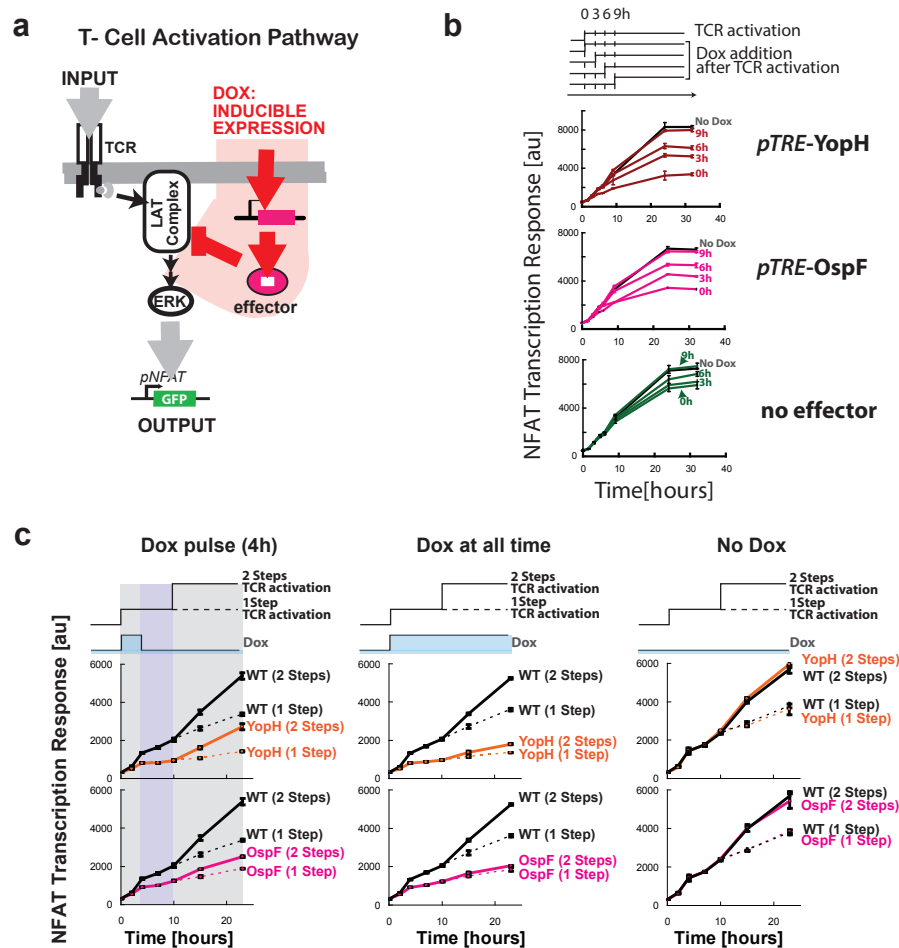
b



Supplementary Figure 7. Mechanism of amplitude limiter circuit: Introduction of OspF negative feedback loop causes transient Erk activation (instead of sustained), leading to lower steady pathway output amplitude. **a**, Histogram of the phospho-ERK at different time when stimulated with anti-TCR and PMA. PMA was used to sustain a normally transient pERK response, thus allowing the dynamics of negative feedback to be demonstrated. When OspF is expressed, a population of low pERK level appears. Constitutive expression of OspF has only low ppERK level while Jurkat without any OspF has only high of OspF population. With feedback loop, however, all cells displays high level of ppERK level after 5 minutes of activation, until after 1 hours of activation, when NFAT begins to express OspF and create a population of low pERK cells. The percentage of active ERK as a function of time. **(B)** The dose response profile of NFAT transcription response for cells containing negative feedback loops built from YopH or OspF controlled by variant activity dependent promoters (*pNFAT*, *pAP1*), with or without the degnon (*PEST*), induced by anti-TCR alone or anti-TCR supplemented with PMA. Constitutively expressed effectors (*pEF*) were used as negative controls.

Supplementary Figure 8

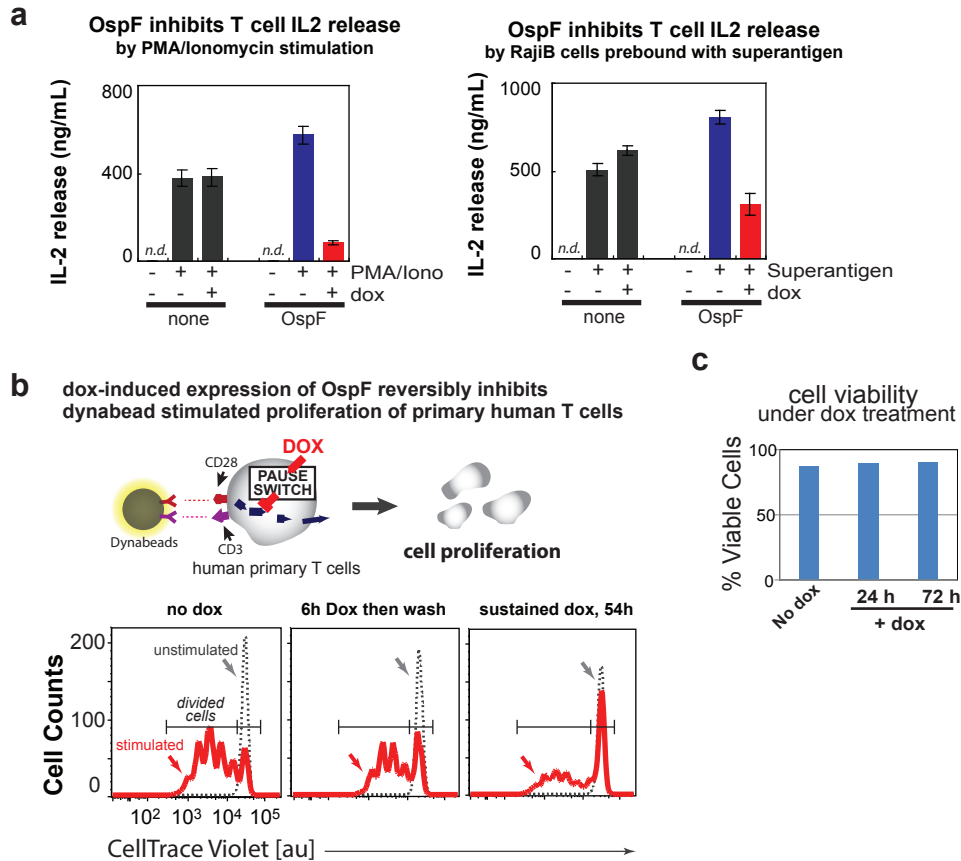
Bacterial effectors can be engineered as pause switch to control T cell activation in Jurkat T cell



Supplementary Figure 8. Synthetic pause switch: Transient inhibition of TCR activation with a pulse induction of bacterial effectors. **a**, Using a tetracycline inducible promoter (*pTRE*), the expression of YopH and OspF can be controlled by the addition of doxycycline (dox). **b**, Dox induced expression of YopH and OspF at various time points after TCR activation. **c**, TCR is activated along with the addition of dox. In the left, after 4 hours, the cells were washed away of dox and incubate for 6 hours before the TCR is further stimulated (solid line) or unstimulated (dash line). In the middle, TCR is activated along with the addition of dox, but without dox removal. In the right TCR is activated without any dox addition.

Supplementary Figure 9

OspF can be used as a synthetic pause switch to inhibit the activation of human primary CD4+ T cells



Supplementary Figure 9. OspF was engineered into a synthetic pause switch to control the activation of primary human T cells. **a**, The control T cells and T cells with OspF pause switch were pre-treated with or without 200ng/ml doxycycline for 6 hours and then activated with 10ng/ml PMA+0.5 mM ionomycine or Raji B cells pre-bound with superantigen peptides (1:1 ratio). IL-2 release was measured after 24 hours activation. **b**, The cells with OspF synthetic pause switch were treated without (left), with 6 hours (middle) or sustained dox (54 hours total) (right) were activated with anti-CD3 and anti-CD28 dynabeads (0.3:1 beads/cells ratio) for 4 days. Cells were labeled with CellTrace violet dye before beads activation and measured with flow cytometry. The cells with low fluorescence density (red) indicated divided cells (diluted labeling dye in each single cell). The unstimulated cells with each dox-treatment did not proliferate (dot line, grey). **c**, The cell viability was measured after addition of 200ng/ml dox with live/dead cells dye. There is no evident of toxicity to human primary CD4+ T cells upon dox addition at 200ng/ml.

Chapter 5. Concluding Remarks

The use of cells as effective therapeutic agents in the clinic is a reality in the present day. Successes in the field in preclinical and clinical studies have largely been in two types of situations: 1) where the endogenous therapeutic capabilities of cells has been sufficient to heal disease or replace depleted cells (hematopoietic stem cell transplant, organ transplant, dendritic cell-based vaccines for cancer, regulatory T cells for Graft versus Host Disease, mesenchymal stem cells for immune modulation), and 2) where genetic engineering has been used to enhance the therapeutic properties of the cells (chimeric antigen receptor-based T cell therapy for cancer).

Thus, the ability to augment and unlock the potential of therapeutic cells through genetic engineering in at least some key leading application areas (such as cancer) has been firmly established. Now it remains to extend and generalize the lessons learned from past successes. We believe that building a systematic therapeutic cell engineering science that allows us to precisely and predictably tune, optimize, and control therapeutic cell behavior will be critical for the advancement of this field.

One aspect of this new discipline will be the continued development, testing, characterization, and eventual application of toolkit parts that rewire cellular behaviors in understandable and generalizable ways. This dissertation described our efforts at two such classes of tools: orthogonal engineered GPCRs to control cell migration to arbitrary locations in the body, and bacterial pathogen effectors to rewire MAPK signaling cascades.

In these projects, we used an iterative engineering approach to the design and testing of new toolkit parts. First the new parts were tested *in vitro* and in relevant simple

cell types (e.g. yeast, cancer cell lines) to test hypotheses on how our design system should behave and generate data for further optimization. We then moved to more “complex” and technically challenging experiments such as those in primary cell culture and finally, to mouse models to demonstrate proof-of-principle or efficacy against disease. Experiments at each stage inform the iterative process of designing optimization that is important to the development of robust new toolkit parts.

Challenges remain for the developing field of therapeutic cell engineering. Some of the key ones include:

- Our basic mechanistic understanding of disease remains incomplete. Knowledge gained from basic research will inform the generation of ever better tools for therapeutic cellular engineering. In addition, by studying the effects of cellular therapeutic agents on disease, researchers may actually be able to gain deeper mechanistic insights.
- Further development of basic enabling technologies will be invaluable to the field. This includes advances in genetic/genomic engineering, gene synthesis, and sequencing, as well as tools for the sophisticated perturbation of cell state and cellular engineering (including in optogenetics and chemical biology). This is especially true in primary human cells, which are often slower to grow, challenging to work with, and more complex than cells such as bacteria and yeast that traditionally have been favored by synthetic biologists.
- Engineering cellular behaviors and cell “state” is more complex than inducing isolated biochemical changes into cells. In contrast to metabolic engineering or microbial biofuel production using synthetic biology where the primary endpoint is often a natural product, the desired end “product” for therapeutic cellular

engineering is often a desirable cellular behavior that likely involves a confluence of signaling, genetic, epigenetic, proteomic, and other biological factors.

- Better predictive modeling of the effects of engineering perturbations on cellular systems biology will likely facilitate more reproducible and robust cellular engineering. This work should integrate the complexity of predicting how synthetic parts will “wire into” existing cellular architecture.
- Engineered therapeutic cells that are infused into patients must work predictably and effectively in the context of the human body. Within the body, therapeutic cells are exposed to complex biochemical signals, novel cell-cell interactions with diverse cell types, inflammatory mediators in many settings of disease, the immune system and the potential for rejection, and other factors that are difficult to recapitulate in *in vitro* assays or even in mouse models of disease. Even in a “simple” case as cancer adoptive immunotherapy, where the goal for the engineered cell is relatively straightforward (i.e. attack cancer cells and spare normal cells), the therapeutic cell must carry out its tasks in a complex environment. The complexity of accounting for host – therapeutic cell interactions is likely to grow even greater in more complicated disease settings such as those seen in indications for regenerative medicine. The best path forward is likely to be to expect that therapy will be complicated by such effects and to carefully design preclinical and clinical studies with an eye toward learning key principles regarding the design of cellular therapies to avoid the compromise of therapeutic functionality within the body.

Still, the future is bright for the field of engineered cellular therapeutics. Our vision for successful cell therapies of the future is one in which engineered cells will be precisely and reproducibly manufactured tunable biological devices that silently and continuously

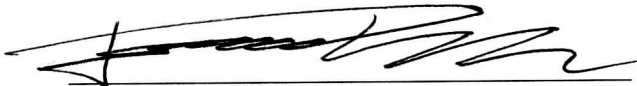
interrogate the health of the body's tissues and organs, sensing aberrant physiological signals, and responding appropriately to disease. With great control and sophistication, they will deliver therapeutic molecules, modulate inflammation, stimulate regenerative and reparative processes, attack diseased cells, and assist the body in maintaining homeostatic balance in its organ systems. When the job is done, they will revert to a quiescent sentinel state or perhaps eliminate themselves from the body. Certainly much exciting work remains to be done in the years to come.

Publishing Agreement

It is the policy of the University to encourage the distribution of all theses, dissertations, and manuscripts. Copies of all UCSF theses, dissertations, and manuscripts will be routed to the library via the Graduate Division. The library will make all theses, dissertations, and manuscripts accessible to the public and will preserve these to the best of their abilities, in perpetuity.

Please sign the following statement:

I hereby grant permission to the Graduate Division of the University of California, San Francisco to release copies of my thesis, dissertation, or manuscript to the Campus Library to provide access and preservation, in whole or in part, in perpetuity.

A handwritten signature in black ink, appearing to be "James M. Smith", written over a horizontal line.

Author Signature

6/7/2013

Date